

**VISCO-PLASTIC RATCHETING EVALUATION OF STEEL ALLOYS UNDERGOING  
VARIOUS STEP-LOADING CONDITIONS BY MEANS OF ISOTROPIC-KINEMATIC  
HARDENING RULES**

By

Poorya Karvan

B.Sc. in Mechanical Engineering, Razi University, Iran, 2013

M.Sc. in Mechanical Engineering, Razi University, Iran, 2016

A dissertation  
presented to Ryerson University  
in partial fulfillment of the  
requirements for the degree of

**Doctor of Philosophy  
in the Program of  
Mechanical and Industrial Engineering**

Toronto, Ontario, Canada, 2020

© Poorya Karvan, 2020

## AUTHOR'S DECLARATION FOR ELECTRONIC SUBMISSION OF A DISSERTATION

I hereby declare that I am the sole author of this dissertation. This is a true copy of the dissertation, including any required final revisions, as accepted by my examiners.

I authorize Ryerson University to lend this dissertation to other institutions or individuals for the purpose of scholarly research.

I further authorize Ryerson University to reproduce this dissertation by photocopying or by other means, in total or in part, at the request of other institutions or individuals for the purpose of scholarly research.

I understand that my dissertation may be made electronically available to the public.

# ABSTRACT

## **Visco-Plastic Ratcheting Evaluation of Steel Alloys undergoing various Step-Loading Conditions by means of Isotropic-Kinematic Hardening Rules**

Poorya Karvan, Doctor of Philosophy Mechanical and Industrial Engineering, Ryerson University, Toronto, Canada, 2020

The present thesis develops visco-plastic constitutive equations to assess ratcheting response of several steel alloys of 304, austenitic Z2CND18.12N, U71Mn, and 316 examined under various step-loading conditions through use of the Ohno-Wang (O-W) and Ahmadzadeh-Varvani (A-V) kinematic hardening rules. The framework of hardening rules was incorporated isotropic hardening rules of Lee and Zavrel (Iso-LZ), Chaboche (Iso-C), and Kang (Iso-K) to emulate expansion of yield surfaces. The unified visco-plastic flow rule was adapted to account for the effects of stress rate and time-dependency in ratcheting assessment of steel samples. Kang's function on dynamic strain aging was employed to further evaluate time-dependent ratcheting response at operating room and elevated temperatures. This function was integrated to the dynamic recovery terms leading to drop in ratcheting magnitude and rate resulting in plastic shakedown shortly after a few stress cycles over Low-High loading sequence. The effect of the presence of peak/valley holding time resulting in static recovery was introduced into the kinematic hardening rules through inclusion of a backstress-dependent function proposed earlier by Ding. This integration enabled hardening rules to predict the excess of ratcheting strain values generated by static loading at maximum and minimum stresses over each loading cycle.

Visco-plastic ratcheting evaluation of various stainless steel samples were evaluated at various stress rate, stress levels, loading steps and sequences, operating temperatures and holding times through use of the O-W and A-V hardening rules. The predicted ratcheting curves and hysteresis loops by the O-W and A-V frameworks were compared with those obtained experimentally. The predicted ratcheting curves of steel samples tested at Low-High-Low and High-Low-High loading sequences and at room and elevated temperatures revealed that both frameworks elevated ratcheting strains over Low-High loading sequence and dropped them over High-Low loading sequence.

Choices of material constants and number of segments taken from stress-strain curve based on the O-W model noticeably influenced ratcheting response of steel samples. The O-W model held more backstress components, and consequently more coefficients, requiring longer Central Processing Unit (CPU) time for ratcheting evaluation than the A-V model which possessed a less complex framework with a fewer number of coefficients.

# ACKNOWLEDGEMENTS

First and foremost, I would like to express my sincere appreciation to my supervisor, Professor A. Varvani-Farahani for his persistent and friendly support, encouragement, and patience. The joy and enthusiasm he has for his research was contagious and motivational for me, even during tough times in the Ph.D. pursuit. He has definitely contributed to the success of this work very much.

Sincere thanks are extended to Dr. Reza Ahmadzadeh who morally supported me over the period of this study.

The financial supports through Ryerson Graduate Scholarship Program (RGS) and Natural Sciences and Engineering Research Council (NSERC) of Canada are greatly appreciated.

I would like to thank my parents for their love and support throughout my life. Thank you both for giving me the strength to reach for the stars and chase my dreams. My sister, niece and nephew deserve my wholehearted thanks as well.

I would like to express my sincerest gratitude to my lovely fiancée, Maryam, for her patience, inspiration, unconditional support, and love. I undoubtedly owe her greatly for being able to complete my studies and perform this work.

# Table of Contents

ABSTRACT.....	iii
ACKNOWLEDGEMENTS.....	v
LIST OF TABLES.....	viii
LIST OF APPENDICES.....	ix
LIST OF FIGURES .....	x
NOMENCLATURE .....	xiii
PREFACE.....	xiv
CHAPTER ONE.....	1
INTRODUCTION .....	1
1.1. Overview and background .....	1
1.2. Objective and scope .....	2
CHAPTER TWO .....	4
LITERATURE SURVEY.....	4
2.1. Physics of ratcheting.....	4
2.2. Importance of Ratcheting.....	5
2.3. Isotropic and kinematic hardening rules .....	5
2.3.1. A-F type hardening models and ratcheting assessment .....	7
2.4. Visco-plastic flow rules and affecting parameters in hardening rules .....	12
2.4.1. Use of visco-plastic flow description in hardening rules.....	12
2.4.2. The effect of stress/strain rate .....	13
2.4.3. The influence of operating temperature .....	14
2.4.4. Holding time effect .....	14
2.5. Summary .....	15
CHAPTER THREE.....	17
FUNDAMENTALS OF CYCLIC VISCO-PLASTICITY< HARDENING RULES AND CONSTITUTIVE EQUATIONS.....	17
3.1. Fundamental of constitutive model and formulation .....	17
3.1.1. Elements of plasticity and visco-plasticity.....	17
3.1.2. Isotropic hardening rules.....	19

3.1.3. Kinematic hardening rules .....	23
3.2. Visco-plastic flow rule .....	28
3.2.1. The influence of operating temperature .....	29
3.2.2. The influence of holding time .....	30
3.3. Algorithm of ratcheting assessment .....	31
3.4. Summary .....	33
CHAPTER FOUR.....	34
RESULTS OF RATCHETING EVALUATION AND DISCUSSION.....	34
4.1. Materials and Testing Conditions .....	34
4.2. Coupled isotropic-kinematic hardening rules .....	36
4.2.1. Testing conditions and models coefficients .....	36
4.2.2. Ratcheting evaluation through isotropic-kinematic hardening rules .....	37
4.3. Visco-plastic constitutive frameworks.....	45
4.3.1. Stress level and rate on ratcheting response.....	45
4.3.2. Step-loading conditions .....	48
4.3.3. Operating temperatures .....	54
4.3.4. Holding time .....	65
4.4. Summary .....	70
CHAPTER FIVE.....	72
CONCLUSIONS AND RECOMMENDATIONS .....	72
5.1. Conclusions .....	72
5.2. Recommendations for future research .....	74
APPENDIX A.....	76
APPENDIX B.....	96
REFERENCES .....	115

# LIST OF TABLES

<b>Table 4.1.</b> Mechanical properties of studied materials .....	36
<b>Table 4.2.</b> Testing conditions for SS304 steel samples tested at room temperature .....	37
<b>Table 4.3.</b> Coefficients of the A-V and O-W isotropic-kinematic hardening rules.....	37
<b>Table 4.4.</b> Testing conditions for Z2CND18.12N and SS304 alloys at room temperature.....	46
<b>Table 4.5.</b> Coefficients for the O-W and A-V frameworks for Z2CND18.12N and SS304 alloys.....	46
<b>Table 4.6.</b> Ratcheting tests and stress-steps for SS304, SS316L, U71Mn steel samples tested at room temperature	49
<b>Table 4.7.</b> Coefficients of the O-W and A-V frameworks for SS304, SS316, U71Mn steel samples .....	49
<b>Table 4.8.</b> Ratcheting tests and stress-steps on SS304 samples at various temperatures .....	55
<b>Table 4.9.</b> Coefficients for the O-W and A-V frameworks for SS304 samples at various temperatures.....	56
<b>Table 4.10.</b> Ratcheting tests and stress-steps on SS304 samples with holding time.....	65
<b>Table 4.11.</b> Coefficients for the O-W and A-V frameworks for SS304 samples with holding time.....	66

# LIST OF APPENDICES

<b>Table A.1</b> Symbols and terms employed in the MATLAB programming .....	76
<b>Table B.1</b> Mechanical properties of studied materials .....	97
<b>Table B.2</b> Experimental ratcheting strain of SS304 in Figure 4.2.....	98
<b>Table B.3</b> Experimental ratcheting strain of SS304 in Figure 4.6(a-c) .....	99
<b>Table B.4</b> Experimental ratcheting strain of Z2CND18.12 N steel with constant stress amplitude and various mean stresses in Figure 4.8a.....	100
<b>Table B.5</b> Experimental ratcheting strain of Z2CND18.12 N steel with constant mean stress and various stresses amplitude in Figure 4.8b.....	101
<b>Table B.6</b> Experimental ratcheting strain of Z2CND18.12 N steel with constant stress level of $150\pm 150$ MPa and various stress rates Figure 4.9a.....	102
<b>Table B.7</b> Experimental ratcheting strain of SS304 with constant stress level of $78\pm 234$ MPa and various stress rates Figure 4.9b and Figure 4.15.....	103
<b>Table B.8</b> Experimental ratcheting strain of SS304 over three steps of loading in Figure 4.10 .....	104
<b>Table B.9</b> Experimental ratcheting strain of SS316L over four steps of loading in Figure 4.11 .....	105
<b>Table B.10</b> Experimental ratcheting strain of U71Mn over seven steps of loading in Figure 4.12 .....	106
<b>Table B.11</b> Experimental ratcheting strain of U71Mn over four steps of loading in Figure 4.13a.....	107
<b>Table B.12</b> Experimental ratcheting strain of U71Mn over six steps of loading in Figure 4.13b.....	108
<b>Table B.13</b> Experimental ratcheting strain of SS316L over four steps of loading in Figure 4.13c .....	109
<b>Table B.14</b> Experimental ratcheting strain of SS304 at $700^{\circ}\text{C}$ in Figure 4.16.....	110
<b>Table B.15</b> Experimental ratcheting strain of SS304 over three steps of loading at $200^{\circ}\text{C}$ in Figure 4.17 .....	111
<b>Table B.16</b> Experimental ratcheting strain of SS304 over three steps of loading at $400^{\circ}\text{C}$ in Figure 4.18 .....	112
<b>Table B.17</b> Experimental ratcheting strain of SS304 over three steps of loading at $600^{\circ}\text{C}$ in Figure 4.20 .....	113
<b>Table B.18</b> Experimental ratcheting strain of SS304 over three steps of loading at $700^{\circ}\text{C}$ in Figure 4.21 .....	114

# LIST OF FIGURES

<b>Figure 2.1.</b> Stress-strain hysteresis loops based on Prager model for SS304.....	8
<b>Figure 2.2.</b> Stress-strain hysteresis loops of SS304 based on A-F model.....	9
<b>Figure 2.3.</b> Stress-strain hysteresis loops of SS304 based on Bower model.....	10
<b>Figure 2.4.</b> Stress-strain hysteresis loops of SS304 based on (a) O-W Model I and (b) O-W Model II.....	11
<b>Figure 2.5.</b> Stress-strain hysteresis loops of SS304 based on A-V model .....	12
<b>Figure 3.1.</b> Maximum tensile stress in each cycle versus the accumulated plastic strain .....	20
<b>Figure 3.2.</b> Schematic presentation of strain range memory and its variables.....	21
<b>Figure 3.3.</b> Superposition of components of backstress.....	24
<b>Figure 3.4.</b> Backstress at different activation functions .....	25
<b>Figure 3.5.</b> (a) Increments taken over uniaxial cyclic stress–strain to determine constants $\gamma_i$ and $r_i$ , and (b) exponent $m$ in the O-W model .....	26
<b>Figure 3.6.</b> Schematic presentation of the experimental and predicted hysteresis loops based on the A-V model: (a) coefficients $C$ and $\gamma_1$ through cyclic stress-strain loops, and (b and c) variation of coefficients $C$ and $\gamma_1$ to achieve consistency condition.....	27
<b>Figure 3.6.</b> Continued.....	28
<b>Figure 3.7.</b> determination of coefficient $\gamma_2$ through best-fit curve of ratcheting strain data .....	28
<b>Figure 3.8.</b> Ratcheting prediction based on plasticity and visco-plasticity constitutive theory on (a) the A-V model and (b) the O-W model.....	29
<b>Figure 3.9.</b> Flowchart of the algorithm developed on the basis of visco-plastic framework of O-W and A-V .....	32
<b>Figure 4.1.</b> Stress-strain curves of studied materials.....	35
<b>Figure 4.2.</b> Uniaxial ratcheting prediction by means of the O-W and the A-V kinematic hardening rule. ....	38
<b>Figure 4.3.</b> Predicted ratcheting curves based on (a) the A-V framework, and (b) the O-W framework as compared with experimental data.....	39
<b>Figure 4.4.</b> Hysteresis loops generated over ratcheting progress based on the O-W and A-V hardening rules (a) experimental data, (b1-b4) the O-W kinematic model, and (c1-c4) the A-V kinematic model, without and with inclusion of Iso-LZ, Iso-C and Iso-K models.....	41
<b>Figure 4.5.</b> (a) Evolution of yield stress in the O-W and A-V hardening rules, (b) the predicted hysteresis loop for the 16 <sup>th</sup> cycle based on the A-V model, and (c) the predicted hysteresis loop for the 16 <sup>th</sup> cycle based on the O-W model. ....	42
<b>Figure 4.5.</b> Continued.....	43
<b>Figure 4.6.</b> Predicted ratcheting strains based on the A-V and O-W frameworks for various loading conditions of (a) 10±260MPa, (b) 65±260MPa, (c) 65±325MPa.....	44
<b>Figure 4.7.</b> Experimental ratcheting rate over 100 cycles and those predicted by means of the A-V and O-W hardening rules.....	44

<b>Figure 4.8.</b> Experimental and predicted ratcheting curves of Z2CND18.12 N steel by means of visco-plastic frameworks of O-W and A-V for various (a) mean stresses and (b) stress amplitudes .....	47
<b>Figure 4.9.</b> Experimental and predicted ratcheting curves by means of visco-plastic frameworks of O-W and A-V for various stress rates (a) Z2CND18.12 N steel and (b) SS304.....	48
<b>Figure 4.10.</b> (a) Experimental ratcheting data and (b) their measured hysteresis loops at room temperature plotted versus predicted ratcheting curves by means of the O-W and A-V models at constant stress amplitude of 248 MPa and different mean stress of 78→117→78 MPa.....	50
<b>Figure 4.11.</b> (a) Experimental and predicted ratcheting data over four stress-steps, and (b) experimental and predicted hysteresis loops generated by means of the O-W and A-V models for four-step stress levels for a SS316L sample tested at constant stress amplitude of 195 MPa and different means stresses of 0→39.7→66.2→105.8 MPa .	51
<b>Figure 4.12.</b> (a) Experimental and predicted ratcheting data over seven Low-High/ High-Low stress-steps, and (b) experimental and predicted hysteresis loops generated by means of the O-W and A-V models for seven-step stress levels for a U71Mn sample tested at constant stress amplitude of 449 MPa and mean stresses of 0→308→359→411→308 →359→411MPa.....	53
<b>Figure 4.13.</b> Experimental and predicted ratcheting values by means of the O-W and A-V models for (a and b) U71Mn and (c) SS316 alloys. ....	54
<b>Figure 4.14.</b> Experimental uniaxial tensile stress-strain data for (a) various strain rates at room and 700°C temperatures, and (b) various strain rates at 350°C.....	57
<b>Figure 4.15.</b> (a) Experimental ratcheting data and (b) their measured hysteresis loops plotted versus predicted ratcheting curves and hysteresis loops for 304 steel sample T1 by means of the O-W and A-V models at 78±234 MPa and at room temperature.....	58
<b>Figure 4.16.</b> Experimental ratcheting data and their measured hysteresis loops at 700°C plotted versus predicted ratcheting curves for 304 steel sample T5 by means of the O-W and A-V models at 40±100 MPa and at stress rate of 10MPa/sec .....	59
<b>Figure 4.17.</b> Experimental ratcheting data and their measured hysteresis loops at 200°C plotted versus predicted ratcheting curves for 304 steel sample T2 by means of the O-W and A-V models stress amplitude of 248 MPa and different mean stress of 39→78→39 MPa .....	60
<b>Figure 4.18.</b> Experimental ratcheting data and their measured hysteresis loops at 400°C plotted versus predicted ratcheting curves for 304 steel sample T3 by means of the O-W and A-V models at constant stress amplitude of 208 MPa and different mean stress of 39→78→39 MPa.....	61
<b>Figure 4.19.</b> (a) Variation of exponential function $\psi$ over loading cycles for sample T3 tested at 400°C based on the hardening rules O-W and A-V, and (b, c) predicted ratcheting results in the presence and absence of function $\psi$ in the dynamic recovery terms of the hardening rules.....	62
<b>Figure 4.20.</b> Experimental ratcheting data and their measured hysteresis loops plotted at 600°C versus predicted ratcheting curves for 304 steel sample T4 by means of the O-W and A-V models at constant stress amplitude of 195 MPa and mean stress of 26→39→26 MPa.....	63

**Figure 4.21.** Experimental ratcheting data and their measured hysteresis loops for 304 steel sample T6 tested at 700°C plotted versus predicted ratcheting data by means of the O-W and A-V models at constant stress amplitude of 102 MPa and different mean stress of 0→26→52 MPa..... 64

**Figure 4.22.** (a) experimental ratcheting data without and with holding time and (b) measured hysteresis loops with hold time is plotted versus those predicted by means of O-W and A-V frameworks for sample H1 at 78±234 MPa..... 67

**Figure 4.23.** (a) experimental ratcheting data without and with holding time and (b) measured hysteresis loops with holding time is plotted versus those predicted by means of O-W and A-V frameworks for sample H1 tested at 40±100 MPa..... 68

**Figure 4.24.** Predicted ratcheting curves in the presence and absence of static recovery function for sample H1 tested at room temperature by means of the (a) O-W and (b) A-V model ..... 69

**Figure 4.25.** Predicted ratcheting results in the presence and absence of static recovery function for sample H2 tested at 700°C temperature by means of the (a) O-W and (b) A-V model..... 69

# NOMENCLATURE

$\bar{n}^*$  = Unit normal to plastic strain surface

$A_1, A_2, A_3$  = Kang's isotropic internal variables

$Q_0$  = Initial value of saturated yield surface

$Q_M$  = Saturated value of yield surface

$\bar{a}$  = Backstress tensor

$\bar{b}$  = Internal variable of the A-V model

$\bar{n}$  = Unit normal to yield surface

$\gamma^i, r^i, m^i$  = Coefficients of the O-W model

$\gamma_1, \gamma_2, C, \delta$  = Coefficients of the A-V model

$\bar{\zeta}$  = Tensor representing movement of the center of plastic strain surface

$\sigma_y$  = Actual yield Stress

$\sigma_y^0$  = Initial yield stress

$R$  = Internal variable of isotropic hardening (i.e. saturated value of yield surface)

$Q$  = Saturated value of internal variable  $R$

$d\bar{\epsilon}^p$  = Increment of plastic strain

$dp$  = Increment of equivalent plastic strain

$p$  = Accumulated plastic strain

$q$  = Internal variable retains the previous larger plastic strain amplitude

$\beta$  = Exponent defining evolution rate of  $R$

$\eta$  = Constant defining the number of cycles require for stabilization

$\mu$  = Exponent defining evolution rate of  $Q_M$

$\varsigma$  = Constant defining the evanescent (i.e. fading) memory function in Kang's isotropic model

$\dot{\bar{\epsilon}}^{vp}$ : Visco-plastic strain rate

$q$  : Radius of the envelope surface of plastic strain trajectory

$K$ : Drag stress

$n$  : Visco-plastic strain growth exponent

$\sigma_v$  : Viscous stress

# PREFACE

This current dissertation holds five chapters followed by two appendices A and B. The following briefs materials covered in the chapters and appendices of this thesis. At the end of each chapter a summary is given highlighting important remarks.

**Chapter 1** presents the background and overview of ratcheting evaluation. This chapter features the objective and scope of the research work.

**Chapter 2** initially highlights physics of ratcheting and its importance in engineering practice. It further reviews literature on cyclic plasticity and visco-plasticity with an emphasis on coupled kinematic hardening rules of Prager, Armstrong-Fredrick, Bower, Ohno-Wang, and Ahmdazadeh-Varvani including their formulations, terms, and coefficients.

**Chapter 3** discusses the fundamental elements of cyclic plasticity and the developed visco-plastic constitutive frameworks of O-W and A-V. The formulation of isotropic hardening rules and expansion of yield surface and its impact on ratcheting assessment over the first stage are discussed. The importance of visco-plastic flow rule to evaluate ratcheting assessment of time-dependent materials is extensively reviewed. This includes dynamic strain aging effect introduced into the dynamic recovery term of the frameworks through an exponential function. This chapter further presents details of the algorithm developed through use of MATLAB program to include visco-plasticity for stainless steel alloys.

**Chapter 4** presents and discusses results of ratcheting curves predicted based as isotropic and kinematic hardening rules were coupled. Predicted visco-plastic ratcheting values by the O-W and A-V frameworks for steel samples under various single and multi-step loading spectra at room and elevated temperature are discussed. Three isotropic hardening rules were introduced into the frameworks and the capability of each was studied. The predicted visco-plastic ratcheting values through O-W and A-V visco-plastic were discussed as generated stress-strain hysteresis loops were compared with those of experimental data. This chapter further discusses the influence of stress rate, loading sequence, operating temperature and holding-time in ratcheting assessment of steel samples.

**Chapter 5** presents the concluding points for the conducted research work. It also holds a section as future recommendations listing more aspects of research to be conducted.

**Appendix A** details the MATLAB programming code developed based on the original Ahmadzadeh-Varvani program with inclusion of isotropic and visco-plastic description. The frameworks and procedure of ratcheting assessment based on the A-V and O-W are detailed in this appendix.

**Appendix B** tabulates materials properties, coefficients, and measured ratcheting data employed in this study.

# CHAPTER ONE

## INTRODUCTION

### 1.1. Overview and background

Engineering and structural components in industries such as offshore structures, pressure vessels, and airplane landing gears are constantly subjected to cyclic loading conditions leading to catastrophic failure as plastic strain accumulation over loading cycles becomes inevitable. Failure of these components in low-cycle fatigue (LCF) regime is highly attributed to irreversible inelastic deformation developed over asymmetric stress cycles. The progressive plastic strain accumulation under asymmetrical stress-controlled cycles is referred as ratcheting strain. Ratcheting response of materials is highly influenced by microstructural properties, stress levels and rates, operating temperatures, loading histories, steps, sequences and holding-time.

An indispensable step for reliable design of load-bearing engineering components to assess ratcheting response of materials is to employ cyclic plasticity constitutive equations and hardening rules. The framework of constitutive models is categorized into two classes of plasticity and viscoplasticity theories. These models are employed as materials undergo elastic-plastic or elastic-viscoplastic deformation over loading cycles. The former involves materials deformation to fading memory over hardening process, while the latter is attributed to viscous deformation as materials deformation becomes time-dependent. The backbone of constitutive models is structured on the basis of the hardening rules. These rules control the evolution of yield surface within deviatoric stress space as loading exceeds elastic domain. The yield surface evolution in size is controlled through isotropic hardening rules and the transition of the yield surface is governed by kinematic hardening rules. The current study evaluates two well-known kinematic hardening rules

developed earlier namely the Ohno-Wang (O-W) and Ahmadzadeh-Varvani (A-V) along with isotropic hardening rules to assess ratcheting of various steel alloys under step-loading conditions. The framework of models involved use of visco-plastic flow rule to address time-dependent ratcheting response of materials. The choice of A-V and O-W models in ratcheting assessment were discussed as both frameworks were evaluated through their structures, terms, and coefficients.

## **1.2. Objective and scope**

This research intends to evaluate visco-plastic ratcheting of different steel alloys subjected to asymmetric uniaxial loading cycles based on the Ohno-Wang (O-W) and Ahmadzadeh-Varvani (A-V) hardening rules. As a primary step, isotropic descriptions are integrated to the kinematic hardening models to assess expansion of yield surface where ratcheting over stage I is controlled with different yield values. The initial yield stress is taken as the onset of yielding through the O-W model and yield surface is expanded over first few cycles resulting in yield stress to mature. On the other hand, in the A-V model, the stabilized yield surface is employed through entire ratcheting progress. Involving isotropic hardening rules will enable both kinematic hardening rules to stabilize yield surface through hardening/softening over longer cycles in stage I. The engagement of isotropic hardening rule highly influences ratcheting over the first stage promoting to a steady state condition.

To address the influence of rate-dependency in ratcheting assessment of materials, the O-W and A-V hardening rules will be further employed along with the unified visco-plastic flow rule. Through this inclusion, visco-plastic ratcheting of stainless steel alloys is evaluated through various stress rates and at room and elevated temperatures. Rate-dependency in materials deformation is faded at a given range of temperature. This minimized time-dependency will be described through dynamic strain ageing, an exponential function as a part of the dynamic recovery term in the kinematic hardening rule. This function is expected to provoke peculiar ratcheting response resulting in a sharp buildup over a few number of cycles followed by a plateau as stress level dropped over High-Low loading sequence.

Further objective of this research is to take into account the effect of peak/valley holding-time over visco-plastic ratcheting assessment. The presence of hold-time over loading spectra results in static recovery effect leading to accumulation of larger values of ratcheting strain. Longer holding-time critically will impact ratcheting elevation resulting in an accelerated failure.

The ultimate objective is to comprehensively evaluate cyclic hardening and visco-plastic ratcheting response of materials. These responses are investigated at various step-loading conditions through inclusion of stress level, stress rate, loading sequence, operating temperature, and holding-time.

# CHAPTER TWO

## LITERATURE SURVEY

This chapter presents a thorough review on elements of cyclic plasticity, hardening rules, and ratcheting assessment of materials developed earlier in literature. The coupled hardening rules of Armstrong-Fredrick type including Prager, Armstrong-Fredrik (A-F), Bower, Ohno-Wang (O-W), and Ahmadzadeh-Varvani (A-V) were introduced. The importance of ratcheting and variables involved in assessing of this phenomenon was highlighted.

### 2.1. Physics of ratcheting

Ratcheting accumulation over asymmetric stress cycling is known as a tri-phasic phenomenon, similar to creep trend, however, different in nature. The ratcheting strain is caused by the formation of cells, the dislocations movement and/or slip, and the interaction of dislocations. Cyclic hardening and softening are the dominant factors affecting ratcheting in stage I. Ratcheting accumulation as a result of hardening phenomenon in this stage is due to gradual dislocation pile-up as cyclic load is applied. Cyclic softening feature contributes to ratcheting buildup by dislocation motion. In the second stage, ratcheting rate decays steadily until it reaches a constant value. In the final stage, the number of active dislocations increases leading to necking and ductile fracture in materials [1–4]. The magnitude of ratcheting and number of cycles to failure can be impacted by stress rate and operating temperature. A lower value of the former results in larger values of ratcheting. This response is associated with the higher number of active dislocations at lower stress rates [2]. Operating temperature causes fading time-dependency in materials deformation at given range of temperatures, resulting in premature ratcheting shakedown. This

phenomenon, ascribed as the dynamic strain aging, was reported to strengthening mechanism as mobile dislocations interacted with diffusing solute atoms [5,6].

## **2.2. Importance of Ratcheting**

Reliable design of engineering components in various industries such as automotive, aerospace, power plant, pressure vessel and pipeline is rigorously hinged upon materials integrity, complexity of geometry, operating temperature, and loading conditions. Such components undergo asymmetric loading cycles during their lifespan resulting in accumulation of plastic strain, known as ratcheting strain. While rate-dependent response in materials deformation has been reported in engineering alloys as early as 1909 [7], ratcheting was first evidenced in steel samples by Bairstow [8] in 1911. Machinery parts in service inevitably experience catastrophic failure due to progressive damage. The evidence of progressive damage in materials as a result of integrating ratcheting and fatigue was first documented by Coffin [9] in 1970. Following sections review fundamental of isotropic and those A-F type kinematic hardening rules and related parameters developed over the last half-century.

## **2.3. Isotropic and kinematic hardening rules**

The paramount asset for evaluation of ratcheting is hardening rules responsible for evolution of yield surface. This evolution can be through yield surface transition, kinematic hardening rule, or expansion/contraction, isotropic hardening rule. Experimental studies collectively reported that materials exhibit hardening/softening over the first 10 to 1000 cycles before they stabilize [10]. The dominance of isotropic hardening rules to control progressive plastic strain merely over the initial loading cycles as well as its incapability in prediction of cyclic phenomena, such as Bauschinger's effect, relaxation, and ratcheting was a prime notion to further promote research to develop kinematic hardening rules [11].

Lee and Zavrel [12] were first to introduce a function to correlate the expansion of yield surface to plastic strain accumulation. Chaboche [13] experimentally argued that the traditional isotropic hardening was yet to adequately predict hardening/softening as it is saturated towards a unique value. To address this shortcoming, Chaboche [13] introduced an internal variable retaining

the prior largest plastic strain amplitude. This internal variable was defined based on hypersphere in the plastic strain space; later referred as non-hardening region by Ohno [14]. As long as plastic strain moves within this region, no isotropic hardening would occur. This was associated to the direction and mobility of dislocations over loading and unloading paths. Nouailhas et al. [15] included an evanescent part to the strain memory concept developed earlier by Chaboche to study the hardening and softening of quenched and cold-work samples of SS316. Kang [16] made further adjustments to Chaboche's and Nouailhas's postulations by modifying the evanescent part to a function referred to as fading memory which could trace the largest plastic strain range.

Isotropic and kinematic hardening rules are both responsible for evolution of yield surface. By implementing both hardening rules, yield surfaces are allowed to expand and translate simultaneously until they reach their saturated values. A simple kinematic hardening rule was first proposed by Prager [17]. This linear hardening rule was capable of addressing Bauschinger's effect but incapable of ratcheting prediction. The Armstrong-Fredrick [18] (A-F) model modified the Prager's model by introducing a dynamic recovery term. This term prevented closed hysteresis loops as expected over asymmetric cycles to promote ratcheting deformation. The rate of ratcheting in the A-F model remained unchanged throughout loading cycles which resulted in over-estimation of ratcheting. Bower [19] further modified the dynamic recovery part and managed to decay the rate of ratcheting. However, after a certain number of cycles ratcheting arrest appeared through a plateau. Chaboche's postulation [20] of decomposing total backstress into backstress increments was used by Ohno and Wang [21,22] to introduce a new kinematic hardening rule. Ohno and Wang presented a threshold for each increment of backstress by means of a Heaviside and power law functions respectively in their models I and II. The former failed to predict ratcheting and resulted in closed hysteresis loops. The latter was however successful in predicting ratcheting. Jiang and Sehitoglu [23] modified the O-W model by a controlling exponent and employed accumulated plastic strain instead of plastic strain increment to predict ratcheting under non-proportional loading conditions. McDowell [24] modified the exponent  $m$  in the O-W dynamic recovery term and replaced it with a function indicating the effect of uniaxial and multiaxial loading. Chen et al. [25] developed a model incorporating new factor in the second model of O-W. This factor was associated with backstress and non-coaxiality of plastic strain rate and took into account the effect of non-proportionality. Their hardening rule was reported

promising in ratcheting assessment under multiaxial loading conditions. Varvani and coworkers [26,27] developed the A-F model through new parameters adapted in the dynamic recovery and predicted ratcheting of various loading spectra. Their framework consisted of a few material coefficients and an internal variable in the dynamic recovery to control backstress increments and corresponding yield surface translation over loading paths. However, this model was yet to include the effect of cyclically hardening/softening on ratcheting prediction as well as rate-dependent materials' ratcheting prediction. To address the former issue, Karvan and Varvani [28,29] further adhered isotropic hardening description to the A-V model. They employed isotropic-kinematic hardening rule to further improve ratcheting underestimation predicted by the A-V model through initial cycles in the absence of isotropic description.

### **2.3.1. A-F type hardening models and ratcheting assessment**

#### **2.3.1.1. The Prager Model**

Prager [17] (1955) was first to introduce a kinematic hardening rule capable of tracking the transition of the yield surface. This model relates plastic strain and applied stress with a linear correlation as:

$$d\mathbf{a} = C d\boldsymbol{\varepsilon}^p \quad (2.1)$$

tensor  $\mathbf{a}$  corresponds to backstress and term  $C$  is a material constant. According to this model, the value of modulus of plasticity remains unchanged over loading and unloading condition, causing generation of closed hysteresis loops and zero ratcheting strain. Figure 2.1 presents stress-strain hysteresis loops drawn based on Prager kinematic hardening rule. In this figure, it is evident that even in the presence of mean stress, progression of hysteresis loops did not occur.

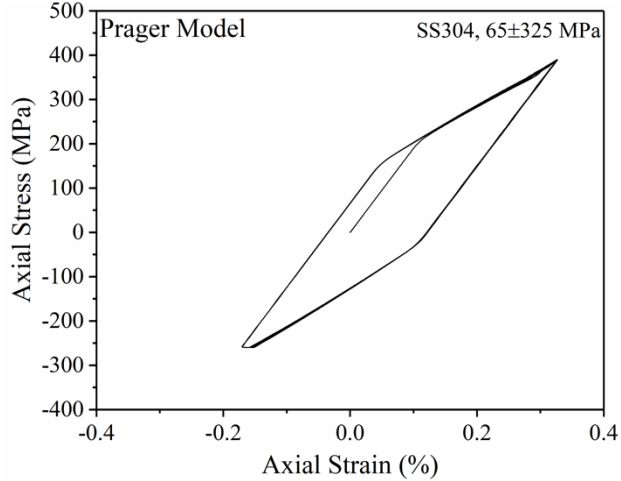


**Figure 2.1.** Stress-strain hysteresis loops based on Prager model for SS304

### 2.3.1.2. The Armstrong-Frederick Model

Armstrong and Fredrick [18] (1966) proposed the A-F hardening rule by inclusion of a non-linear term, known as dynamic recovery, into the Prager's model as:

$$d\mathbf{a} = C d\boldsymbol{\varepsilon}^p - \gamma \mathbf{a} dp \quad (2.2)$$

coefficients  $C$  and  $\gamma$  are material constants obtained from uniaxial stress-controlled hysteresis loops. Increment of accumulated plastic strain,  $dp$ , is defined as,  $dp = \sqrt{d\boldsymbol{\varepsilon}^p \cdot d\boldsymbol{\varepsilon}^p}$ . The second term in equation (2.2) introduces nonlinearity into the A-F model resulting in inequality in the modulus of plasticity over loading and unloading parts. Figure 2.2 shows that the inclusion of the dynamic recovery term has resulted in open hysteresis loops and consequently non-zero ratcheting strain. The A-F kinematic hardening rule however fell short in estimating ratcheting strain rate decay by generating equally-distant hysteresis loops as the stress cycles progressed.

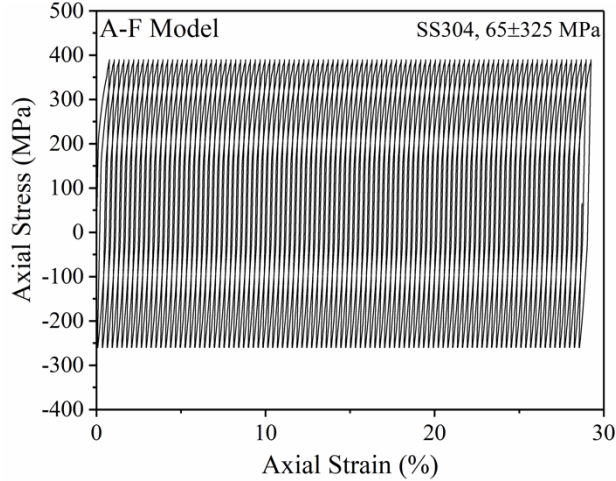


**Figure 2.2.** Stress-strain hysteresis loops of SS304 based on A-F model

### 2.3.1.3. The Bower Model

Bower [19] (1989) further modified the A-F model to overcome its over-prediction. In this model, an internal variable,  $\mathbf{b}$ , was introduced into the dynamic recovery term to simulate evolution of yield surface more accurately. This internal variable was defined similarly to dynamic recovery term as:

$$d\mathbf{a} = C d\boldsymbol{\varepsilon}^p - \gamma_1 (\mathbf{a} - \mathbf{b}) dp \quad (2.3a)$$

$$d\mathbf{b} = \gamma_2 (\mathbf{a} - \mathbf{b}) dp \quad (2.3b)$$

coefficients  $C$  and  $\gamma$  are material constants and obtained similar to the A-F model. Constant  $\gamma_2$  is responsible for ratcheting rate decay. Tensor  $\mathbf{b}$ , follows backstress,  $\mathbf{a}$ , over stress cycles and causes additional hardening and decrease in magnitude of ratcheting strain as stress cycles continue. Figure 2.3 displays that generated hysteresis loops through Bower model caused gradual decrease in the distance of stress-strain loops, however, after a few cycles, this distance becomes zero and causes premature ratcheting arrest. In other words, the magnitude of term  $(\mathbf{a} - \mathbf{b})$  becomes zero which consequently cancels out the dynamic recovery term and the Bower model reduces to the Prager model.

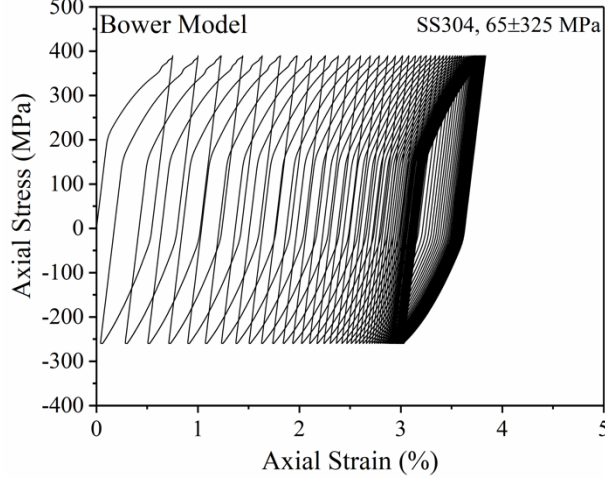


**Figure 2.3.** Stress-strain hysteresis loops of SS304 based on Bower model

#### 2.3.1.4. The Ohno-Wang Model

Ohno and Wang [21,22] (1993) developed a kinematic hardening rule on the basis of Chaboche [13] decomposing backstress into several increments, by introducing respectively a Heaviside (Model I) in equation (2.4a) and power function (Model II) in equation (2.4b) into dynamic recovery terms defining thresholds to activate backstress increments. The Model I and Model II are described as:

$$d\bar{a}^i = \gamma^i \left[ \frac{2}{3} r^i d\bar{\epsilon}^p - H(f_i) \left\langle d\bar{\epsilon}^p, \frac{\bar{a}^i}{|\bar{a}^i|} \right\rangle \bar{a}^i \right] \quad (2.4a)$$

$$d\mathbf{a}^i = \gamma^i \left[ \frac{2}{3} r^i d\boldsymbol{\epsilon}^p - \left( \frac{|\mathbf{a}^i|}{r^i} \right)^{m^i} \left\langle d\boldsymbol{\epsilon}^p, \frac{\mathbf{a}^i}{|\mathbf{a}^i|} \right\rangle \mathbf{a}^i \right] \quad (2.4b)$$

The McCauley function ensures to account for the effects of loading path and direction under multiaxial loading conditions. This function is simplified to  $dp = \sqrt{\frac{2}{3}} d\boldsymbol{\epsilon}^p \cdot d\boldsymbol{\epsilon}^p$  under uniaxial loading condition. Exponent  $m^i$  controls ratcheting decay and is determined from the curve of uniaxial ratcheting strain data plotted versus loading cycles. A smaller value of  $m^i$  results in over-prediction similar to the A-F model and a larger value of this exponent develops the

Prager's shakedown. Terms  $\gamma^i$  and  $r^i$  are material coefficients determined from uniaxial stress-strain curve. Equations (2.5a) and (2.5b) define material dependent coefficients of  $\gamma^i$  and  $r^i$  as:

$$\gamma^i = \frac{1}{\varepsilon^{p(i)}} \quad (2.5a)$$

$$r^i = \left( \frac{\sigma^{(i)} - \sigma^{(i-1)}}{\varepsilon^{p(i)} - \varepsilon^{p(i-1)}} - \frac{\sigma^{(i+1)} - \sigma^{(i)}}{\varepsilon^{p(i+1)} - \varepsilon^{p(i)}} \right) \quad (2.5b)$$

Figure 2.4 presents hysteresis loops generated by means of the Ohno –Wang models. The Model I (Figure 2.4a) failed to produce open hysteresis loops under uniaxial loading condition and resulted in premature shakedown, while the Model II (Figure 2.4b) was capable to generate progressive open hysteresis loops.

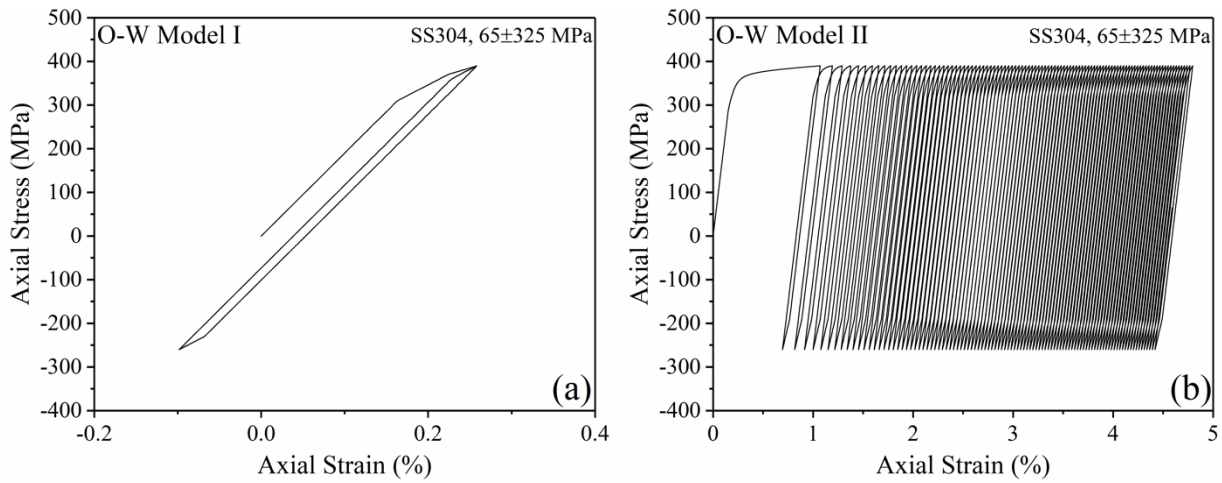


**Figure 2.4.** Stress-strain hysteresis loops of SS304 based on (a) O-W Model I and (b) O-W Model II

### 2.3.1.5. The Ahmadzadeh-Varvani Model

Ahmadzadeh and Varvani [30] (2013) developed a hardening rule by introducing an internal variable  $\mathbf{b}$  into dynamic recovery part of the A-F model to control the evolution of backstress. Term  $(\mathbf{a} - \delta\mathbf{b})$  enabled yield surface to evolve and decrease ratcheting strain rate. The general structure of the A-V hardening rule is presented through equation (2.6a) [23] as:

$$d\mathbf{a} = Cd\boldsymbol{\varepsilon}^p - \gamma_1 \left( \mathbf{a} - \left( \frac{|\mathbf{a}|}{k} \right)^m \mathbf{b} \right) dp \quad (2.6a)$$

$$d\mathbf{b} = \gamma_2 (\mathbf{a} - \mathbf{b}) dp \quad (2.6b)$$

where  $C$  and  $\gamma_1$  are material constants and are determined to preserve consistency condition and to control width of open hysteresis loops. Material constant  $\gamma_2$  is the secondary coefficient responsible to calibrate ratcheting rate and its decay over stage II. Coefficient  $k$  is defined as  $C/\gamma_1$  and exponent  $m$  is a value close to zero.

Figure 2.5 demonstrates that the A-V model successfully overcame the deficiencies of the A-F and Bower model in producing respectively loops with constant distance and premature shakedown. Term  $\delta$  in the A-V model precludes additional hardening and ensures the evolution of backstress  $\mathbf{a}$  along with the internal variable  $\mathbf{b}$  maintain parallel to each other as the number of cycles progresses resulting in prevention of ratcheting arrest.

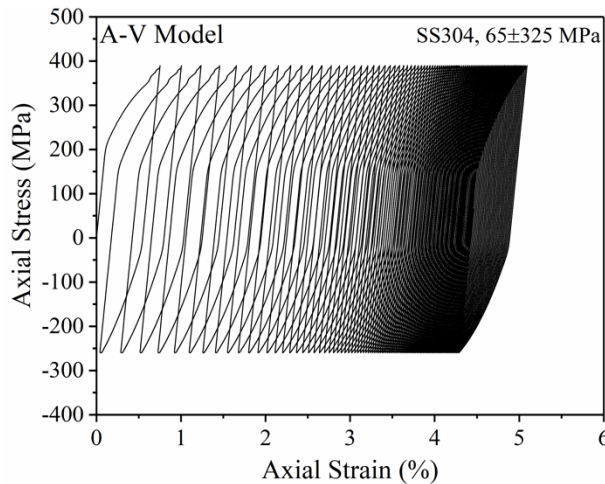


**Figure 2.5.** Stress-strain hysteresis loops of SS304 based on A-V model

## 2.4. Visco-plastic flow rules and affecting parameters in hardening rules

### 2.4.1. Use of visco-plastic flow description in hardening rules

A plasticity flow rule, initially proposed by Drucker [31], includes modulus of plasticity possessing two unique values, over loading and unloading conditions. The framework of plastic flow rule lacks inclusion of applied stress rate and materials time-dependent ratcheting. To address

this shortcoming, Chaboche [32] formulated a visco-plastic constitutive equation on the basis of Perzyna's classical visco-plastic theory [33] through introducing a McCauley function with an exponent known as viscous exponent. This formulation later reflected in a number of research work [34–39] to mostly predict ratcheting in stainless steel samples. Kang et al. [38] introduced visco-plastic flow rule into the AK-O model to assess time-dependent ratcheting response in 304 steel samples subjected to various stress levels and rates at room temperature. Yu et al. [36] further employed visco-plastic description and a new exponential function replacing the exponent in the dynamic recovery of the O-W model to evaluate ratcheting response of austenitic stainless steel samples at different stress magnitudes. Zhao et. al [39] performed analysis on ratcheting behavior of SS304 samples by means of the AK-O model and a visco-plastic constitutive description. The A-V kinematic hardening model was employed [37] along with visco-plastic constitutive equation to address ratcheting response of stress rate-dependent alloys of Z2CND18.12N , Zircaloy-4, and solder 63Sn37Pb under single-step loading conditions at room temperature.

#### **2.4.2. The effect of stress/strain rate**

Loading rate is a key factor on ratcheting evaluation of rate-dependent materials. It is widely reported in literature that even at room temperature, ratcheting increases in magnitude as the stress rate decreases. This feature is attributed to the activation of larger number dislocations under smaller stress rate [2]. Yoshida [40] reported that ratcheting response of samples of SUS304 is highly rate sensitive even at room temperature. They showed experimentally that ratcheting increases by %40 upon decreasing strain-rate from 0.0001/sec. to 0.01/sec. Ratcheting tests conducted by Mizuno et. al [41] on samples of 316FR at room temperature revealed that change of stress rate from 10 to 1 MPa/sec. increased ratcheting strain over %50. Tested samples of 63Sn37Pb solder, Zircaloy-4 and Z2CND18.12N stainless steel at room temperature under various stress rates showed the similar ratcheting behavior [36,42,43]. It was observed that ratcheting increases for samples of Zircaloy-4 and Z2CND18.12N stainless steel by %40 under decreasing stress rate from respectively 1000 to 100 MPa/sec. and 200 to 20 MPa/sec. For samples of 63Sn37Pb solder this increase was more than 5 times when stress rate plunged from 4 to 2 MPa/sec.

### **2.4.3. The influence of operating temperature**

While metallic materials are generally regarded as rate-dependent at elevated temperature, evidence has shown that materials rate-dependency lessens as operating temperatures varied between 350°C and 650°C for SS304 steel alloy [38]. Drop in rate-dependency was further observed in SS316L and SS316LN steel samples by Hong and Lee [44] and Sarkar et al. [45] respectively at temperatures 250°C-600°C and 550°C. Stainless steel samples of Z2CND18.12N tested under uniaxial stress cycles at 350°C [46] have also shown a drop in rate-independency response. De Almeida et al. [47] reported that austenitic stainless steels are prone to time-independency at 200°C-800°C. Models were developed to address isothermal and an-isothermal loading conditions and to introduce dynamic strain aging effect into the constitutive models [48–53]. Tests on 35CrMo and 25Cr2MoVA steel samples [54,55] at elevated temperature were conducted at various stress rates to assess ratcheting under asymmetric load cycles. Yu et al. [36] applied asymmetric uniaxial loading cycles on stainless steel samples at various loading conditions at room temperature and reported that an increase in stress level and a drop in the applied stress rate noticeably promoted ratcheting over loading cycles. Zheng et. al [56] employed the O-W model [21] in the framework of a visco-plastic constitutive model to address uniaxial ratcheting response of 35CrMo at 500°C subjected to various stress cycles with zero stress ratio,  $R=0$ . They achieved more promising results for loading histories possessing smaller stress ranges. Kang et al. [38,57] employed AbdelKarim-Ohno (AK-O) model [58] to assess ratcheting of SS316 and SS304 steel samples at various temperatures. They addressed the influence of dynamic strain aging in ratcheting response through inclusion of an exponential function into the dynamic recovery term of the AK-O model. Their predicted ratcheting results at various temperatures were found to follow the experimental data.

### **2.4.4. Holding time effect**

Imposition of peak/valley holding time to asymmetric stress-controlled loading cycles, results in creep-ratcheting phenomenon leading to higher ratcheting progress. Yoshida [40] conducted cyclic tests including holding time in each peak/valley on samples of SUS304 at room temperature. He predicted ratcheting response of steel samples through use of the Krempl visco-

plastic model [59] and reported the shortcomings of the model to assess experimental ratcheting data obtained at stress ratios of  $R < 0$ . Kang et al. [38] further reported that holding time escalated ratcheting progress at room temperature and at elevated temperature of  $700^{\circ}\text{C}$ . They found predicted ratcheting and hysteresis loops by means of the Abdel-Karim and Ohno hardening rule constantly collapsed below experimental data obtained at various stress rates and holding times. To overcome this drawback, Ding et al. [60] introduced an exponential function of backstress into the dynamic recovery part to account for the static recovery effect emanating from holding times. The proposed model was then employed to simulate ratcheting response of Al 6061-T6 samples undergoing various cyclic stress rates, stress levels, and holding times. The predicted uniaxial ratcheting curves were reported to closely agree with those measured experimentally at operating temperatures of  $25^{\circ}\text{C}$  and  $150^{\circ}\text{C}$ .

## 2.5. Summary

The frameworks of several kinematic hardening rules were discussed. The Prager linear kinematic hardening rule fell short to generate open hysteresis loops and consequently ratcheting strain. Introduction of dynamic recovery term through the A-F model tackled this deficiency resulting in open stress-controlled loops. However, constant ratcheting rate caused significant over-prediction of ratcheting by the A-F model. While the internal variable  $\mathbf{b}$  in Bower model lessened the effect of dynamic recovery part leading to ratcheting rate decay, it became equal to backstress  $\mathbf{a}$  after a few number of cycles and neutralized the dynamic recovery part contribution in ratcheting prediction by creating a plateau similar to Prager model. To overcome this drawback, Ahmadzadeh and Varvani alleviated the influence of internal variable  $\mathbf{b}$ , and the additional hardening caused by it, by introducing coefficient  $\delta$ . Through this modification, the A-V model successfully controlled the ratcheting rate decay over stage II. Chaboche's breakthrough on decomposing the total backstress and controlling each component of backstress by a critical value inspired Ohno and Wang to develop a kinematic hardening rule. The Heaviside function as a concept of critical value in the O-W Model I precluded the model to develop open hysteresis loops. By substituting this function with a power function, the O-W Model II managed to generate progressive stress-controlled loops. Adapting the unified visco-plastic flow rule enabled hardening

rules to evaluate ratcheting response of materials in the presence of influential parameters including stress and strain rates, room and elevated operating temperatures, and holding time.

# CHAPTER THREE

## FUNDAMENTALS OF CYCLIC VISCO-PLASTICITY, HARDENING RULES AND CONSTITUTIVE EQUATIONS

This chapter presents the constitutive equations to evaluate ratcheting response of steel samples over asymmetric cyclic loading at room and elevated temperatures. Isotropic-kinematic hardening rules of Ohno-Wang (O-W) and Ahmadzadeh-Varvani (A-V) were employed along with cyclic plasticity/visco-plasticity flow rules to mainly assess time-dependent ratcheting response of materials. An exponential function developed by Kang was adapted to the frameworks of the hardening rules through dynamic strain aging function. This function enabled the dynamic recovery terms of the hardening rules to account for ratcheting at different operating temperatures. The algorithm of the O-W and A-V frameworks were developed to analyse backstress increments over the loading process and to evaluate the ratcheting strain over the asymmetric stress cycles through a MATLAB programming code presented in Appendix A.

### 3.1. Fundamental of constitutive model and formulation

#### 3.1.1. Elements of plasticity and visco-plasticity

Constitutive models are structured through constituents of yield function, strain increments, Hooke's law, flow rule, hardening rule and consistency condition. Yield surface demarks elastic and plastic deformation of materials and is defined through von-Mises criterion as:

$$f(\mathbf{s}, \mathbf{a}, \sigma_y) = \sqrt{\frac{3}{2}(\mathbf{s} - \mathbf{a}) \cdot (\mathbf{s} - \mathbf{a})} - \sigma_y \quad (3.1)$$

tensor  $\mathbf{s}$  presents the state of stress in deviatoric space and is denoted as:

$$\mathbf{s} = \boldsymbol{\sigma} - \frac{1}{3}(\boldsymbol{\sigma} \cdot \mathbf{I})\mathbf{I} \quad (3.2)$$

terms  $\boldsymbol{\sigma}$  and  $\mathbf{I}$  in equation (3.2) correspond respectively to applied stress and unit tensor. The total strain is portioned into elastic and plastic components as:

$$\boldsymbol{\varepsilon} = \boldsymbol{\varepsilon}^e + \boldsymbol{\varepsilon}^p \quad (3.3)$$

Elastic strain is defined by Hooke's law as:

$$\boldsymbol{\varepsilon}^e = \frac{\boldsymbol{\sigma}}{2G} - \frac{\nu}{E}(\boldsymbol{\sigma} \cdot \mathbf{I})\mathbf{I} \quad (3.4)$$

where  $E$  and  $G$  are elastic and shear moduli. Constant  $\nu$  is the Poisson's ratio. The stress-strain relation within plastic domain is defined through a flow rule. Plasticity and visco-plasticity flow rules for time-independent and time-dependent materials are respectively:

$$d\boldsymbol{\varepsilon}^p = \frac{1}{H_p} \langle d\mathbf{s} \cdot \mathbf{n} \rangle \mathbf{n} \quad (3.5a)$$

$$\dot{\boldsymbol{\varepsilon}}^{vp} = \sqrt{\frac{3}{2}} \left\langle \frac{\sigma_v}{K} \right\rangle^n \frac{(\mathbf{s} - \mathbf{a})}{|\mathbf{s} - \mathbf{a}|} \quad (3.5b)$$

where  $H_p$  is modulus of plasticity and  $\mathbf{n}$  in equation (3.5a) is the normal vector to the yield surface:

$$\mathbf{n} = \frac{(\mathbf{s} - \mathbf{a})}{|\mathbf{s} - \mathbf{a}|} \quad (3.6)$$

In equation (3.5a), terms  $K$  and  $n$  are associated with the visco-plastic effect and correspond to respectively drag stress and viscous exponent. The visco-plastic overstress,  $\sigma_v$ , is defined identical to von-Mises yield function through equation (3.7):

$$\sigma_v = \sqrt{\frac{3}{2}(\mathbf{s} - \mathbf{a}) \cdot (\mathbf{s} - \mathbf{a})} - \sigma_y \quad (3.7)$$

where  $\mathbf{a}$  and  $\sigma_y$  denote backstress and yield stress, respectively. The former is governed through kinematic hardening rules and the latter is associated with isotropic hardening rule. Symbols/terms in bold correspond to tensors and those in regular font denote scalar values.

### 3.1.2. Isotropic hardening rules

#### 3.1.2.1. Isotropic hardening rule of Lee and Zarvel (Iso-LZ)

Over the first stage of ratcheting, yield surface undergoes expansion/contraction. Lee and Zarvel (1978) [12] introduced an isotropic model structured through an internal variable as a function of accumulated plastic strain. They defined the yield stress through integrating the initial yield stress,  $\sigma_y^0$ , and an internal variable,  $R$ :

$$\sigma_y = \sigma_y^0 + R(p) \quad (3.8)$$

where the isotropic internal variable is defined as an exponential function of accumulated plastic strain,  $p$ :

$$R = Q(1 - e^{-\beta p}) \quad (3.9)$$

terms  $Q$  and  $\beta$  are material constants obtained from regression of the maximum stress plotted versus the accumulated plastic strain (see Figure 3.1) [36,61]. Initially,  $p$  possesses a small value eliminating the effect of  $R$  in the yield surface whereas upon progression of stress cycles  $p$  grows resulting in saturation of  $R$  as  $R \rightarrow Q$ .

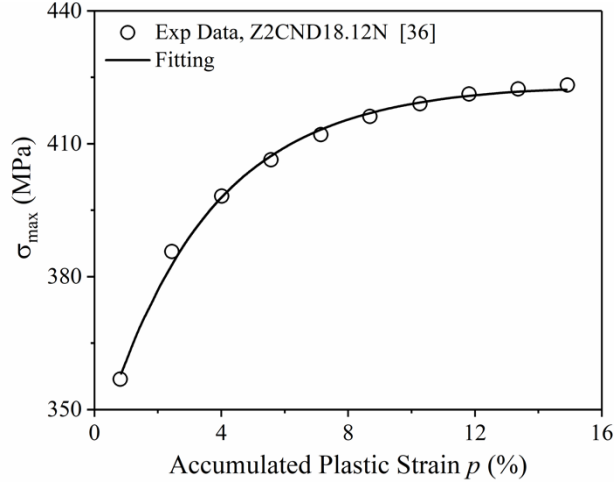


**Figure 3.1.** Maximum tensile stress in each cycle versus the accumulated plastic strain

### 3.1.2.2. Isotropic Hardening Rule of Chaboche (Iso-C)

Chaboche [13] reported that cyclic hardening was built-up in SS316L samples even after stabilization upon an increase in the applied stress amplitude. Test samples initially were hardened due to higher strain amplitude ranges, and then softened as strain amplitudes dropped. To address the multiple hardening events as a result of transient process in isotropic hardening, the concept of a memory surface was introduced by Chaboche [13]. An internal variable,  $q$ , was introduced to account for the prior maximum plastic strain. Term  $Q$  in equation (3.9) was defined [13] as a function of variable  $q$  as:

$$Q = Q_M + (Q_0 - Q_M)e^{-2\mu q} \quad (3.10)$$

where  $Q_M$  and  $Q_0$  are saturated and initial value of  $Q$ ; and exponent  $\mu$  are material dependent [15]. The latter controls the rate of this saturation. A larger value of exponent  $\mu$  delays saturation of  $Q$  and prolongs isotropic yield surface expansion over stress cycles and promotes ratcheting progress. This exponent is determined through the best-fit curve of peak stresses of progressing hysteresis loops plotted versus plastic strain range values [28]. Figure 3.2 schematically presents variables involved in the strain range memory. Internal variable  $q$  in this figure is defined through a memory function, similar to von-Mises in three-dimensional strain space as:

$$F = \frac{2}{3}(\boldsymbol{\varepsilon}_p - \boldsymbol{\xi}) \cdot (\boldsymbol{\varepsilon}_p - \boldsymbol{\xi}) - q^2 \quad (3.11)$$

Changes in memory state is permitted only if  $F = 0$  and  $\frac{\partial F}{\partial \boldsymbol{\varepsilon}_p} \cdot \dot{\boldsymbol{\varepsilon}}_p > 0$  [34]. Memory surface (non-hardening region) corresponds to a domain where isotropic hardening is absent. This domain is defined and controlled by means of radius  $q$  and center position  $\boldsymbol{\xi}$ . The movement of memory surface  $\boldsymbol{\xi}$  and radius  $q$  are defined (see Figure 3.2) as:

$$\dot{\boldsymbol{\xi}} = \sqrt{3/2} (1 - \eta) H(F) \langle \mathbf{n} \cdot \mathbf{n}^* \rangle \mathbf{n}^* \dot{p} \quad (3.12a)$$

$$\dot{q} = \eta H(F) \langle \mathbf{n} \cdot \mathbf{n}^* \rangle \dot{p} \quad (3.12b)$$

Strain range values influence variables  $q$  and  $\boldsymbol{\xi}$  through accumulated plastic strain  $p$  as of equation (3.12). In this equation,  $\mathbf{n}^*$  is defined as the normal vector to memory surface:

$$\mathbf{n}^* = \frac{(\boldsymbol{\varepsilon}_p - \boldsymbol{\xi})}{|(\boldsymbol{\varepsilon}_p - \boldsymbol{\xi})|} \quad (3.13)$$

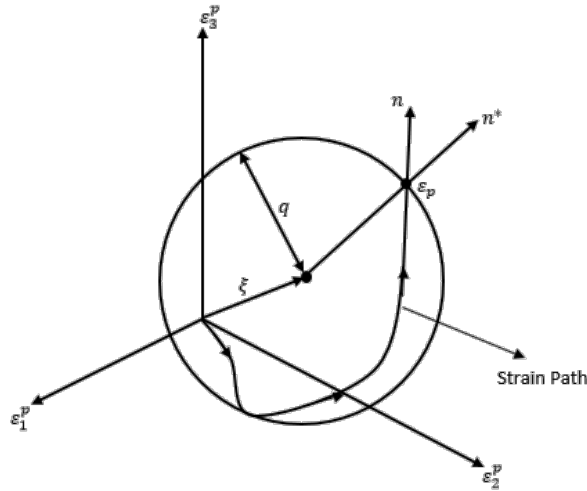


**Figure 3.2.** Schematic presentation of strain range memory and its variables

Memory surface or non-hardening region is associated with the postulation that isotropic hardening cannot be generated while the plastic strain path moves inside the spherical region. The center and radius of this region are defined by two plastic strain points. If the plastic strain stays

on the boundary of this region and moves outwards, this region expands, translates, and results in isotropic hardening, while it remains unchanged when the plastic strain moves inside these two points and inside the region as reported by Ohno and Kachi [62]. The inclusion of McCauley function in equation (3.12) ensured that isotropic hardening was inactivated during unloading condition. Chaboche [10] put forth four possibilities to introduce isotropic hardening descriptions into visco-plastic framework through use of (i) isotropic variable  $R$ ,  $R = R(p)$ , (ii) drag stress as a function of accumulated plastic strain,  $K = K(p)$ , (iii) modifications in the kinematic hardening rule, and (iv) proportional correlation between  $R$  and  $K$  as  $K(p) = K + \zeta R(p)$ . In the latter approach, term  $\zeta$  is a constant between zero and unity imposing the weight of isotropic variable on drag stress and term  $K$  is defined as an initial value of drag stress. In a special case for  $\zeta = 1$ , this term becomes equal to the initial value of yield stress [10,33]. Parameter  $\eta$  was later added to the equation (3.12) by Ohno [14] to account for stress-controlled loading condition. This parameter is associated with the rate of memory storage and varies between zero and half. Larger values of  $\eta$  increased internal variable  $q$  accelerating the evolution of  $Q \rightarrow Q_M$  through equation (3.10). For  $\eta = 0.5$ , equation (3.12) turns into Chaboche's memorization of maximum plastic strain range and stabilization occurs in one cycle [34]. Ohno and Kachi [62] and Chaboche [34] reported that  $\eta$  values noticeably less than 0.50 imply that materials with higher isotropic hardening response result in a more accurate prediction of ratcheting under stress-controlled loading condition.

### 3.1.2.3. Isotropic Hardening Rule of Kang (Iso-K)

Kang [16] argued that the isotropic hardening cannot be restricted to the loading part and introduced a fading function into the Iso-C model to address the rate of softening/hardening. The memory surface  $F$  was defined based on equation (3.11), however, functions defining the movement of its surface and the internal variable were modified as:

$$\dot{\xi} = 0.5H(F)(\dot{\epsilon}^p \cdot \bar{\mathbf{n}}^*)\bar{\mathbf{n}}^* \quad (3.14a)$$

$$\dot{q} = [0.5H(F)(\bar{\mathbf{n}}^* \cdot \bar{\mathbf{n}}') - (H(F) - 1)\Lambda(q)]\dot{p} \quad (3.14b)$$

where  $\Lambda(q)$  is the fading function defined as:

$$\Lambda(q) = \zeta q \quad (3.15)$$

term  $\zeta$  is a material constant obtained from uniaxial cyclic tests [63]. Vector  $\bar{n}'$  in equation (3.14a) is defined as:

$$\bar{n}' = \frac{\dot{\boldsymbol{\epsilon}}^p}{|\dot{\boldsymbol{\epsilon}}^p|} \quad (3.16)$$

Like the Iso-C model, if the plastic strain is positioned outside the memory surface, equation (3.14) acts similarly to equation (3.12) as the second term becomes zero. For plastic strain within the memory surface, equation (3.14) reduces to  $\dot{q} = -\zeta q \dot{p}$ . In Kang's model, term  $Q$  in equation (3.9) is defined as:

$$Q = A_1 + A_2(1 - e^{-A_3 q}) \quad (3.17)$$

where  $A_1$ ,  $A_2$ , and  $A_3$ , are material constants extracted from the uniaxial and strain cyclic experiments [63].

### 3.1.3. Kinematic hardening rules

#### 3.1.3.1. Kinematic hardening rule of Ohno-Wang (O-W)

Ohno and Wang [21,22] developed a kinematic hardening rule on the bases of Chaboche's [13] postulation of backstress decomposition. According to this postulation (illustrated in Figure 3.3), the total backstress is decomposed into components of backstress as:

$$d\mathbf{a} = \sum_{i=1}^M d\bar{\mathbf{a}}^i \quad (3.18)$$

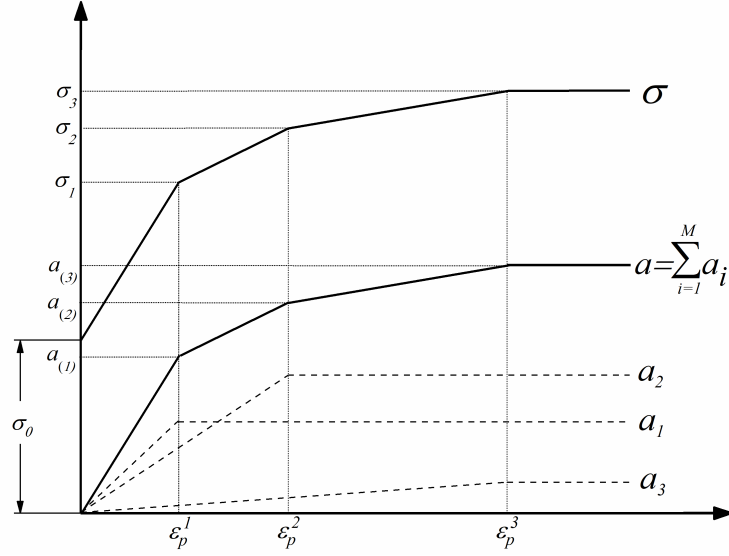


**Figure 3.3.** Superposition of components of backstress

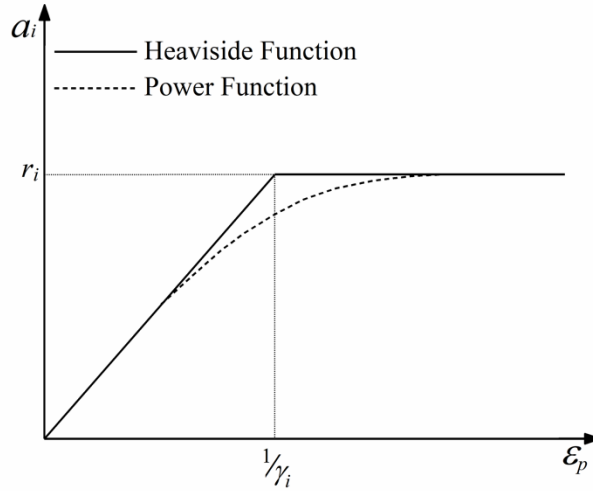
A threshold is defined for each component of backstress to cause full activation of dynamic recovery term. In the O-W Model I (equation(3.19a)) and Model II (equation (3.19b)) a Heaviside function and a power function was employed as the concept of threshold:

$$d\bar{\mathbf{a}}^i = \gamma^i \left[ \frac{2}{3} r^i d\boldsymbol{\varepsilon}^p - H(f_i) \left\langle d\bar{\boldsymbol{\varepsilon}}^p \cdot \frac{\bar{\mathbf{a}}^i}{|\bar{\mathbf{a}}^i|} \right\rangle \bar{\mathbf{a}}^i \right] \quad (3.19a)$$

$$d\mathbf{a}^i = \gamma^i \left[ \frac{2}{3} r^i d\boldsymbol{\varepsilon}^p - \left( \frac{|\mathbf{a}^i|}{r^i} \right)^{m^i} \left\langle d\boldsymbol{\varepsilon}^p \cdot \frac{\mathbf{a}^i}{|\mathbf{a}^i|} \right\rangle \mathbf{a}^i \right] \quad (3.19b)$$

The backstress  $\mathbf{a}^i$  cannot increase beyond the surface  $f^i = 0$  in Model I. This surface is similar to the yield surface of perfectly plastic materials and is defined to be a hypersphere of radius  $r^i$  in the space of  $\mathbf{a}^i$  as  $f^i = \mathbf{a}^{i2} - r^{i2} = 0$ . Backstress for the  $i^{\text{th}}$  component ( $i=1, 2, \dots, M$ ) is defined as  $a^i = \sqrt{\left(\frac{3}{2} \mathbf{a}^i \cdot \mathbf{a}^i\right)}$ . Based on the Model I (equation (3.19a)), each decomposed backstress is either within or acts on the yield surface. If the backstress is less than  $r^i$ , the O-W model changes to the Prager's model and fails to predict ratcheting. When backstress  $\bar{\mathbf{a}}^i$  approaches its limit, the first and second terms of the Model I cancel out each other, resulting in closed stress-strain hysteresis loops and no ratcheting progress after a few stress cycles. Unlike the

Model I, the threshold function never becomes zero in the Model II (equation (3.19b)). In other words, even if backstress does not reach  $r^i$ , the entire power function in Model II acts as a non-zero value, preventing the model to reduce to the Prager's model. Figure 3.4 shows the impact of activation function for variation of backstress,  $a^i$ , at the transient stage.



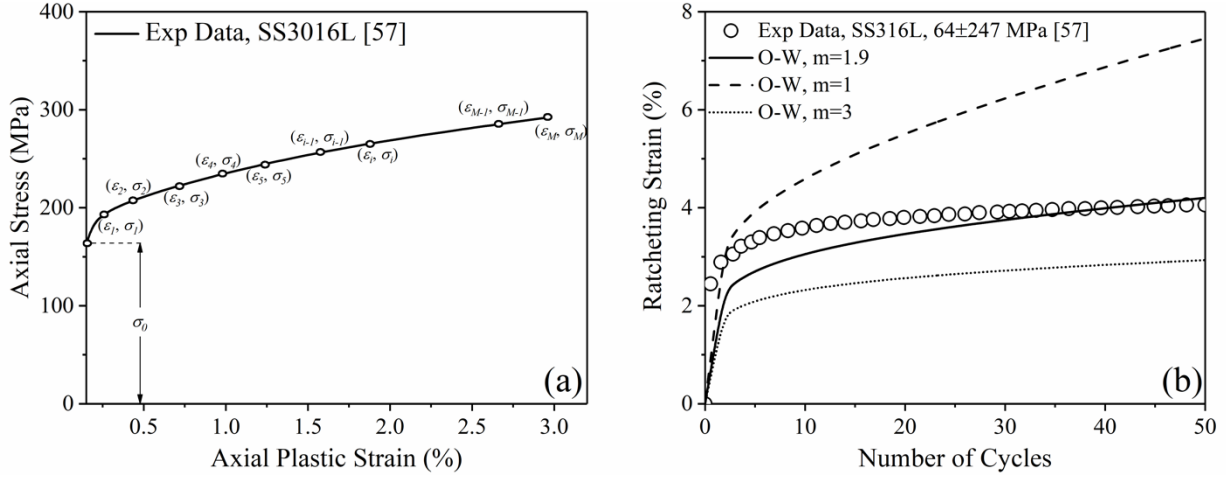
**Figure 3.4.** Backstress at different activation functions

Figure 3.5 along with equation (3.20) describes how material constants  $\gamma^i$  and  $r^i$  are determined through increments taken from the uniaxial stress-strain curve (see Figure 3.5a).

$$\gamma^i = \frac{1}{\epsilon p^{(i)}} \quad (3.20a)$$

$$r^i = \left( \frac{\sigma^{(i)} - \sigma^{(i-1)}}{\epsilon p^{(i)} - \epsilon p^{(i-1)}} - \frac{\sigma^{(i+1)} - \sigma^{(i)}}{\epsilon p^{(i+1)} - \epsilon p^{(i)}} \right) \quad (3.20b)$$

The exponent  $m^i$  in the Model II is determined through regression of ratcheting data as schematically presented in Figure 3.5b. In this figure, a larger value of exponent  $m^i$  promotes ratcheting rate decays and when  $m^i$  becomes small enough, the dynamic recovery term drops to zero and the model reduces to the Prager's model to control rate and magnitude of plastic strain accumulation over uniaxial stress cycles.



**Figure 3.5.** (a) Increments taken over uniaxial cyclic stress–strain to determine constants  $\gamma^i$  and  $r^i$ , and (b) exponent  $m$  in the O-W model (I will generate for SS316L later)

### 3.1.3.2. Kinematic hardening rule of Ahmadzadeh-Varvani (A-V)

Ahmadzadeh-Varvani (A-V) model [30] was developed on the basis of Armstrong-Fredrick (A-F) kinematic hardening rule to control the evolution of backstress increments over the loading process through adapting an internal variable,  $\mathbf{b}$ , into the dynamic recovery term. The dynamic recovery term in the A-V model includes term  $(\mathbf{a} - \delta\mathbf{b})$  to enable evolution of yield surface on the deviatoric stress space to evaluate ratcheting strain with a gradual decreasing rate. The difference of backstress  $\mathbf{a}$  and internal variable  $\mathbf{b}$  controlled yield stress evolution and calibrated its motion over the loading process. The framework of the hardening rule consists of fewer coefficients simplifying the framework to assess ratcheting with less computation/CPU time. The general form of the A-V model is expressed as:

$$d\mathbf{a} = C d\boldsymbol{\varepsilon}^p - \gamma_1(\mathbf{a} - \delta\mathbf{b})d\boldsymbol{\varepsilon}^p \quad (3.21a)$$

$$d\mathbf{b} = \gamma_2(\mathbf{a} - \mathbf{b})d\boldsymbol{\varepsilon}^p \quad (3.21b)$$

coefficients  $C$  and  $\gamma_1$  in equation (3.21a) are determined from uniaxial stress-strain hysteresis loops. Both coefficients  $\gamma_2$  and  $\delta$  were defined to be material dependent [64]. Term  $\delta$  is then defined as a function of backstress through  $(|\mathbf{a}|/k)^m$ , where constant  $k = C/\gamma_1$  and exponent  $m$  are material constants. Coefficient  $\delta$  prevents the dynamic recovery term to fall below zero as

backstress and internal variable  $\mathbf{b}$  are subtracted as  $(\mathbf{a} - \delta\mathbf{b})$ . While coefficients  $C$  and  $\gamma_1$  are to control size and shape of hysteresis loops (Figure 3.6a),  $\gamma_2$  controls ratcheting strain rate and its decay over stage II (Figure 3.7). For smaller values of  $\gamma_1 \rightarrow 0$ , the A-V model reduces to the Prager's model and as  $\delta$  approaches to unity, it is simplified to the Bower's model. Accurate choice of these coefficients ensures the consistency condition in the governing of the constitutive model, resulting in uniform non-closed hysteresis loops generated over asymmetric stress cycles. Figure 3.6a presents coefficients  $C$  and  $\gamma_1$  at which the consistency condition is satisfied. In Figure 3.6b with  $C = 88$  GPa and  $\gamma_1 = 1000$  the generated hysteresis loops lacked a consistency condition while choice of  $C = 185$  GPa and  $\gamma_1 = 1500$  (Figure 3.6c) enabled the model to construct consistent and uniform open hysteresis loops. Larger values of coefficient  $\gamma_2$  increase the internal variable  $\mathbf{b}$  in magnitude resulting in a drop in term  $(\mathbf{a} - \delta\mathbf{b})$  and eventually closed hysteresis loops similar to those predicted by the Prager model. Smaller values of  $\gamma_2$  however alleviate the effect of  $\mathbf{b}$  and result in dynamic recovery term analogous to the A-F model.

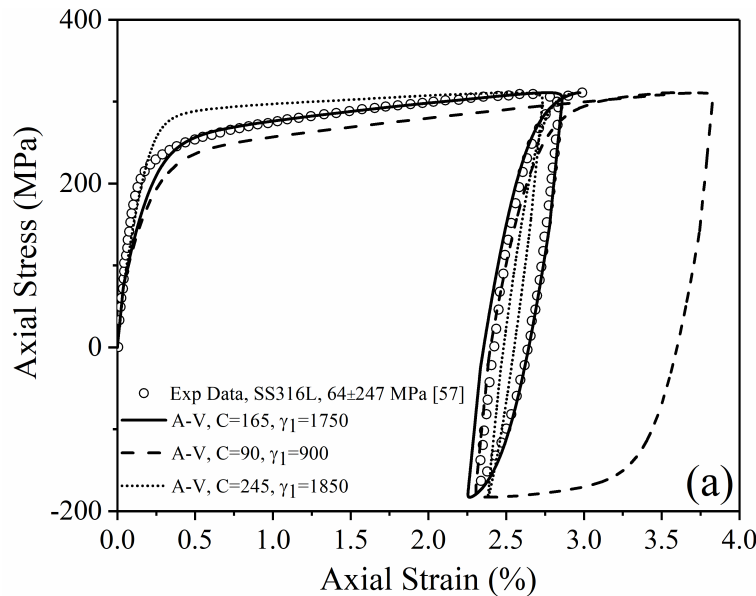


**Figure 3.6.** Schematic presentation of the experimental and predicted hysteresis loops based on the A-V model: (a) coefficients  $C$  and  $\gamma_1$  through cyclic stress-strain loops, and (b and c) variation of coefficients  $C$  and  $\gamma_1$  to achieve consistency condition

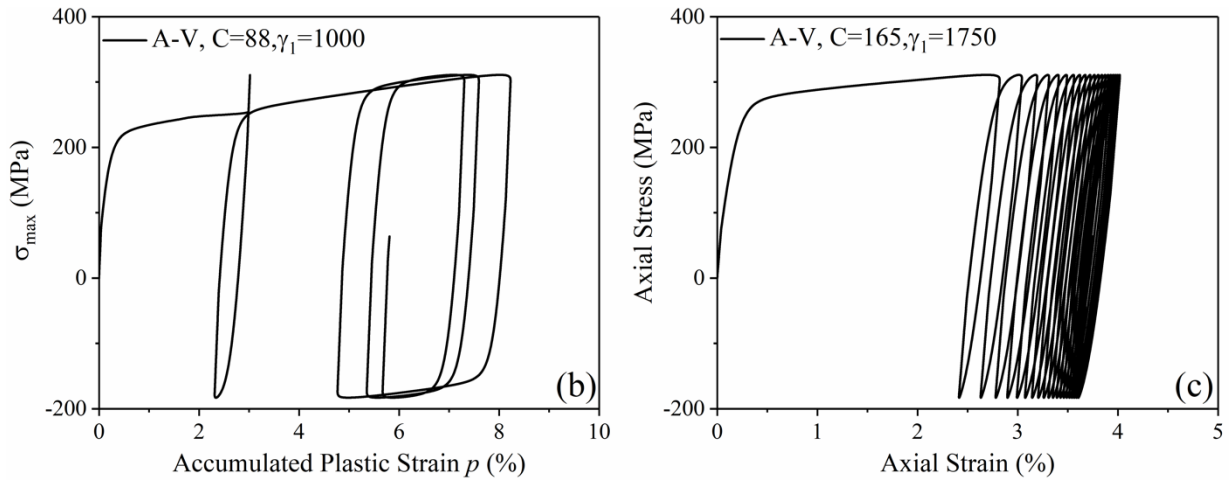


**Figure 3.6.** Continued.

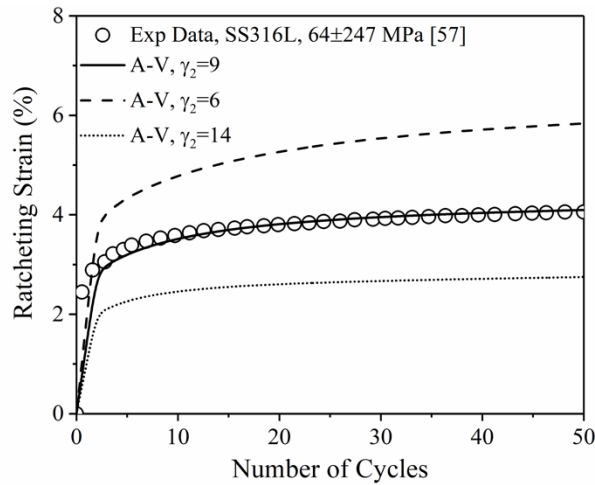


**Figure 3.7.** determination of coefficient  $\gamma_2$  through best-fit curve of ratcheting strain data

### 3.2. Visco-plastic flow rule

Plastic deformation in some engineering alloys is affected by the rate of loading even at room temperature. The rate of applied stress noticeably influences ratcheting response of these materials over asymmetric stress cycles. Stainless steel alloys are categorized within visco-plastic materials. The present study employs several steel alloys to examine ratcheting response at various stress rates, temperatures and holding times. The visco-plastic flow rule enables the constitutive model to relate plastic strain to applied stress at every instant as oppose to relate them

incrementally. Through plastic flow rule (equation (3.5a)) increments of deviatoric stress are associated to plastic strains regardless of the current state of stress. However, in visco-plastic flow rule (equation (3.5b)), at various applied stress rates and backstresses, corresponding ratcheting strains are affected at every instant of time. While in the former equation,  $d\mathbf{s}$  is defined regardless of stress rate, in the latter equation, term  $(\mathbf{s} - \mathbf{a})$  varies as the stress rate changes. Depending on whether material deforms time-dependently or independently, plasticity and visco-plasticity flow rules are adapted. Figure 3.8 presents ratcheting response of Z2CND18.12N stainless steel at room temperature through use of plastic and visco-plastic flow rules. This figure shows the substantial impact of flow rules on the ratcheting response of time-dependent materials.

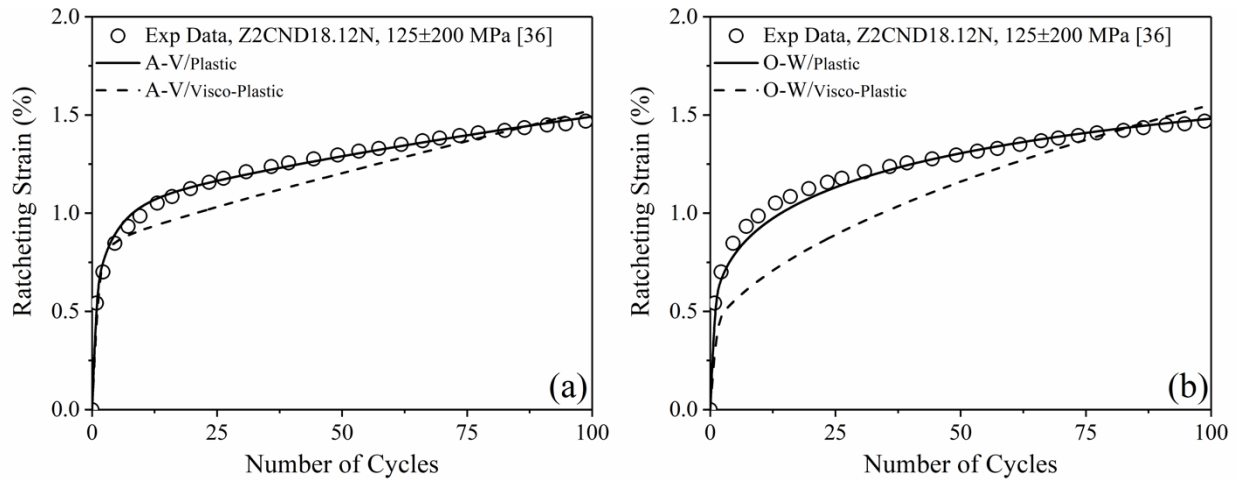


**Figure 3.8.** Ratcheting prediction based on plasticity and visco-plasticity constitutive theory on (a) the A-V model and (b) the O-W model.

### 3.2.1. The influence of operating temperature

To account for the influence of various operating temperatures on ratcheting assessment of stainless steel samples, dynamic strain aging function  $\psi(p, T)$  developed earlier by Kang and coworkers [65] was introduced into the dynamic recovery terms of the O-W and A-V hardening rules. Stainless steel 304 samples have shown that at elevated temperature range of 300-600°C the time-dependency of the material is faded. Dynamic strain aging function enabled to account for the extent of time-dependency over various temperatures and was exponentially related to plastic strain accumulation  $p$  as:

$$\psi(p, T) = \psi_\infty(T) + [1 - \psi_\infty(T)]e^{-\lambda p} \quad (3.22)$$

where  $\psi_\infty(T)$  and  $\lambda$  are temperature dependent and are obtained from experimental stress-strain data at elevated temperatures. Function  $\psi$  is excluded from hardening rules at ambient temperature and temperatures at which material deformation is rate-dependent.

Dynamic strain aging effect was introduced into the O-W and A-V models through function  $\psi$  to account for the influence of the temperature range at which ratcheting of stainless steel samples paused rate-dependency response. Inclusion of the dynamic strain aging phenomenon into the dynamic recovery of the O-W model and the A-V model restructured these models through equations (3.23) and (3.24) respectively as:

$$d\bar{\mathbf{a}}^i = \gamma^i \left[ \frac{2}{3} r^i d\boldsymbol{\varepsilon}^p - \psi(p, T) H(f_i) \langle d\bar{\boldsymbol{\varepsilon}}^p \cdot \frac{\bar{\mathbf{a}}^i}{|\bar{\mathbf{a}}^i|} \rangle \bar{\mathbf{a}}^i \right] \quad (3.23a)$$

$$d\mathbf{a}^i = \gamma^i \left[ \frac{2}{3} r^i d\boldsymbol{\varepsilon}^p - \psi(p, T) \left( \frac{|\mathbf{a}^i|}{r^i} \right)^{m^i} \langle d\boldsymbol{\varepsilon}^p \cdot \frac{\mathbf{a}^i}{|\mathbf{a}^i|} \rangle \mathbf{a}^i \right] \quad (3.23b)$$

$$d\mathbf{a} = C d\boldsymbol{\varepsilon}^p - \psi(p, T) \gamma_1 (\mathbf{a} - \delta \mathbf{b}) dp \quad (3.24a)$$

$$d\mathbf{b} = \gamma_2 (\mathbf{a} - \mathbf{b}) dp \quad (3.24b)$$

### 3.2.2. The influence of holding time

In the presence of loading cycles with holding time at peak/valley, the static recovery effect was introduced to accommodate for larger ratcheting strains. To account for this effect, Kang et al. [60] introduced an exponential function,  $\chi(a)^{e^{-1}} \mathbf{a}$ , holding backstress component. Infusion of this function into the dynamic recovery terms in the O-W and A-V models converted these models to equations (3.25) and (3.26), respectively:

$$d\bar{\mathbf{a}}^i = \gamma^i \left[ \frac{2}{3} r^i d\boldsymbol{\varepsilon}^p - \left\{ \left( \chi^i(a^i)^{e^{-1}} \right) + H(f_i) \langle d\bar{\boldsymbol{\varepsilon}}^p \cdot \frac{\bar{\mathbf{a}}^i}{|\bar{\mathbf{a}}^i|} \rangle \right\} \bar{\mathbf{a}}^i \right] \quad (3.25a)$$

$$d\mathbf{a}^i = \gamma^i \left[ \frac{2}{3} r^i d\boldsymbol{\varepsilon}^p - \left\{ \left( \chi^i (a^i)^{\varrho^i - 1} \right) + \left( \frac{|\mathbf{a}^i|}{r^i} \right)^{m^i} \left\langle d\bar{\boldsymbol{\varepsilon}}^p \cdot \frac{\bar{\mathbf{a}}^i}{|\bar{\mathbf{a}}^i|} \right\rangle \right\} \mathbf{a}^i \right] \quad (3.25b)$$

and

$$d\mathbf{a} = C d\boldsymbol{\varepsilon}^p - \{ \chi (a)^{\varrho - 1} + \gamma_1 dp \} (\mathbf{a} - \delta \mathbf{b}) \quad (3.26a)$$

$$d\mathbf{b} = \gamma_2 (\mathbf{a} - \mathbf{b}) dp \quad (3.26b)$$

coefficient  $\chi$  and exponent  $\varrho$  in these functions are determined from cyclic stress-strain curves with holding time. This function controls the evolution of yield surface by enhancing the influence of dynamic recovery term in the kinematic hardening rules and addressing the excess of ratcheting strains.

### 3.3. Algorithm of ratcheting assessment

To assess visco-plastic ratcheting response of materials subjected to uniaxial asymmetric cyclic loading based on the framework of O-W and A-V, plasticity constitutive equations were employed. The procedure of analysis was programmed using MATLAB (R2019a) software [66]. The algorithm of visco-plastic ratcheting assessment for both hardening rules with plastic and visco-plastic flow rules is presented in Figure 3.9. Details of MATLAB code and analysis procedure are presented in Appendix A.

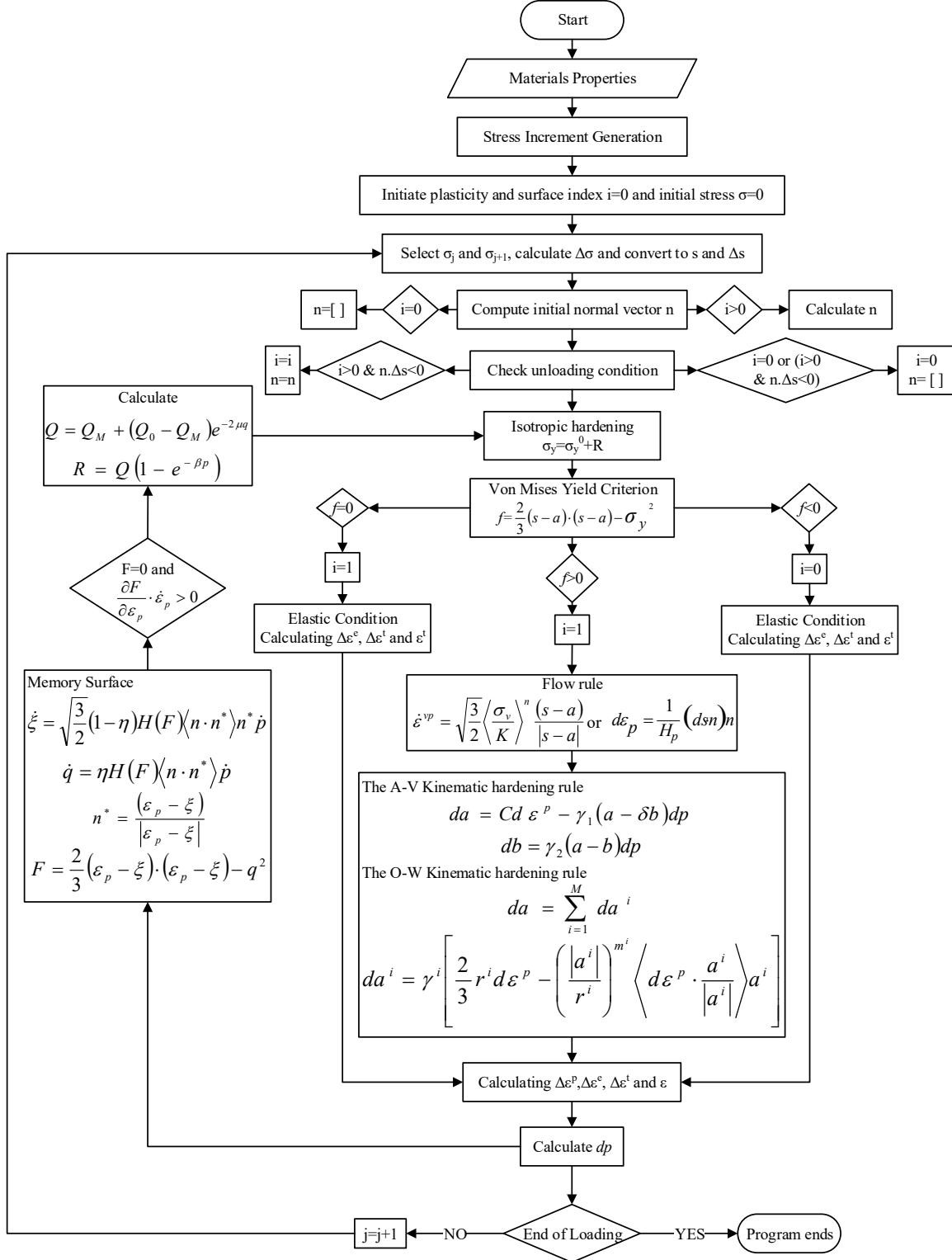


Figure 3.9. Flowchart of the algorithm developed on the basis of visco-plastic framework of O-W and A-V

### 3.4. Summary

There are various factors to consider when developing frameworks of cyclic plasticity and its constitutive equations. To accommodate for ratcheting evaluation of rate-dependent steel alloys, the frameworks developed on the basis of the O-W and A-V models were employed involving isotropic hardening rules. This rigorously improved the framework over the initial step of ratcheting. The use of visco-plastic flow rule further enabled the O-W and A-V hardening rules to assess time-dependent ratcheting response of steel alloys and to manifest the impact of stress rate, operating temperature and holding time. At elevated temperature, SS304 steel samples exhibited negative rate sensitivity, resulting in the fading of their rate-dependency effect. This influence was described through dynamic strain aging function. The dynamic strain aging was introduced into the dynamic recovery term of the frameworks by means of an exponential function, responsible for decaying ratcheting strain as the number cycles increased. This function was defined to address the range of temperature (300-600°C) in 304 steel samples eliminating the rate-dependency of samples. Holding-time was found to noticeably influences visco-plastic ratcheting values. Holding time at peak/valley of stress cycles created a phenomenon known as ratcheting-creep, resulting in elevation of ratcheting magnitude. This surge was introduced into dynamic recovery terms of the hardening rules by the infusion of an exponential function to account for the static recovery effect. The developed algorithm enabled a rather comprehensive assessment of ratcheting through use of the O-W and A-V models to evaluate time-dependent ratcheting response of stainless steel samples subjected to various uniaxial stress rates at different temperatures and holding times.

## **CHAPTER FOUR**

# **RESULTS OF RATCHETING EVALUATION AND DISCUSSION**

Ratcheting response of steel alloys was evaluated through use of the Ohno-Wang (O-W) and Ahmadzadeh-Varvani (A-V) hardening rules under various loading conditions. The hardening rules with different dynamic recovery terms, variables and influential parameters enabled in assessment of time-dependent ratcheting responses of various steel alloys through the involvement of different isotropic hardening rules and a unified visco-plastic flow rule description. The frameworks of these models were developed to predict ratcheting at various stress levels, loading steps and sequences, and stress rates. The influence of operating temperatures and holding times were further discussed.

### **4.1. Materials and Testing Conditions**

Visco-plastic ratcheting responses of steel alloys tested under single- and multi-step loading conditions at room and elevated temperatures were studied as experimental data were taken from references [36,38,57,67–74]. Figure 4.1 presents monotonic stress-strain curves of steel alloys of 304 [38,68–72], Z2CND18.12N [36], U71Mn [73,74], 316 [57,67] examined in this chapter. In this figure an increase in strain rate imposed no change in elastic and plastic moduli of stress-strain curves. Table 4.1 tabulates tensile properties of steel alloys defined from stress-strain curves in Figure 4.1.

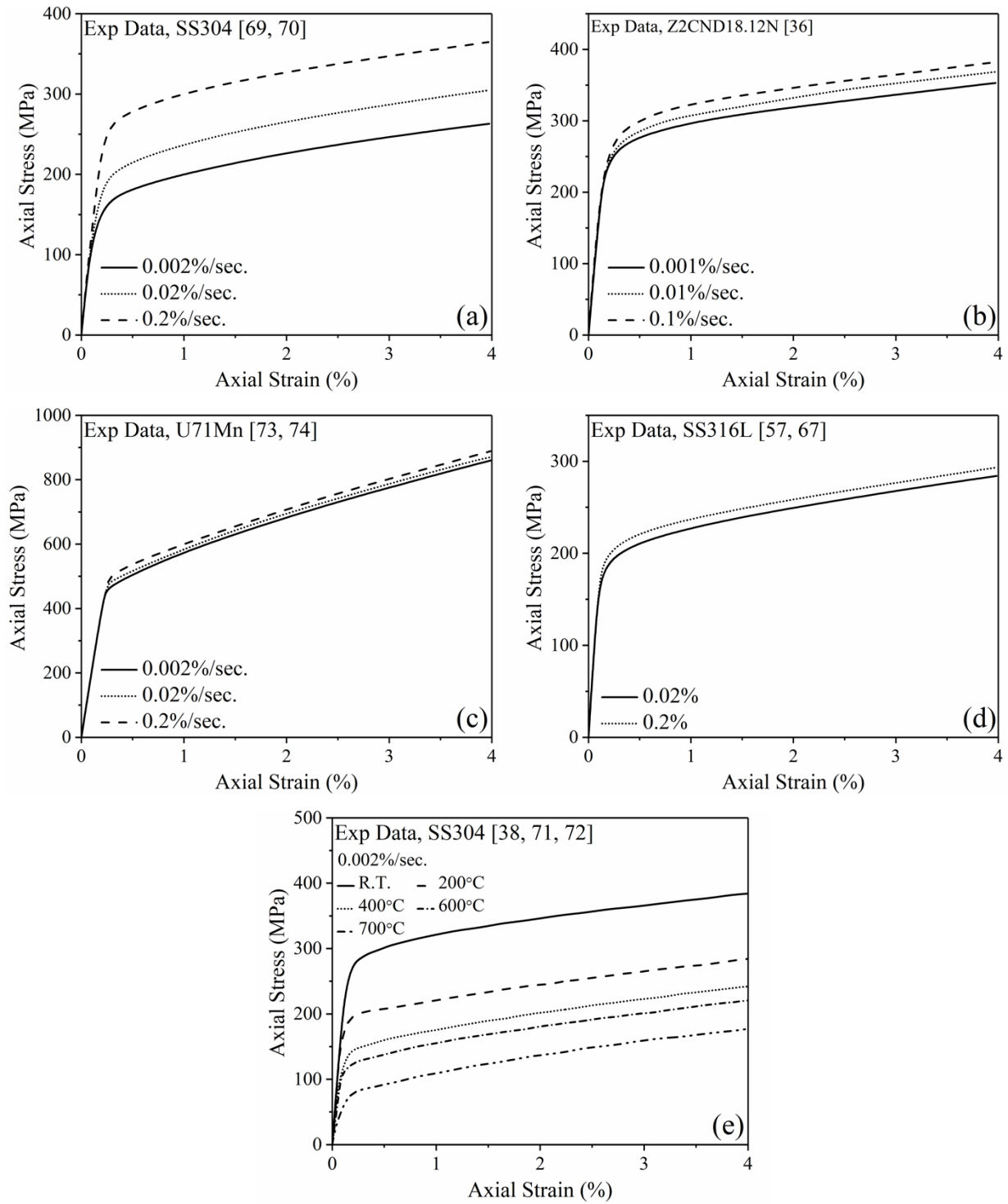


**Figure 4.1.** Stress-strain curves of studied materials

**Table 4.1.** Mechanical properties of studied materials

Material	$\sigma_y$ (MPa)	$E$ (GPa)	$K'$ (MPa)	$n'$
SS304 [69,70]	270	209	560	0.12
Z2CND18.12N [36]	265	165	590	0.094
U71Mn [73,74]	500	204	1854	0.28
SS316L [57,67]	200	176	430	0.13
SS304 [38,71,72]	290	211	570	0.12

## 4.2. Coupled isotropic-kinematic hardening rules

Ratcheting response of materials by means of kinematic hardening rules of the Ohno-Wang (O-W) and Ahmadzadeh-Varvani (A-V) coupled with three distinct isotropic hardening rules of Lee and Zavrel (Iso-LZ), Chaboche (Iso-C), and Kang (Iso-K) is assessed. While kinematic hardening rule is responsible for transition of the yield surface, isotropic hardening rule deals with changes in the size of the yield surface. The inclusion of isotropic hardening rules in the framework of these models improves ratcheting predictions within stage I, resulting in more realistic predictions in stages II and III when material becomes stabilized in terms of softening/hardening. The combined isotropic-kinematic frameworks of the O-W and A-V models are employed to assess ratcheting data and stress-strain hysteresis loops for various samples of SS304.

### 4.2.1. Testing conditions and models coefficients

To evaluate the capabilities of isotropic-kinematic hardening rules, measured ratcheting strains of 304 stainless steel samples subjected to asymmetric stress cycles using MTS servo-hydraulic machines were taken from references [68–70].

Table 4.2 lists loading conditions for SS304 samples tested at room temperature. Table 4.3 lists coefficients of the A-V and O-W hardening rules employed to assess the ratcheting response

of 304 stainless steel specimens. Thorough explanation on how to determine coefficients is detailed in Chapter 3.

**Table 4.2.** Testing conditions for SS304 steel samples tested at room temperature

Material	Test	$\sigma_m \pm \sigma_a$ (MPa)
SS304 [68]	S1	150 ± 200
SS304 [69,70]	S2	10 ± 260
	S3	65 ± 260
	S4	65 ± 325

**Table 4.3.** Coefficients of the A-V and O-W isotropic-kinematic hardening rules

Materials	Coefficients
SS304 [68]	$C$ (GPa) = 40, $\gamma_1 = 180, \gamma_2 = 35$ $Q$ (MPa) = 30, $\beta = 125, Q_0$ (MPa) = 10, $\mu = 150, \eta = 0.042, \zeta = 10$ $A_1 = 10, A_2 = 20, A_3$ (MPa) = 300 $\gamma_{1-5} = 1400, 500, 250, 90, 20$ $r_{1-5} = 58, 61, 47, 34, 60$ (MPa) $m_{1,2} = 1.1, m_{3-5} = 8$
SS304 [69,70]	$C$ (GPa) = 35, $\gamma_1 = 200, \gamma_2 = 20$ $Q$ (MPa) = 100, $\beta = 100, Q_0$ (MPa) = 30, $\mu = 125, \eta = 0.04, \zeta = 5$ $A_1 = 30, A_2 = 70, A_3$ (MPa) = 150 $\gamma_{1-8} = 3341, 1833, 765.6, 210.4, 69.92, 35.91, 23.04, 13$ $r_{1-8} = 37.85, 33.16, 18.89, 10.92, 8.38, 6.74, 12.41, 70.33$ (MPa) $m_i = 0.1$

#### 4.2.2. Ratcheting evaluation through isotropic-kinematic hardening rules

The predicted ratcheting curves for a 304 steel sample by means of the A-V and O-W kinematic hardening rules are compared with those of experimentally obtained at 150±200MPa in Figure 4.2. In this figure, the predicted ratcheting curve by means of the O-W model positioned above experimental data, while the curve predicted by the A-V model fell below measured values. This discrepancy in the two hardening rules is attributed to the use of the initial yield stress,  $\sigma_y^0$ , in the O-W model, while the A-V hardening rule is governed through the saturated yield surface with  $\sigma_y$  magnitude. For the former model, this postulation resulted in a good agreement over the initial

few cycles and an overprediction of ratcheting beyond the first 10 cycles before hardening occurred. However, the latter model predicted lower ratcheting values up until the first 60-70 cycles and agreed well with experimental as the number of cycles increased.

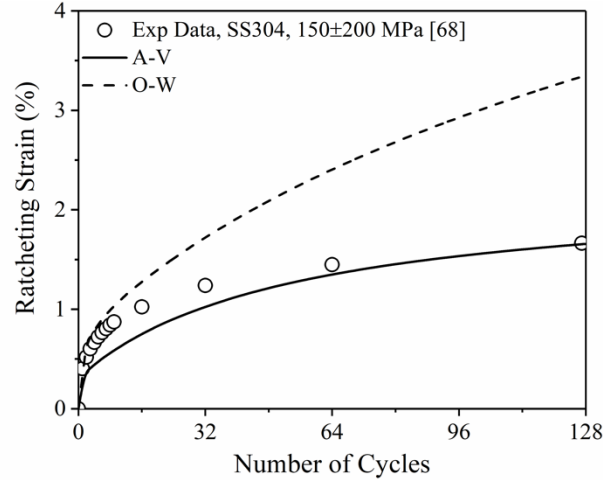


**Figure 4.2.** Uniaxial ratcheting prediction by means of the O-W and the A-V kinematic hardening rule.

The inclusion of isotropic hardening rules in the framework of the O-W and A-V models influenced the predicted ratcheting response of 304 steel samples. Figure 4.3 presents the result of predicted ratcheting strain versus number of asymmetric stress cycles of  $150\pm 200$ MPa for steel sample S1 by means of the A-V and O-W models. The solid lines in this figure present ratcheting prediction through kinematic hardening rules and broken lines are predicted results when models were coupled with three isotropic hardening rules of Iso-LZ, Iso-C, and Iso-K. In the absence of isotropic models, the A-V model underpredicted the ratcheting results as compared to the coupled framework in Figure 4.3a. While adherence of isotropic models to the O-W model noticeably shifted the predicted ratcheting curves below experimental data in Figure 4.3b. This underprediction has been consistently reported by Kang et al. [16], Abdel-Karim [75], and more recently by Chen et al. [76]. This discrepancy between the two frameworks of O-W and A-V is attributed to the definition of initial  $\sigma_y^0$  and actual yield stress  $\sigma_y$ . The initial yield stress based on the O-W kinematic hardening rule is a small magnitude resulting in an overprediction of ratcheting values. As the O-W is coupled with isotropic hardening rules, yield stress magnitude increases

over stress cycles through equation (3.8). This noticeably decreases the predicted ratcheting curves. By contrast the A-V kinematic rule merely translated constant yield surfaces of  $\sigma_y$  magnitude over the loading process, resulting in predicted ratcheting results falling below experimental data in Figure 4.3a. Inclusion of the isotropic models to the A-V framework enabled the expansion of yield surfaces based on isotropic hardening models within  $\sigma_y^0$  and  $\sigma_y$  over the first 100-150 stress cycles. Imposing initial yield stress  $\sigma_y^0$  at the first cycle and its gradual increase over stress cycles up until 100-150 cycles, at which the size of yield surface was saturated, resulted in an increasing trend of predicted ratcheting values. The inclusion of isotropic models in the O-W and A-V frameworks resulted in closer agreements of the predicted ratcheting data to experimental values, particularly where the Iso-C model adhered to the kinematic hardening rules.

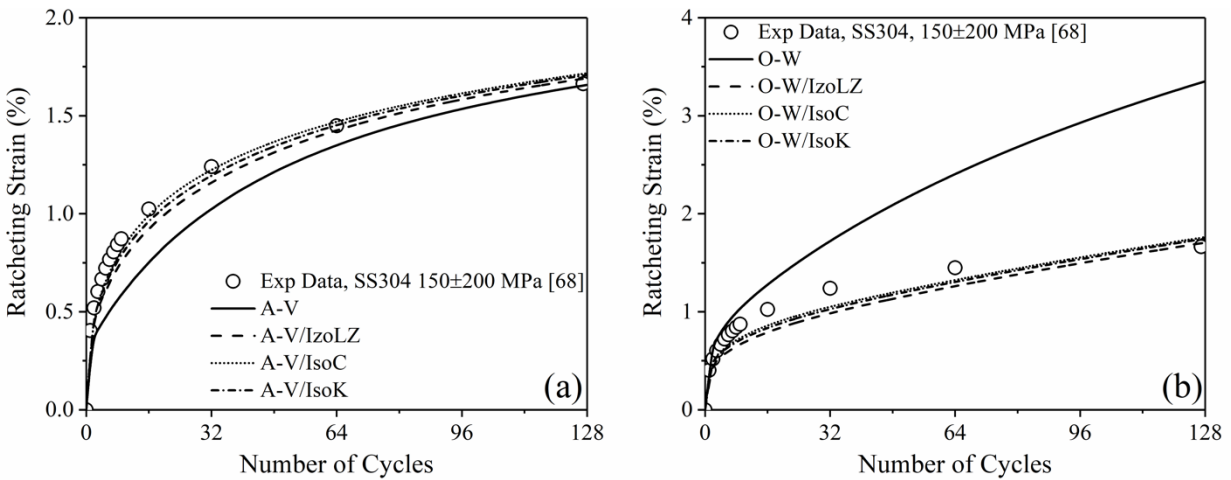


**Figure 4.3.** Predicted ratcheting curves based on (a) the A-V framework, and (b) the O-W framework as compared with experimental data.

Inclusion of isotropic hardening models influenced the magnitude of plastic strain, pushing forward the stress-strain hysteresis loops and changing their widths. As presented in Figure 4.4b and Figure 4.4c, in the absence of isotropic models, the A-V and O-W kinematic hardening rules consisted of hysteresis loops with unchanged widths over loading cycles. On the contrary, the predicted hysteresis loops based on the isotropic-kinematic frameworks showed gradual drops in the widths over loading cycles. The decline in the width of hysteresis loops corresponds to hardening phenomenon within the first hundred cycles. The first hysteresis loop is highly affected

by the magnitude of yield stress. It is evident that over the loading cycles, predicted ratcheting curves by means of combined isotropic-kinematic hardening rules are in greater agreement with experimental data, particularly through the involvement of the Iso-C model. The Iso-LZ model however showed a better agreement at the 128<sup>th</sup> cycle based on the O-W framework. More consistent agreements between experimentally measured loops and those predicted were achieved by means of the A-V model coupled with the Iso-C model. The evolution of yield surface and consequently hysteresis loops are controlled by isotropic parameters such as  $Q$  and  $\beta$  in equation (3.9). The former is associated with the width of the hysteresis loops. Ultimately, the higher the  $Q$ , the wider the loops. The latter is attributed to the rate of change in the width. The smaller the exponent  $\beta$ , the longer it takes for loops to stabilize.

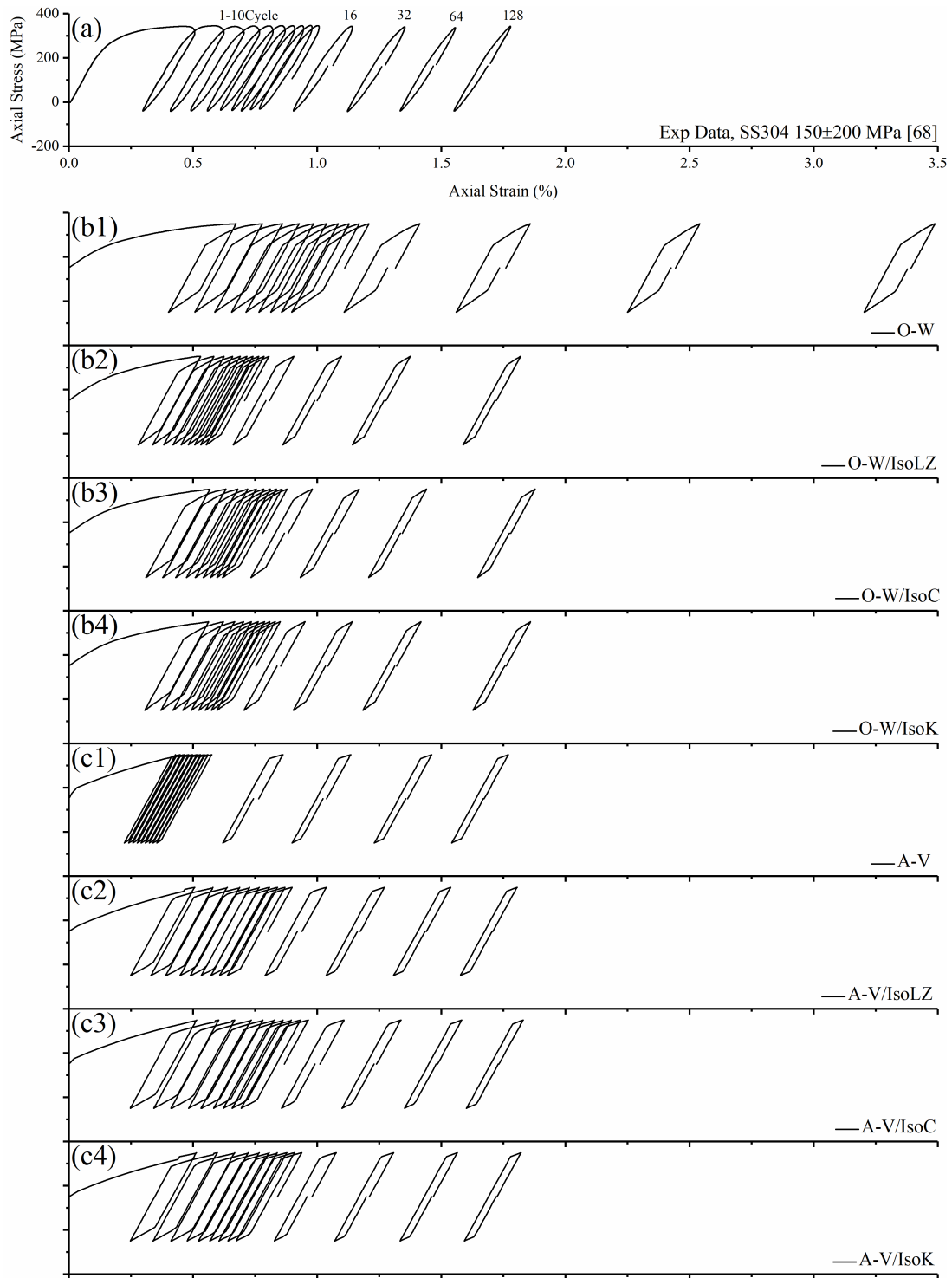


**Figure 4.4.** Hysteresis loops generated over ratcheting progress based on the O-W and A-V hardening rules (a) experimental data, (b1-b4) the O-W kinematic model, and (c1-c4) the A-V kinematic model, without and with inclusion of Iso-LZ, Iso-C and Iso-K models.

The difference in ratcheting responses of the O-W and A-V frameworks is attributed to the employed yield limit/stress in these models. Involvement of the isotropic models facilitated both models to include yield surfaces from an initial to a saturated level over stress cycles. Figure 4.5a presents the yield surface evolution through yield stress values for the 304 steel sample tested at  $150\pm 200$ MPa. Figure 4.5b and Figure 4.5c highlight the predicted hysteresis loops at the 16<sup>th</sup> cycle based on the A-V and O-W frameworks. The change in hysteresis loops shows the influence of yield surface evolution on the ratcheting response of the steel sample. The onset of yielding in the O-W model promoted ratcheting strain and resulted in a wider hysteresis loop in Figure 4.5c. Over the expansion of the yield surface through an inclusion of the isotropic model, the O-W framework predicted a smaller ratcheting strain and a narrower loop comparable to the experimentally obtained loop. The saturated yield surface in the A-V model slightly underpredicted the ratcheting strain and once the isotropic model was implemented, the A-V framework closely agreed with the measured ratcheting strain and the experimentally obtained hysteresis loop (see Figure 4.5b).

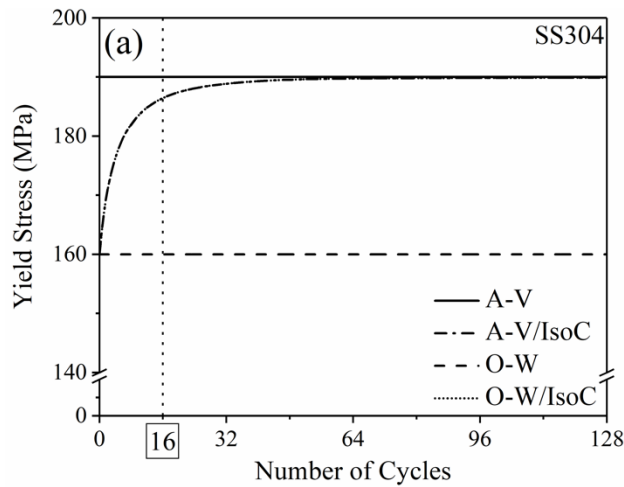


**Figure 4.5.** (a) Evolution of yield stress in the O-W and A-V hardening rules, (b) the predicted hysteresis loop for the 16<sup>th</sup> cycle based on the A-V model, and (c) the predicted hysteresis loop for the 16<sup>th</sup> cycle based on the O-W model.

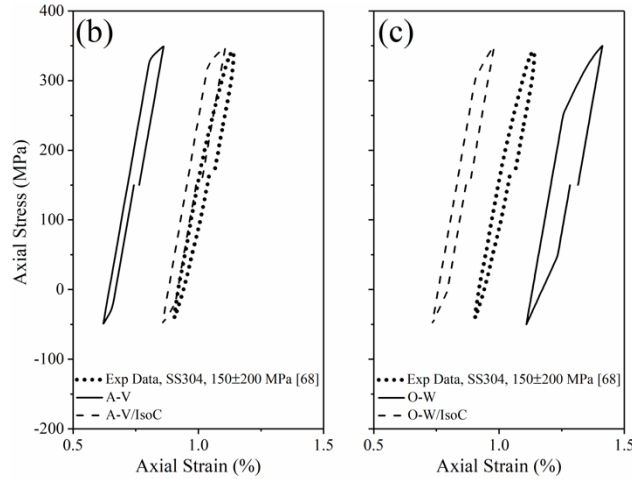


**Figure 4.5.** Continued.

The influence of stress level on ratcheting response of SS304 steel samples S2, S3, and S4 are presented in Figure 4.6. The predicted ratcheting curves based on the A-V and O-W frameworks presented in Figure 4.6a and Figure 4.6b show a better agreement of coupled A-V/Iso-C model for greater mean stress while the stress amplitude remained unchanged. Over the first 70 cycles, the predicted curves based on the A-V framework in Figure 4.6a show a closer agreement to experimental data than those predicted through the O-W framework. Figure 4.6b and Figure 4.6c however show that at the constant mean stress of 65MPa, the lower stress amplitude of 260MPa resulted in a better agreement of predicted ratcheting curves as compared with those of measured values.

Ratcheting progress rate, defined as the increment of the ratcheting strain over each cycle ( $\dot{\epsilon}_r = \frac{d\epsilon_r}{dN}$ ), for the same steel sample is evaluated over loading cycles in Figure 4.7. As expected, ratcheting rate decays as the cycles progress. The predicted ratcheting rates by means of the O-W model in the absence and the presence of isotropic model deviated with experimental data in this figure. The O-W model exhibited a slight increase in rate within the first few cycles once coupled with the isotropic model. While based on the A-V framework, the ratcheting rate was initially built up in an agreeable trend with experimental data. As the number of cycles increased, the A-V model in the presence of Iso-C model closely agreed with data experimentally measured over the first 100 cycles.

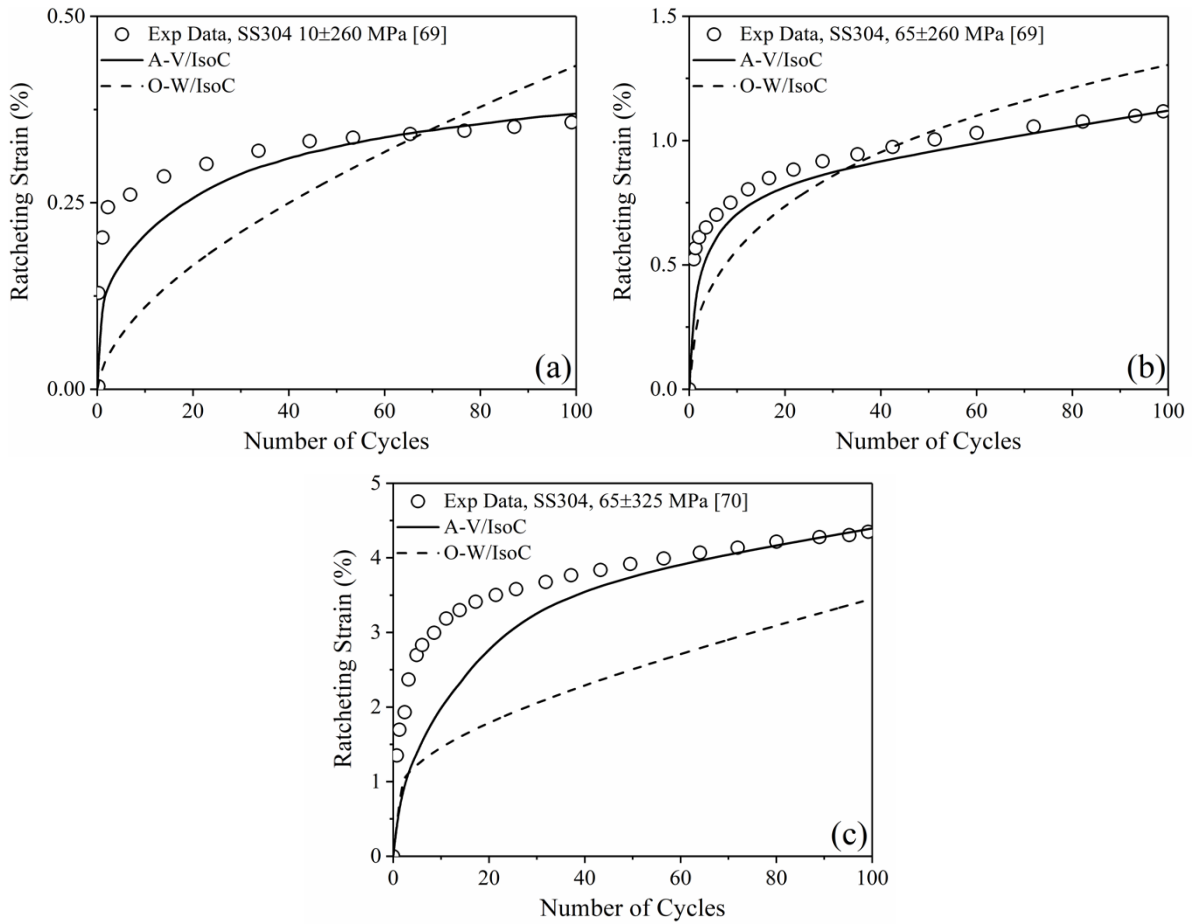


**Figure 4.6.** Predicted ratcheting strains based on the A-V and O-W frameworks for various loading conditions of (a)  $10\pm 260$ MPa, (b)  $65\pm 260$ MPa, (c)  $65\pm 325$ MPa

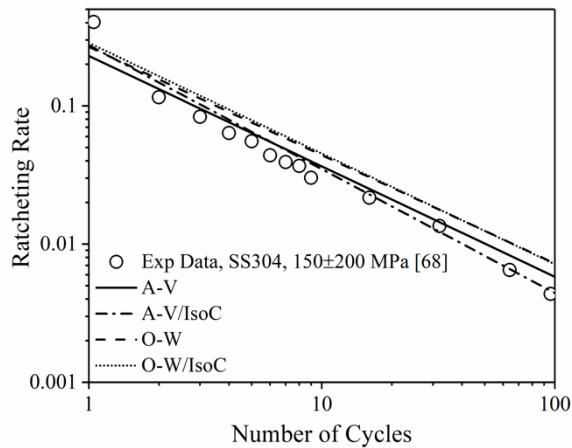


**Figure 4.7.** Experimental ratcheting rate over 100 cycles and those predicted by means of the A-V and O-W hardening rules

### **4.3. Visco-plastic constitutive frameworks**

#### **4.3.1. Stress level and rate on ratcheting response**

To assess visco-plastic ratcheting response of rate-dependent materials at room temperature, hardening rules of Ohno-Wang (O-W) and Ahmadzadeh-Varvani (A-V) were employed along with a unified visco-plastic flow rule to address both transient and steady-state flow under complex loading conditions. The influence of applied stress levels and rates were found noticeable in the ratcheting magnitude and rate for steel samples examined in this section. The frameworks of A-V and O-W were coupled with Chaboche's isotropic hardening model with the memory surface description to emulate the expansion/contraction of yield surfaces. The frameworks were influenced by the visco-plastic description of materials, which enabled models to accurately and realistically assess the ratcheting of materials with rate-dependent responses at room temperature. Hysteresis loops generated through the frameworks were then compared to those obtained experimentally.

##### **4.3.1.1. Testing conditions and hardening rule coefficients**

To examine the capabilities of the A-V and O-W frameworks, ratcheting data of rate-dependant steel samples of Z2CND18.12N [36] and 304 [38], tested at room temperature and under various stress levels and rates, was taken from literature. Ratcheting tests were conducted under single-step uniaxial stress-controlled conditions at ambient temperature. Table 4.4 tabulates the applied stress levels and stress rates of these materials.

Table 4.5 lists coefficients of the O-W and A-V frameworks (equations (3.19) and (3.21)) for Z2CND18.12N austenitic and 304 stainless steels tested at various loading conditions. These coefficients were obtained from regression of stress-strain curves and uniaxial ratcheting data as detailed in references [36,38].

**Table 4.4.** Testing conditions for Z2CND18.12N and SS304 alloys at room temperature

Material	Test	$\sigma_m \pm \sigma_a$ (MPa)	Stress Rate (MPa/sec)
Z2CND18.12N [36]	S5	100 ± 200	100
	S6	125 ± 200	100
	S7	150 ± 200	100
	S8	125 ± 150	100
	S9	125 ± 175	100
	S10	150 ± 150	10
	S11	150 ± 150	100
SS304 [38]	S12	150 ± 150	1000
	S13	78 ± 234	2.6
	S14	78 ± 234	13
	S15	78 ± 234	65

**Table 4.5.** Coefficients for the O-W and A-V frameworks for Z2CND18.12N and SS304 alloys.

Materials	Coefficients
Z2CND18.12N [36]	$C$ (GPa) = 150, $\gamma_1 = 1500$ , $\gamma_2 = 350$ $Q_M = 80$ , $Q_0$ (MPa) = 40, $\beta = 15$ , $\mu = 50$ , $\eta = 0.42$ , $K = 150$ , $n = 7$ $\gamma_{1-8} = 4000, 2000, 1000, 300, 200, 100, 35, 12$ $r_{1-8} = 66, 54, 10, 11, 6, 13, 17, 59$ MPa $m_i = 5.8$
SS304 [38]	$C$ (GPa) = 65, $\gamma_1 = 992$ , $\gamma_2 = 20$ $Q$ (MPa) = 50, $\beta = 12.5$ , $K = 82$ , $n = 15$ $\gamma_{1-8} = 3341, 1833, 756.6, 210.4, 69.92, 35.91, 23.04, 13$ $r_{1-8} = 37.85, 33.16, 18.89, 10.92, 8.38, 6.74, 12.41, 70.33$ MPa $m_i = 1.9$

#### 4.3.1.2. Predicted ratcheting results

Figure 4.8 plots measured ratcheting data versus the predicted curves by means of the O-W and A-V frameworks over loading cycles at various stress levels. In Figure 4.8a, as the mean stress increased from 100→125→150MPa and at constant stress amplitude of 200MPa, the predicted curves through the A-V framework were shifted to higher magnitudes together with experimental data, resulting in a close agreement between them. In this figure, the O-W framework underpredicted ratcheting by nearly 38% as compared to experimental values of sample S7 tested at 150±200MPa load cycles. The ratcheting buildup in Figure 4.8b was found almost identical to measured data and those predicted by the A-V framework as stress amplitude increased from

150→175→200MPa at constant mean stress of 125MPa. The O-W model predicted ratcheting of the steel sample at 125±175MPa loading cycles with a deviation of 40% as compared to experimental data.

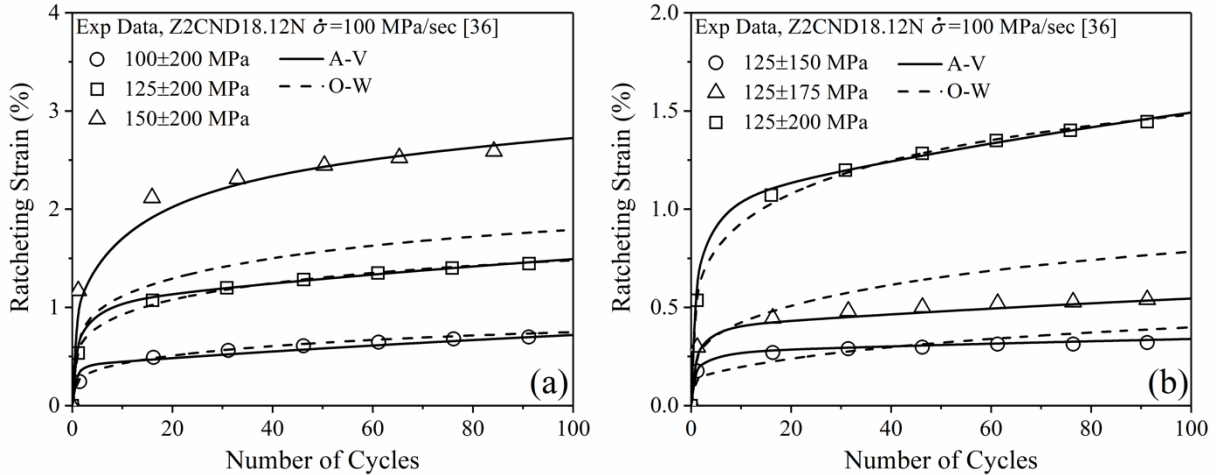


**Figure 4.8.** Experimental and predicted ratcheting curves of Z2CND18.12 N steel by means of visco-plastic frameworks of O-W and A-V for various (a) mean stresses and (b) stress amplitudes

The influence of stress rate on ratcheting response of samples of Z2CND18.12N and SS304 is presented in Figure 4.9. Samples of austenitic steel Z2CND18.12N tested at 150±150MPa in Figure 4.9a showed that as stress rate decreased from 1000→100→10 MPa/sec., ratcheting strains increased in magnitudes. In this figure, ratcheting rate remained nearly constant beyond the 25<sup>th</sup> cycle at stress rates of 10, 100 and 1000 MPa/sec. Figure 4.9b displays samples of SS304 tested at 78±234MPa under three stress rates of 2.6, 13, and 65 MPa/Sec. Similarly, by increasing the stress rate from 2.6→13→65MPa/sec, ratcheting dropped. The constant rate in ratcheting progress coincided with the predicted curves through the A-V model and deviated from the curves predicted by the O-W model.

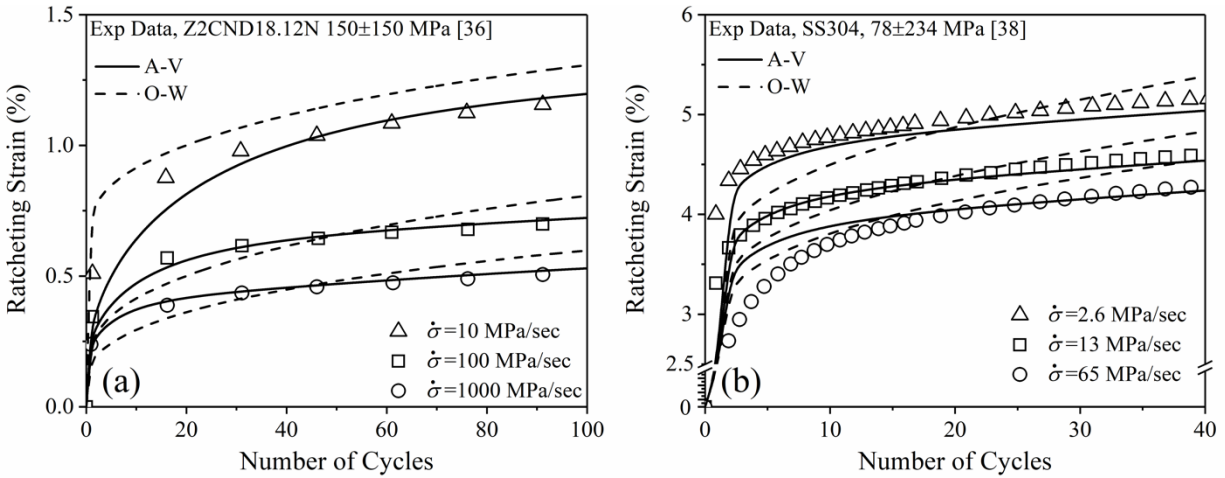


**Figure 4.9.** Experimental and predicted ratcheting curves by means of visco-plastic frameworks of O-W and A-V for various stress rates (a) Z2CND18.12 N steel and (b) SS304

### 4.3.2. Step-loading conditions

The ratcheting response of various steel samples under multi-step loading conditions at room temperature is studied through the use of visco-plastic frameworks of the O-W and A-V hardening rules. The loading sequence has a substantial impact on the ratcheting response over subsequent loading steps and sequences. Chaboche's isotropic hardening model was coupled to the frameworks to realistically track the evolution of yield surface and subsequent softening/hardening occurred as a result of change in stress levels over consecutive steps. Generated hysteresis loops and ratcheting curves were compared to the measured values.

#### 4.3.2.1. Testing conditions and coefficients

Visco-plastic frameworks of A-V and O-W were employed to evaluate the ratcheting response of steel samples of SS304 [38], SS316 L [57,67], and U71Mn [73,74]. Specimens were subjected to various step-loading levels at room temperature. Table 4.6 lists testing conditions and the designated number of cycles over loading steps.

Coefficients of the frameworks were obtained through the best-fit of experimental data [38,57,67,73,74] and are presented in Table 4.7.

**Table 4.6.** Ratcheting tests and stress-steps for SS304, SS316L, U71Mn steel samples tested at room temperature

Materials	Tests	Step I	Step II	Step III	Step IV	Step V	Step VI	Step VII	Stress rate (MPa/sec)
		$\sigma_m \pm \sigma_a$ (MPa)							
SS304 [38]	S16	78±248 (50°)*	117±248 (50°)	78±248 (20°)	---	---	---	---	52
SS316L [57,67]	S17	0±195 (20°)	39.7±195 (10°)	66.2±195 (10°)	105.8±195 (10°)	---	---	---	52
	S18	52±195 (20°)	52±221 (20°)	52±247 (20°)	52±195 (20°)	---	---	---	52
U71Mn [73,74]	S19	205±411 (20°)	256±411 (20°)	308±411 (20°)	256±411 (20°)	---	---	---	52
	S20	359±324 (20°)	359±385 (20°)	359±449 (20°)	359±513 (20°)	359±385 (20°)	359±321 (20°)	---	52
	S21	0±449 (20°)	308±449 (20°)	359±449 (20°)	411±449 (20°)	308±449 (20°)	359±449 (20°)	411±449 (20°)	52

(\*) Number of cycles over loading step

**Table 4.7.** Coefficients of the O-W and A-V frameworks for SS304, SS316, U71Mn steel samples

Materials	Coefficients
SS304 [38]	$C (GPa) = 65, \gamma_1 = 992, \gamma_2 = 20$ $Q(MPa) = 50, \beta = 12.5, K = 82, n = 15$ $\gamma_{1-8} = 3341, 1833, 756.6, 210.4, 69.92, 35.91, 23.04, 13$ $r_{1-8} = 37.85, 33.16, 18.89, 10.92, 8.38, 6.74, 12.41, 70.33MPa$ $m_i = 1.9$
SS316L [57,67]	$C (GPa) = 165, \gamma_1 = 1750, \gamma_2 = 9$ $Q_M = 60, Q_0(MPa) = 30, \beta = 7.5, \mu = 30, \eta = 0.04, K (MPa) = 80, n = 13$ $\gamma_{1-8} = 3448, 1515, 833, 379, 114, 44, 22, 14$ $r_{1-8} = 6.96, 28.73, 73.28, 55.95, 16.99, 10.22, 10.46, 74.41MPa$ $m^i = 1.9$
U71Mn [73,74]	$C (GPa) = 95, \gamma_1 = 490, \gamma_2 = 46$ $Q_M = Q_0(MPa) = 0, \beta = 1, \mu = 1, \eta = 1, K (MPa) = 90, n = 13$ $\gamma_{1-12} = 4444, 2020, 974.6, 343.6, 201.2, 114.8, 66.7, 40.0, 28.6, 22.2, 18.2, 15.4$ $r_{1-12} = 69.5, 43.0, 44.6, 45.2, 27.5, 32.2, 49.5, 43.8, 82.0, 71.9, 80.6, 52.0 MPa$ $m_i = 5.5$

#### 4.3.2.2. Ratcheting evaluation

Experimental and predicted ratcheting values tested at room temperature under consecutive stress steps of  $78\pm 248 \rightarrow 117\pm 248 \rightarrow 78\pm 248$  MPa are presented in Figure 4.10. Stress-strain hysteresis loops were collected over ratcheting progress as asymmetric stress cycles followed Low-High-Low sequence. Accumulation of plastic strain over steps I and II preserved ratcheting strain to largely drop over step III, as evidenced through measured data and hysteresis loops in this figure. Predicted curves through the A-V and O-W models were closely agreed with experimental data. Generated hysteresis loops by means of the A-V model is more agreeable than those of the O-W model.

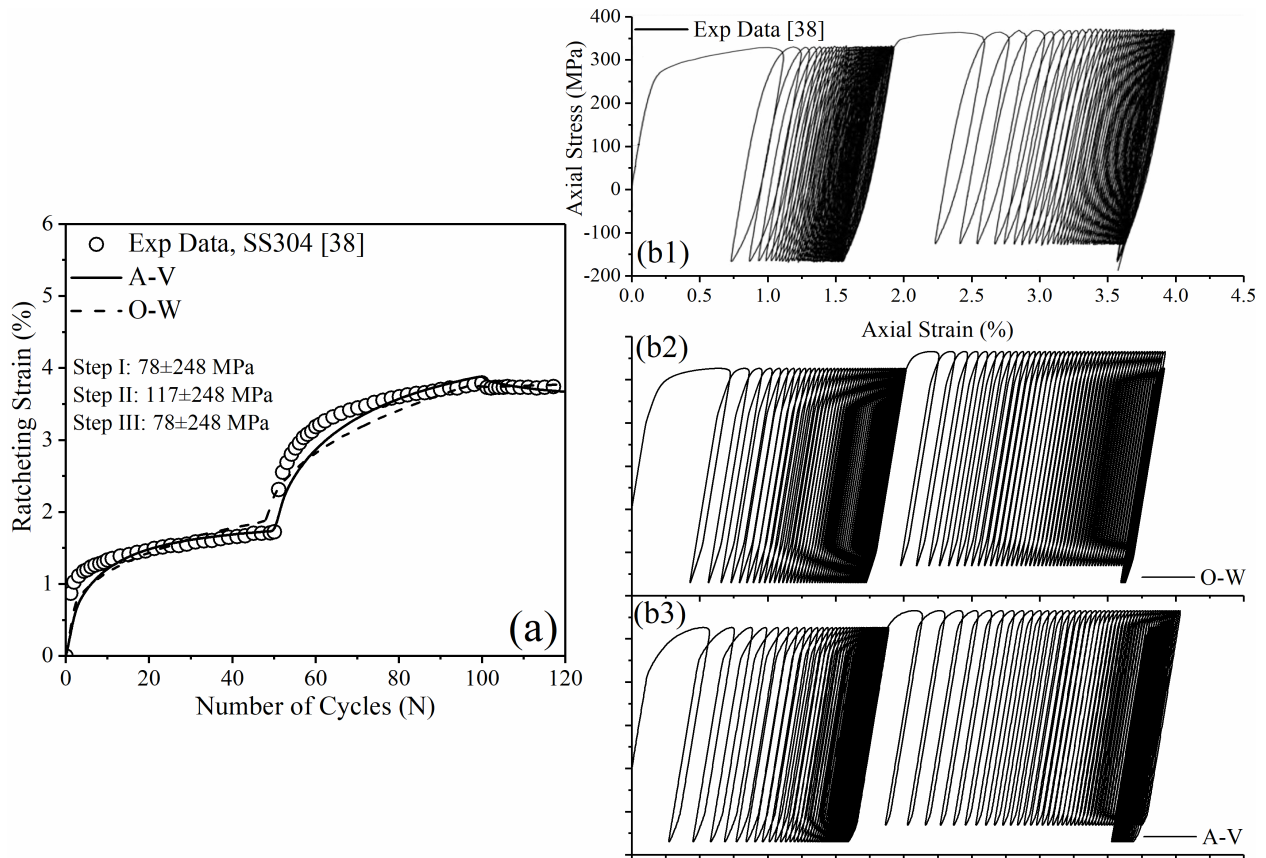


**Figure 4.10.** (a) Experimental ratcheting data and (b) their measured hysteresis loops at room temperature plotted versus predicted ratcheting curves by means of the O-W and A-V models at constant stress amplitude of 248 MPa and different mean stress of  $78 \rightarrow 117 \rightarrow 78$  MPa

A test on sample S17 was carried out under constant  $\sigma_a = 195$  MPa and different mean stresses of  $0 \rightarrow 39.7 \rightarrow 66.2 \rightarrow 105.8$  MPa over stress steps. At the absence of mean stress in the first step, no ratcheting strain is generated. Figure 4.11a shows that, similar to sample S16, as the mean stress increased over the second step, ratcheting strain was built up. Increasing the value of mean stress in each step resulted in promoting the magnitude of ratcheting strain to almost 3% at the end of the 4<sup>th</sup> step. Figure 4.11b compares experimental and predicted loops. Loops predicted based on the A-V model over the fourth step were found in closer agreement with experimental loops. While the width of generated loops through the O-W model were found in the same order of measured loops.

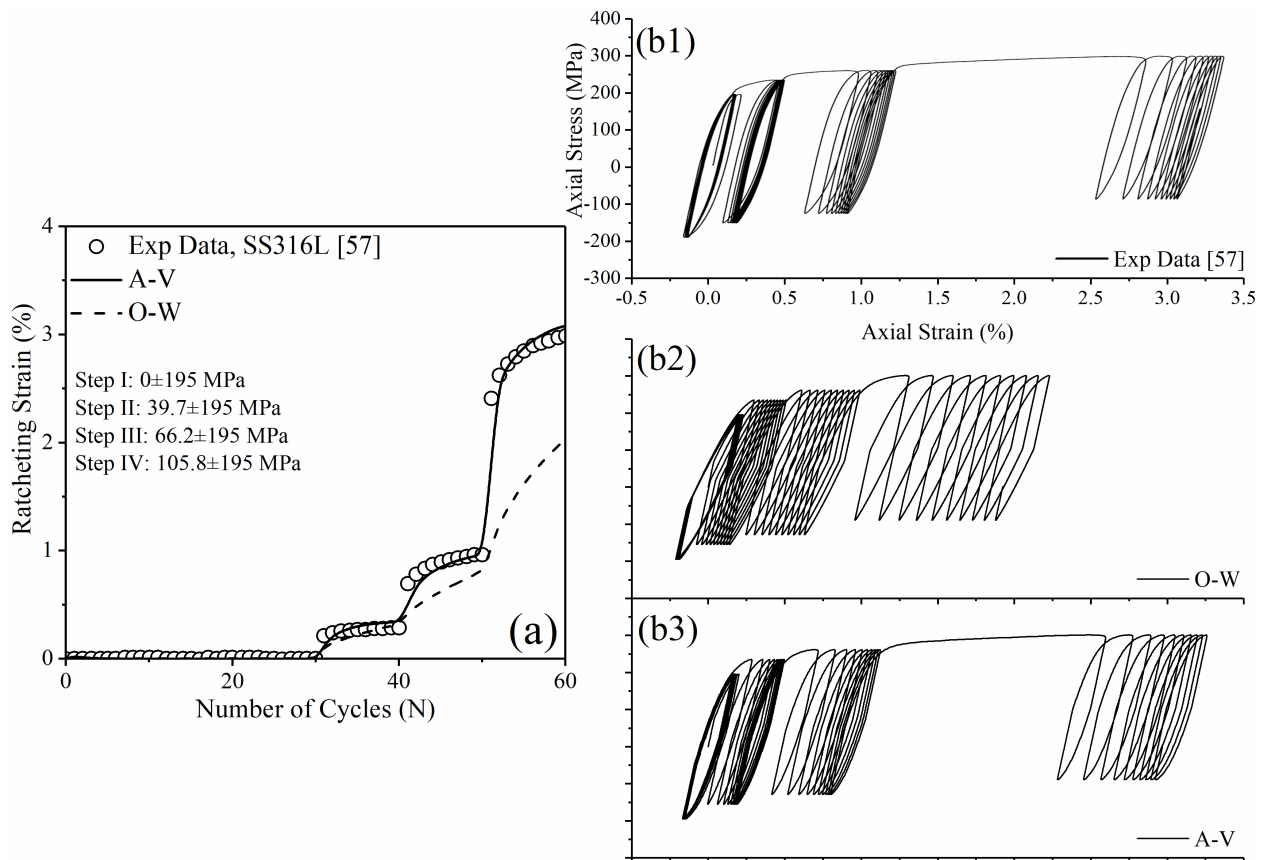


**Figure 4.11.** (a) Experimental and predicted ratcheting data over four stress-steps, and (b) experimental and predicted hysteresis loops generated by means of the O-W and A-V models for four-step stress levels for a SS316L sample tested at constant stress amplitude of 195 MPa and different means stresses of  $0 \rightarrow 39.7 \rightarrow 66.2 \rightarrow 105.8$  MPa

Figure 4.12 presents the ratcheting response of a sample of U71Mn subjected to seven consequential stress steps with a constant  $\sigma_a = 449$  MPa. The test started with no mean stress in the first step, resulting in no ratcheting strain. With an increase in mean stress to  $\sigma_m = 308$  MPa, a surge occurred in the ratcheting curve and it was promoted over steps III and IV as the mean stress increased to 359 and 411MPa, respectively. As the mean stress dropped in the fifth step (411→308MPa), ratcheting progress was halted resulting in shakedown. In Figure 4.12a, the O-W framework predicted ratcheting over the first two Low-High steps. Beyond the second step, the predicted ratcheting curves deviated from experimental ratcheting data. The predicted ratcheting curve by means of the A-V framework showed a close agreement following measured ratcheting data. Figure 4.12b compares experimental and predicted hysteresis loops by means of the O-W and A-V frameworks. While predicted loops by the A-V framework closely agreed with experimentally obtained loops, generated loops by means of the O-W model possessed narrower widths and lower ratcheting strains.

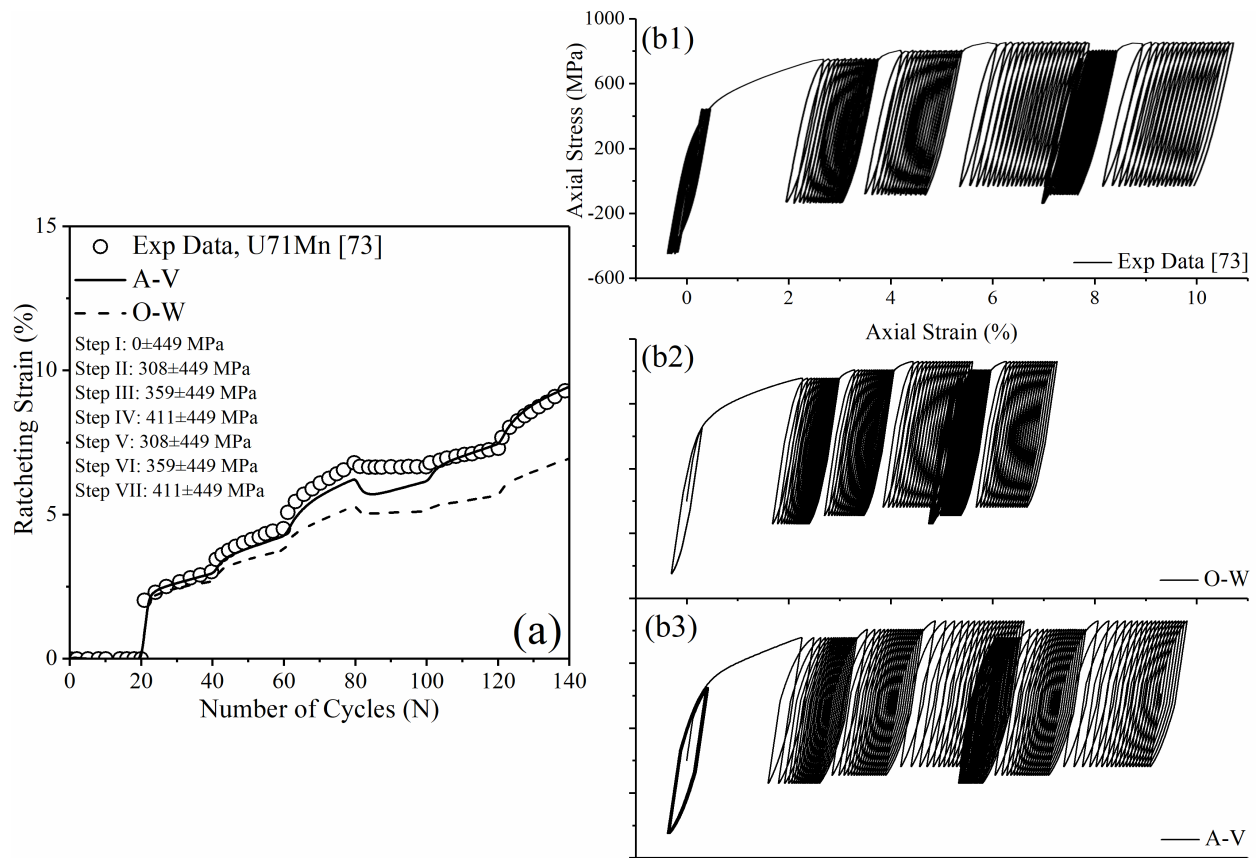


**Figure 4.12.** (a) Experimental and predicted ratcheting data over seven Low-High/ High-Low stress-steps, and (b) experimental and predicted hysteresis loops generated by means of the O-W and A-V models for seven-step stress levels for a U71Mn sample tested at constant stress amplitude of 449 MPa and mean stresses of 0→308→359→411→308 →359→411MPa

Figure 4.13 displays the ratcheting responses of S20 and S21 samples of U71Mn and a S18 sample of SS316L under various High-Low and Low-High sequences. In this figure, an increase in the stress level profoundly affected ratcheting strain accumulation over Low-High sequence, while decreasing the magnitude of stress resulted in a drop in ratcheting. Experimental stress-strain hysteresis of these samples magnifies the accumulation of ratcheting in Low-High sequences as well as a slight drop and eventual ratcheting arrest in High-Low steps. In Figure 4.13a, at a constant stress amplitude of 411 MPa, sample S20 was tested as mean stress increased from 205→256→308 MPa over the first three steps and then decreased to 256 MPa in the fourth step. Sample S21 in Figure 4.13b is subjected to six loading steps with a constant mean stress of 359MPa

and stress amplitudes of 321MPa→385MPa→449MPa→513MPa→385MPa →321MPa. Figure 4.13c shows sample S18 tested with stress amplitudes of 195→221→247→195 MPa and a constant mean stress of 52 MPa. The predicted ratcheting curves by means of O-W fell short to follow the trend of this step-loading test and underpredicted ratcheting curves over last loading steps, while the A-V model developed ratcheting curves in close agreement with those experimentally measured.

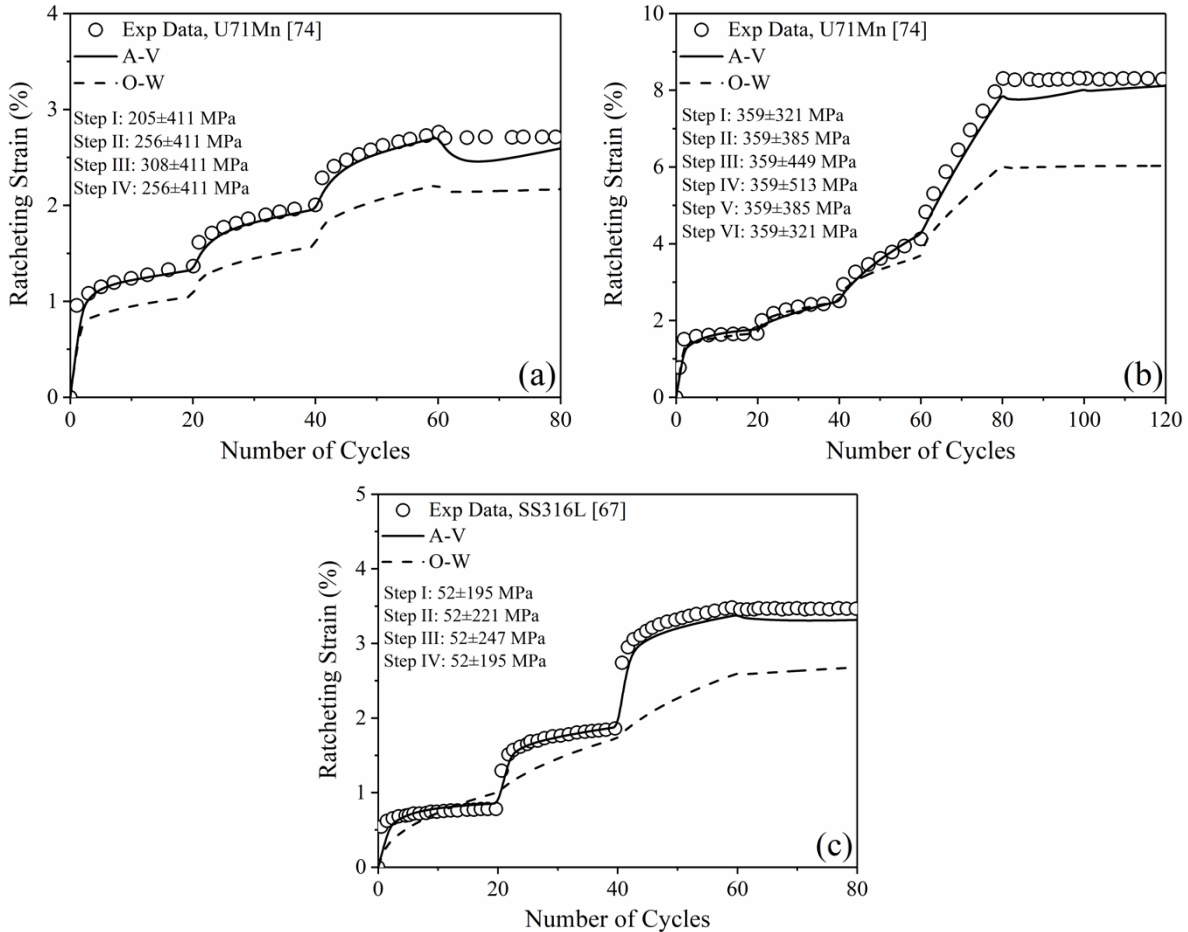


**Figure 4.13.** Experimental and predicted ratcheting values by means of the O-W and A-V models for (a and b) U71Mn and (c) SS316 alloys.

### 4.3.3. Operating temperatures

The visco-plastic ratcheting responses of SS304 samples tested at various step-loading conditions, stress levels, and operating temperatures were investigated. The hardening rules of O-

W and A-V were employed along with visco-plastic flow rule to address ratcheting of time-dependent 304 steel alloy at various temperatures. This alloy demonstrates no/little time-dependency at operating temperatures between 350°C and 650°C, undergoing the dynamic strain aging phenomenon, leading to a sudden escalation of ratcheting strain once mean stress increased over Low-High loading sequence in the beginning of each loading step. These models were further restructured to account for the dynamic strain ageing effect through the inclusion of an exponential function  $\psi$  (equation (3.22)) into the dynamic recovery term of models. Predicted results by means of these modified frameworks are compared to measured values of 304 stainless steel samples.

#### 4.3.3.1. Materials and testing conditions

To assess visco-plastic ratcheting response of SS304 steel samples at room and elevated temperatures under various step-loading, stress levels and rates, a series of experimental test data was taken from references [38,71,72]. Several step-loading tests were conducted under uniaxial strain-controlled and stress-controlled conditions at various rates and temperatures through use of test rig MTS809-250kN. Table 4.8 presents the details of these testing conditions.

**Table 4.8.** Ratcheting tests and stress-steps on SS304 samples at various temperatures

Temperature	Tests	Step I	Step II	Step III	Stress rate (MPa/sec)
		$\sigma_m \pm \sigma_a$ (MPa)	$\sigma_m \pm \sigma_a$ (MPa)	$\sigma_m \pm \sigma_a$ (MPa)	
Room Temperature [38]	T1	78±234 (100°)	---	---	13
200°C [71]	T2	39±248 (50°)*	78±248 (50°)	39±248 (20°)	26
400°C [72]	T3	39±208 (50°)	78±208 (50°)	39±208 (20°)	26
600°C [72]	T4	26±195 (50°)	39±195 (50°)	26±195 (20°)	26
700°C [38]	T5	40±100 (100°)	---	---	10
	T6	0±102 (20°)	26±102 (20°)	52±102 (20°)	40

(\*) Number of cycles over the loading step

Coefficients of the O-W and A-V hardening rules were determined at different operating temperatures at which SS304 steel samples were tested. Stress-strain curves and ratcheting strain

data measured at various temperatures were taken to determine these coefficients of SS304 steel alloy. Table 4.9 lists hardening coefficients determined at various temperature.

**Table 4.9.** Coefficients for the O-W and A-V frameworks for SS304 samples at various temperatures

Temperature	Coefficients
Room Temperature [38]	$C (GPa) = 65, \gamma_1 = 992, \gamma_2 = 20$ $Q (MPa) = 50, \beta = 12.5, K = 82, n = 15$ $\gamma_{1-8} = 3341, 1833, 756.6, 210.4, 69.92, 35.91, 23.04, 13$ $r_{1-8}$ $= 37.85, 33.16, 18.89, 10.92, 8.38, 6.74, 12.41, 70.33MPa$ $m_i = 1.9$
200°C [71]	$C (GPa) = 130, \gamma_1 = 1100, \gamma_2 = 8$ $Q (MPa) = 35, \beta = 13, K = 50, n = 11, \psi_\infty = 1, \lambda = 0$ $\gamma_{1-8} = 3623, 1567, 852.5, 216.8, 62.27, 32.38, 19.85, 12.68$ $r_{1-8}$ $= 1.057, 68.94, 85.21, 26.18, 3.224, 4.835, 6.014, 44.82MPa$ $m_i = 1.8$
400°C [72]	$C (GPa) = 118, \gamma_1 = 1220, \gamma_2 = 8$ $Q (MPa) = 33.5, \beta = 15, K = 40, n = 10, \psi_\infty = 0.08, \lambda = 4$ $\gamma_{1-8} = 3509, 1513, 851.1, 211.1, 70.94, 36.12, 23.80, 16.08$ $r_{1-8}$ $= 2.710, 11.86, 94.51, 25.07, 9.267, 4.432, 6.341, 48.80MPa$ $m_i = 1.6$
600°C [72]	$C (GPa) = 130, \gamma_1 = 1750, \gamma_2 = 7$ $Q (MPa) = 22.5, \beta = 20, K = 40, n = 9, \psi_\infty = 0.06, \lambda = 8$ $\gamma_{1-8} = 3534, 1550, 977.5, 209, 71.22, 36.81, 23.72, 16.32$ $r_{1-8}$ $= 7.968, 74.83, 42.25, 4.720, 4.130, 1.978, 1.954, 42.92MPa$ $m_i = 0.8$
700°C [38]	$C (GPa) = 90, \gamma_1 = 2800, \gamma_2 = 33$ $Q (MPa) = 12.5, \beta = 25, K = 35, n = 8, \psi_\infty = 1, \lambda = 0$ $\gamma_{1-8} = 3306, 1703, 726.7, 208.5, 69.35, 36.15, 22.94, 13$ $r_{1-8}$ $= 12.46, 14.14, 13.39, 3.76, 7.86, 16.08, 9.91, 22.01MPa$ $m_i = 2.8$

Figure 4.14 presents tensile stress-strain diagrams of SS304 steel samples obtained at various temperatures and strain rates. Figure 4.14a shows high rate-dependency of the material at room temperature and 700°C. Figure 4.14b presents the stress-strain curve of SS304 steel sample tested at 350°C with five consecutive strain rates of 0.002→0.02→0.2→0.02→0.002%/sec. This

figure further supports the fact that the stress-strain curve was unaffected by rate-dependency at this temperature.

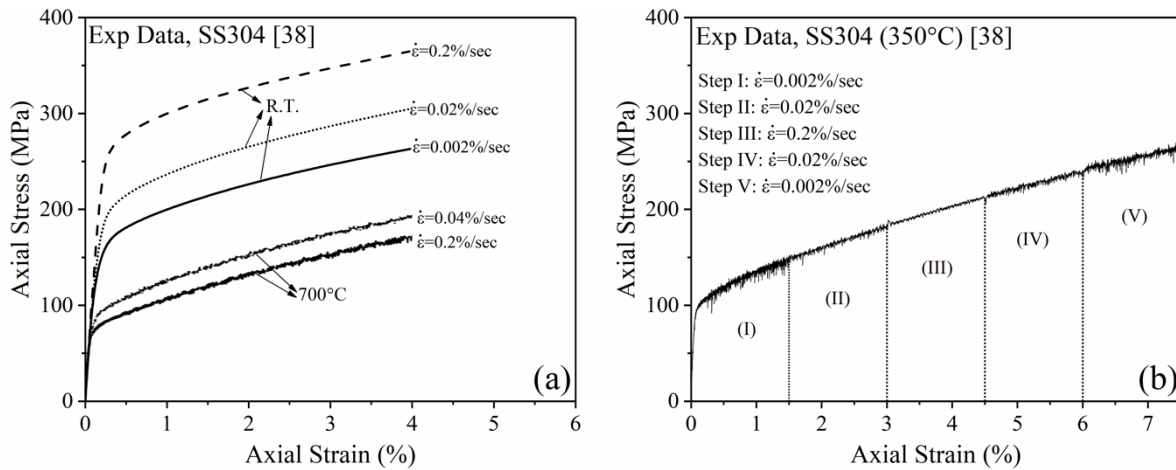


**Figure 4.14.** Experimental uniaxial tensile stress-strain data for (a) various strain rates at room and 700°C temperatures, and (b) various strain rates at 350°C.

#### 4.3.3.2. Visco-plastic frameworks at various temperatures

At ambient and elevated temperature of 700°C, asymmetric single-step cyclic tests were conducted on samples T1 and T5 at respectively  $78 \pm 234$  MPa and  $64 \pm 247$  MPa for 100 cycles. Figure 4.15 and Figure 4.16 present experimental and predicted ratcheting curves and cyclic hysteresis loops for these samples. The predicted ratcheting curve by means of the A-V model was closer to experimental data than the curve generated by the O-W model. The predicted values by the O-W model have shown good agreements over the first 20 and 50 cycles at room and 700°C temperature in Figure 4.15 and Figure 4.16, while beyond these cycles the O-W model overestimated the results as high as 29% and 7%, respectively. Predicted hysteresis loops by means of this model magnify this deviation by the O-W model as compared with measured data. Generated hysteresis loops by means of the A-V model for both samples resulted in agreeable loops in terms of their width and the strain at which they were generated.

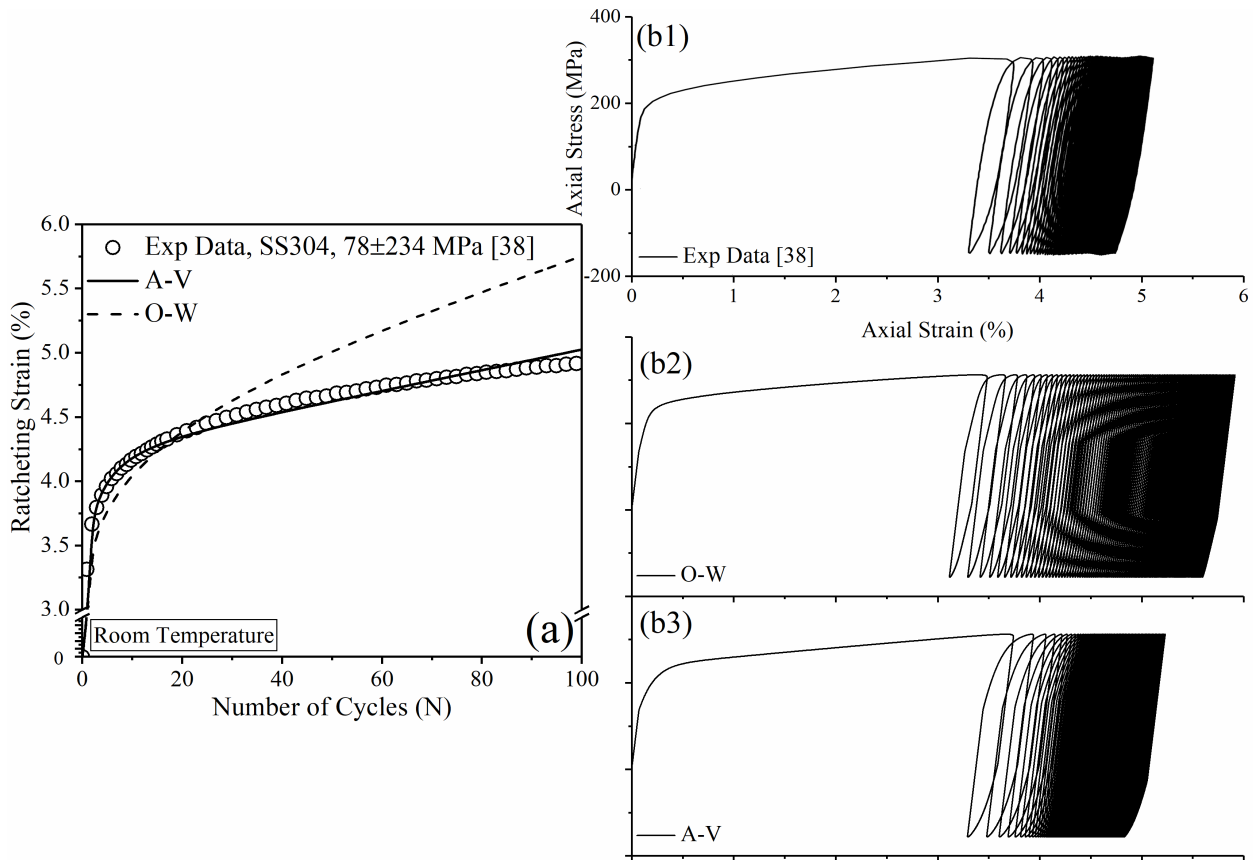


**Figure 4.15.** (a) Experimental ratcheting data and (b) their measured hysteresis loops plotted versus predicted ratcheting curves and hysteresis loops for 304 steel sample T1 by means of the O-W and A-V models at  $78\pm 234$  MPa and at room temperature

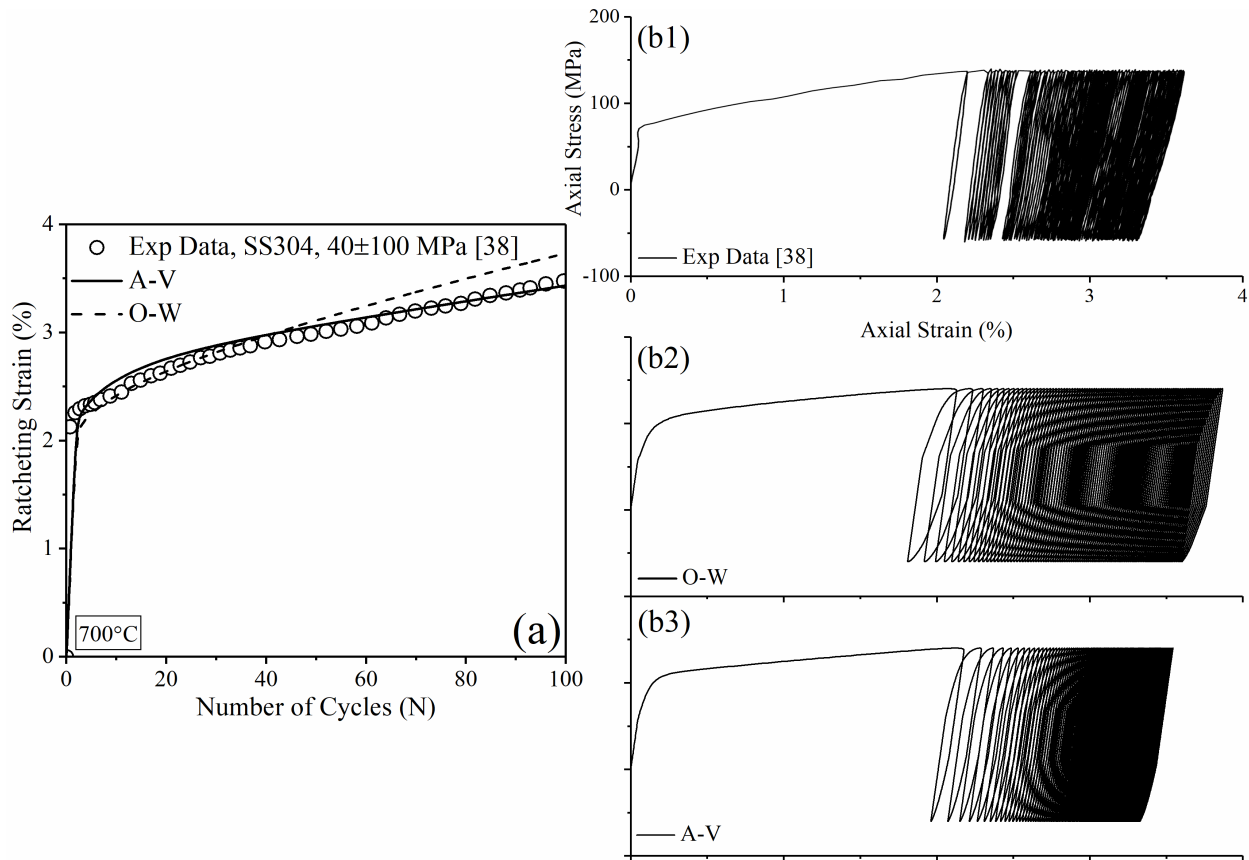


**Figure 4.16.** Experimental ratcheting data and their measured hysteresis loops at 700°C plotted versus predicted ratcheting curves for 304 steel sample T5 by means of the O-W and A-V models at 40±100 MPa and at stress rate of 10MPa/sec

Figure 4.17 presents experimental and predicted ratcheting by means of the O-W and A-V models for sample T2 tested at 39±248→78±248→39±248 MPa and 200°C. Over the first step at 39±248 MPa, after a sudden elevation to 3.32%, ratcheting strain increased steadily to a value of 4.35%. In the second step with a constant  $\sigma_a=248$  MPa, mean stress was doubled to 78 MPa resulting in ratcheting growth to 7.28% at the 80<sup>th</sup> cycle. The last step consisted of a loading condition identical to the first step leading to ratcheting shakedown. A noticeable gap between measured hysteresis loops at the transition of steps I and II in this figure further supports a sudden ratcheting strain buildup in this transition. The drop in ratcheting over the High-Low (steps II-III) transition was insignificant. Ratcheting over steps I and II progressed, resulting in a small drop in ratcheting as the mean stress reduced to half (78→39MPa) over step III. The O-W model predicted

ratcheting with deviations as high as 20% over loading steps. This deviation dropped to 3% for predicted ratcheting values based on the A-V model. The A-V model developed ratcheting strain over the first step, followed experimental data over the second and formed a plateau over the third step.

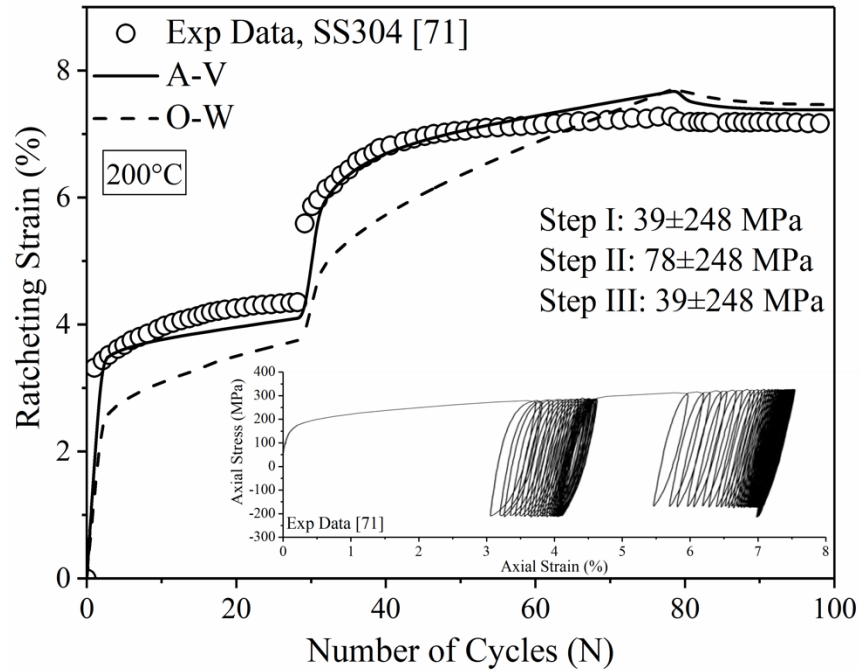


**Figure 4.17.** Experimental ratcheting data and their measured hysteresis loops at 200°C plotted versus predicted ratcheting curves for 304 steel sample T2 by means of the O-W and A-V models stress amplitude of 248 MPa and different mean stress of 39→78→39 MPa

At 400°C, sample T3 was loaded at 39±208→78±208→39±208MPa with a stress rate of 26MPa/sec. The distinct ratcheting response of SS304 alloy at this temperature is presented in Figure 4.18. This figure highlights a sudden ratcheting strain buildup followed by a constant rate resulting in ratcheting shakedown after a few stress cycles, caused by the dynamic strain aging effect. At a constant stress amplitude of 208 MPa, ratcheting strains progressed from 3→5→4.86% as mean stresses varied from 39→78→39MPa over three consecutive loading steps. Models predicted ratcheting curves with close agreements with experimental data over the first step. In the transition from steps I to II, ratcheting strain was built up once more to as high as 5%. The predicted ratcheting curve by the O-W model corresponded large deviations as high as 40% over steps II

and III. Predicted ratcheting curve by the A-V model followed experimental data over steps I and III. A small deviation of 10% was found in the transition from steps I to II. Measured stress-strain hysteresis loops in this figure also show the evidence of sudden ratcheting build ups at the beginning of steps I and II. The drop in ratcheting strain at the third step was minimal as mean stress decreased from 78→39 MPa.

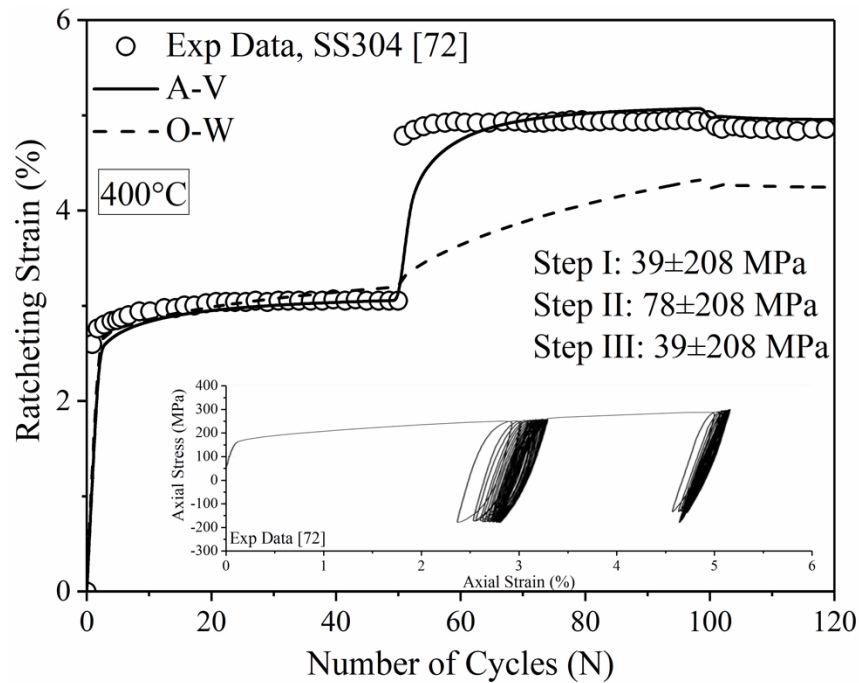


**Figure 4.18.** Experimental ratcheting data and their measured hysteresis loops at 400°C plotted versus predicted ratcheting curves for 304 steel sample T3 by means of the O-W and A-V models at constant stress amplitude of 208 MPa and different mean stress of 39→78→39 MPa

To further discuss the inclusion of function  $\psi$  in the dynamic recovery terms of the O-W and A-V hardening rules, the first stress step of sample T3 tested at 400°C is represented in Figure 4.19. Figure 4.19a shows how function  $\psi$  declines exponentially over stress cycles varying from 1.0 at the first cycle to its saturated value of  $\psi_{\infty} = 0.08$  over longer cycles. Beyond this value no further drop is expected. In this figure, the A-V model with less decay rate requires more stress cycles to converge to  $\psi_{\infty} = 0.08$ , while the decreasing trend of  $\psi$  through the O-W model is sharper, resulting in a fewer number of cycles to approach this value. As a part of dynamic recovery terms in the employed hardening rules, the rate of decay in function  $\psi$  (varying 1.0→0.08) affects

the accumulated plastic strain and backstress components over loading cycles. The predicted ratcheting curves over the first loading step of sample T3 (tested at  $39\pm 208$  MPa) based on the O-W and A-V models at an operating temperature of  $400^\circ\text{C}$  are represented in Figure 4.19b and Figure 4.19c. The hardening rules in the absence of exponential function  $\psi$  at this temperature overpredict ratcheting data noticeably.

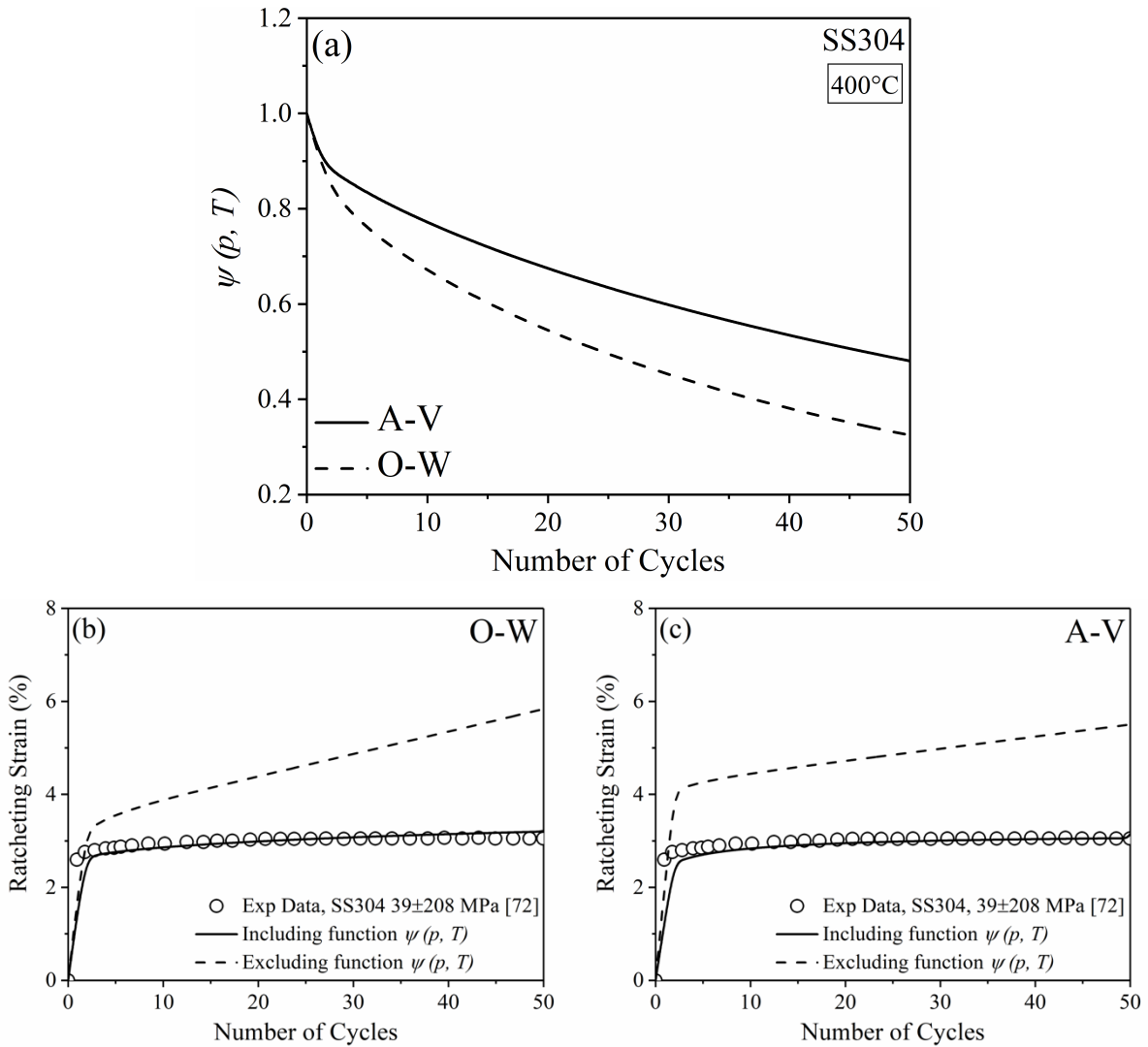


**Figure 4.19.** (a) Variation of exponential function  $\psi$  over loading cycles for sample T3 tested at  $400^\circ\text{C}$  based on the hardening rules O-W and A-V, and (b, c) predicted ratcheting results in the presence and absence of function  $\psi$  in the dynamic recovery terms of the hardening rules.

The tested sample at 400°C exhibited rate-independency for SS304 steel alloy. A similar evidence of abrupt ratcheting increase has been observed in Figure 4.20 for sample T4 tested at 26±195→39±195→26±195MPa and stress rate of 26MPa/sec at 600°C. Hysteresis loops measured for Low-High-Low sequence loading in sample T4 revealed continuous ratcheting shakedown through stress steps and supported the influence of dynamic strain aging at this temperature. An increase in mean stress from 26→39MPa (over Low-High loading sequence) has slightly increased the magnitude of the ratcheting strain. Even with a mean stress drop from 39→26MPa over steps II-III, no noticeable change in the ratcheting strain was observed. The O-W and A-V models predicted ratcheting values in close agreement with those of measured values.

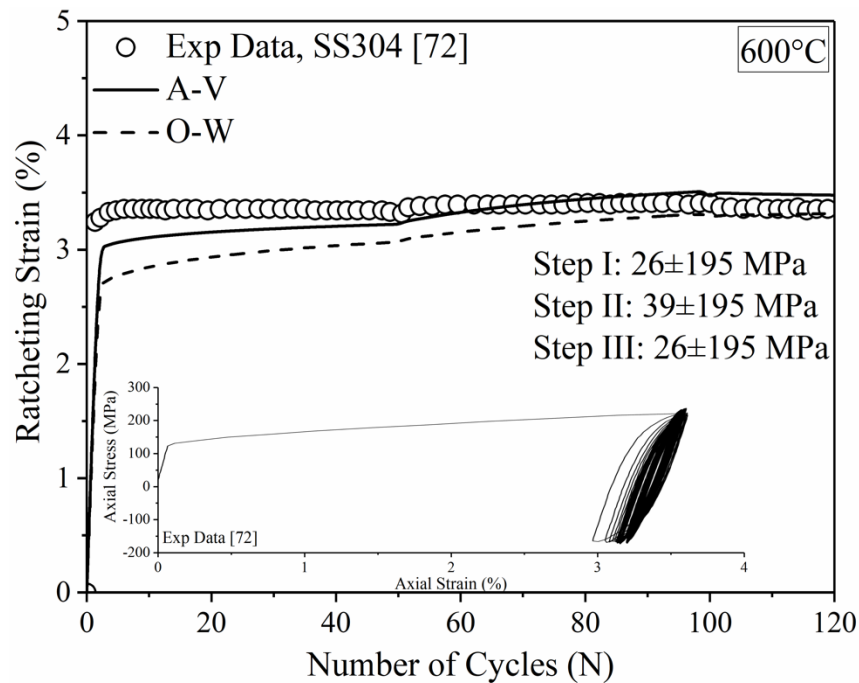


**Figure 4.20.** Experimental ratcheting data and their measured hysteresis loops plotted at 600°C versus predicted ratcheting curves for 304 steel sample T4 by means of the O-W and A-V models at constant stress amplitude of 195 MPa and mean stress of 26→39→26 MPa

Figure 4.21 presents the ratcheting response of sample T6 tested with Low-High-High sequential stress steps of 0±102→26±102→52±102MPa at stress rate of 52MPa/sec and at 700°C. In the first stress step, zero mean stress resulted in no ratcheting strain. An increase in mean stress from 0→26MPa, escalated ratcheting strain to 0.86% in step II. Over an increase from 26→52MPa

in the mean stress, ratcheting was built up significantly to 3.7% over step III. The predicted ratcheting by the A-V model followed the trend of experimental data, while the O-W model over-predicted ratcheting curves up to 12% at the end of the 60<sup>th</sup> cycle. Hysteresis loops and ratcheting data in this figure showed a progressive response. The steady and gradual increase in ratcheting strain verified that sample T6 tested at 700°C resumed its time-dependent response.

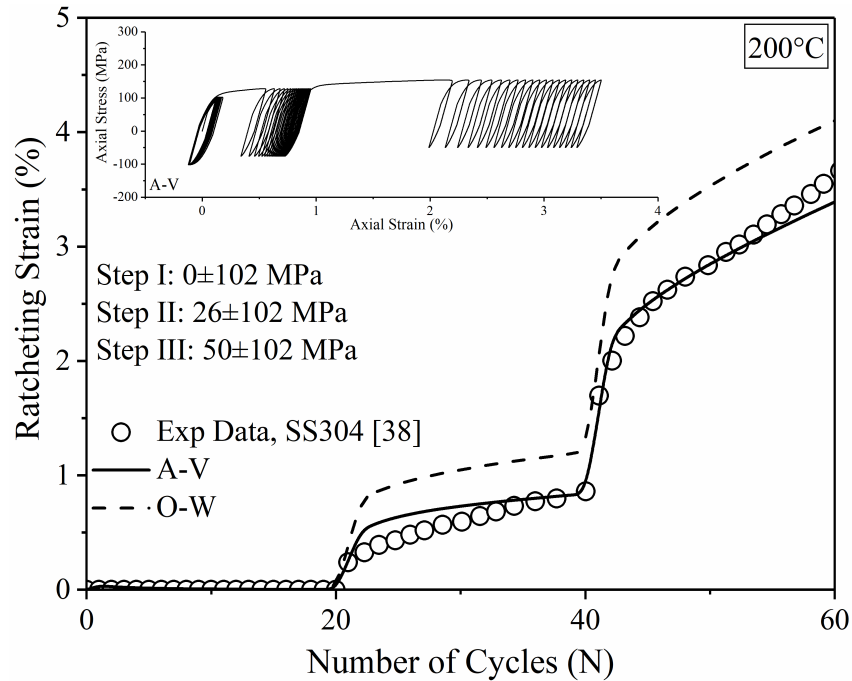


**Figure 4.21.** Experimental ratcheting data and their measured hysteresis loops for 304 steel sample T6 tested at 700°C plotted versus predicted ratcheting data by means of the O-W and A-V models at constant stress amplitude of 102 MPa and different mean stress of 0→26→52 MPa

It is expected that at elevated temperature materials exhibit rate-dependency. However, evidence has shown that various steel alloys, such as SS304, SS316L, and Z2CND18.12N steel, experience negative rate sensitivity resulting in time-independency at a range of temperatures. The evidence of fading time-dependency in the deformation of materials at a given range of temperatures was ascribed to the dynamic strain aging phenomenon. This phenomenon is associated with the interaction of mobile dislocations and point defects in materials upon loading beyond elastic domain, leading to an improved hindrance to deformation and loss of time-dependent viscosity [5,6]. For SS304 steel alloy, rate-dependency was reported to lessen as

operating temperatures varied between 350°C and 650°C [38]. A similar drop in rate-dependency was further observed in SS316L and SS316L(N) steel samples by Hong and Lee [44] and Sarkar et al. [45] respectively at temperatures 250°C-600°C and 550°C. Stainless steel samples of Z2CND18.12N tested under uniaxial stress cycles at 350°C [46] have also shown a drop in the rate-dependency response. De Almeida et al. [47] reported that austenitic stainless steels are prone to time-independency at 200°C-800°C.

#### 4.3.4. Holding time

Visco-plastic ratcheting response of 304 steel samples with peak/valley holding time at room (25°C) and at elevated temperature of 700°C was studied. The infusion of holding time caused the creep-ratcheting phenomenon, resulting in higher ratcheting magnitude when compared to cyclic stress in the absence of holding time. The dynamic recovery terms of the O-W and A-V models were further restructured to account for the static recovery effect as holding time was present over peak/valley of stress cycles. This reconstruction allowed the models to predict larger values of ratcheting strains agreeable with experimental data.

##### 4.3.4.1. Materials and testing conditions

To evaluate ratcheting response of 304 stainless steel samples subjected to stress loading with peak/valley holding time at room temperature and at 700°C, measured ratcheting values and hysteresis loops were taken from literature [38]. Table 4.10 presents testing conditions for SS304 samples tested at various stress levels, rates, holding times, and temperatures.

**Table 4.10.** Ratcheting tests and stress-steps on SS304 samples with holding time

Temperature	Test samples	$\sigma_m \pm \sigma_a$ (MPa)	Holding time (sec.)	Stress rate (MPa/sec)
Room Temperature [38]	H1	78±234 (40°)	10	2.6
700°C [38]	H2	40±100 (100°)	10	10

Coefficients of the O-W and A-V hardening rules were determined from ratcheting and hysteresis loops of SS304 steel samples tested at different operating temperatures and holding times. Table 4.11 lists hardening coefficients determined at room temperature and at 700°C.

**Table 4.11.** Coefficients for the O-W and A-V frameworks for SS304 samples with holding time

Temperature	Coefficients
Room Temperature [38]	$C$ (GPa) = 65, $\gamma_1 = 992$ , $\gamma_2 = 20$ $Q$ (MPa) = 50, $\beta = 12.5$ , $K = 82$ , $n = 15$ $\gamma_{1-8} = 3341, 1833, 756.6, 210.4, 69.92, 35.91, 23.04, 13$ $r_{1-8}$ = 37.85, 33.16, 18.89, 10.92, 8.38, 6.74, 12.41, 70.33MPa $m_i = 1.9$ $\chi = 15e - 10/MPa, \rho = 3.6$
700°C [38]	$C$ (GPa) = 90, $\gamma_1 = 2800$ , $\gamma_2 = 33$ $Q$ (MPa) = 12.5, $\beta = 25$ , $K = 35$ , $n = 8$ , $\psi_\infty = 1$ , $\lambda = 0$ $\gamma_{1-8} = 3306, 1703, 726.7, 208.5, 69.35, 36.15, 22.94, 13$ $r_{1-8} = 12.46, 14.14, 13.39, 3.76, 7.86, 16.08, 9.91, 22.01MPa$ $m_i = 2.8$ $\chi = 2.4e - 7/MPa, \rho = 3.2$

#### 4.3.4.2. Ratcheting prediction

A uniaxial ratcheting test was conducted on a 304 steel sample at room temperature with a stress level of 78±234 MPa and a stress rate of 2.6MPa/sec. The holding time imposed at each peak/valley was 10 seconds. Figure 4.22a shows that peak/valley holding time impacted the ratcheting response of sample H1, resulting in higher values of ratcheting strain as cycles progressed. This elevation mainly occurred in the initial build-up within the first 5 cycles proceeded by an almost steady rate until it reached the value of 5.5% at the 40<sup>th</sup> cycle. The magnitude of ratcheting in the absence of holding time was 5.2% at the same cycle. After a deviation within the first 10 cycles, the A-V model was enabled to predict larger ratcheting strains caused by holding time, while the O-W model neither followed the initial build-up nor the steady condition. Measured ratcheting strains and stress-controlled hysteresis loops were obtained from cycles with a 10sec. holding time in the peak/valley as plotted in Figure 4.22b1. A comparison between this data and the data generated through the O-W and A-V frameworks are presented respectively in Figure 4.22b2 and Figure 4.22b3. These figures further magnify the deviation of

both models in the first few cycles. Hysteresis loops generated through the A-V model were in close agreement with experimental data beyond the initial 5 cycles.

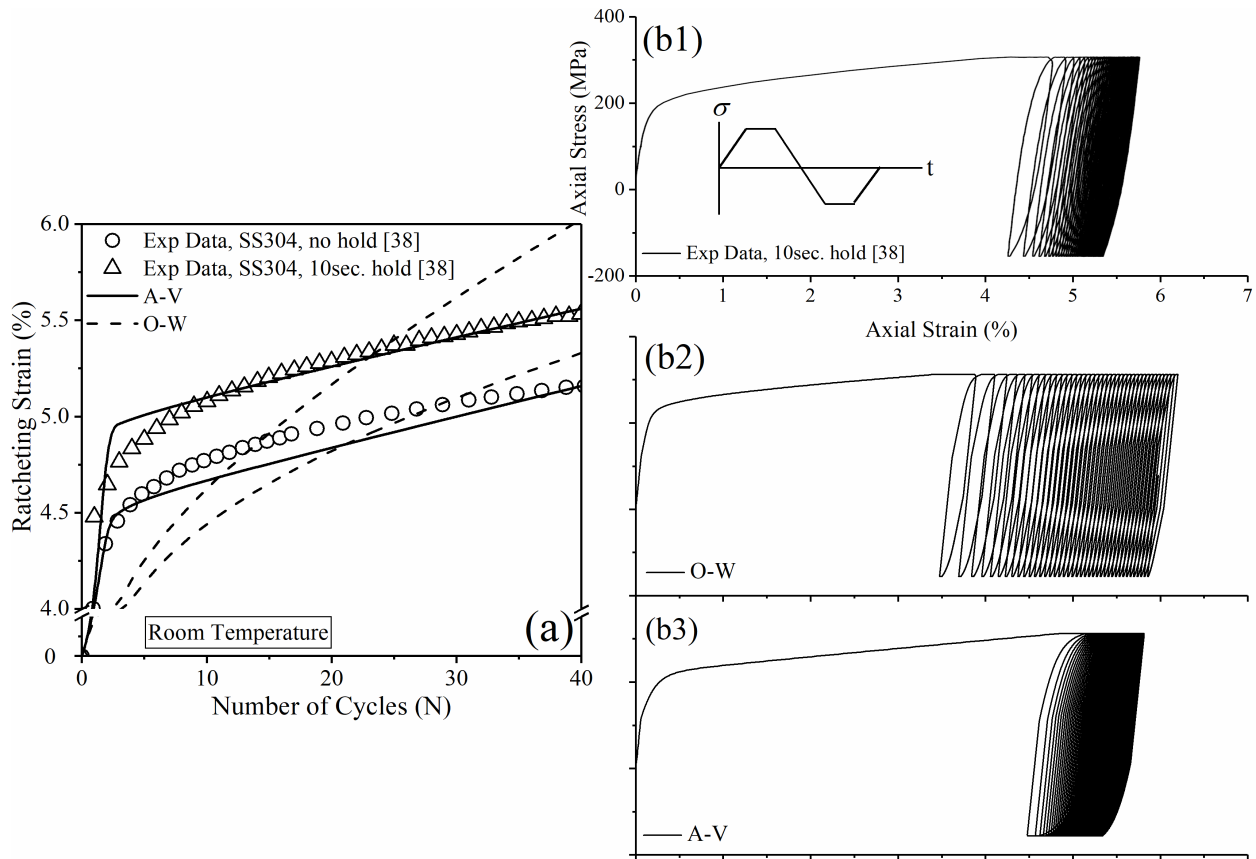


**Figure 4.22.** (a) experimental ratcheting data without and with holding time and (b) measured hysteresis loops with hold time is plotted versus those predicted by means of O-W and A-V frameworks for sample H1 at  $78 \pm 234$  MPa.

Figure 4.23 presents experimental and predicted ratcheting data and hysteresis loops for the H2 sample tested under uniaxial loading cycles with a holding time of 10sec. and at an operating temperature of  $700^{\circ}\text{C}$ . Similar to sample H1, the imposition of holding time at peak/valley increased ratcheting strain substantially to almost 6% at the 100<sup>th</sup> cycle, while it reached 3.3% for samples tested without holding time. In spite of small deviations within the first 40 cycles, predicted ratcheting curves in Figure 4.23a by means of the O-W and A-V models are both in close agreement with measured values. However, the generated hysteresis loops through the A-V framework (Figure 4.23b3) showed that the width and size of the loops closely agreed to

the experimental values (Figure 4.23b1) as compared with those predicted by means of the O-W framework (Figure 4.23b2).

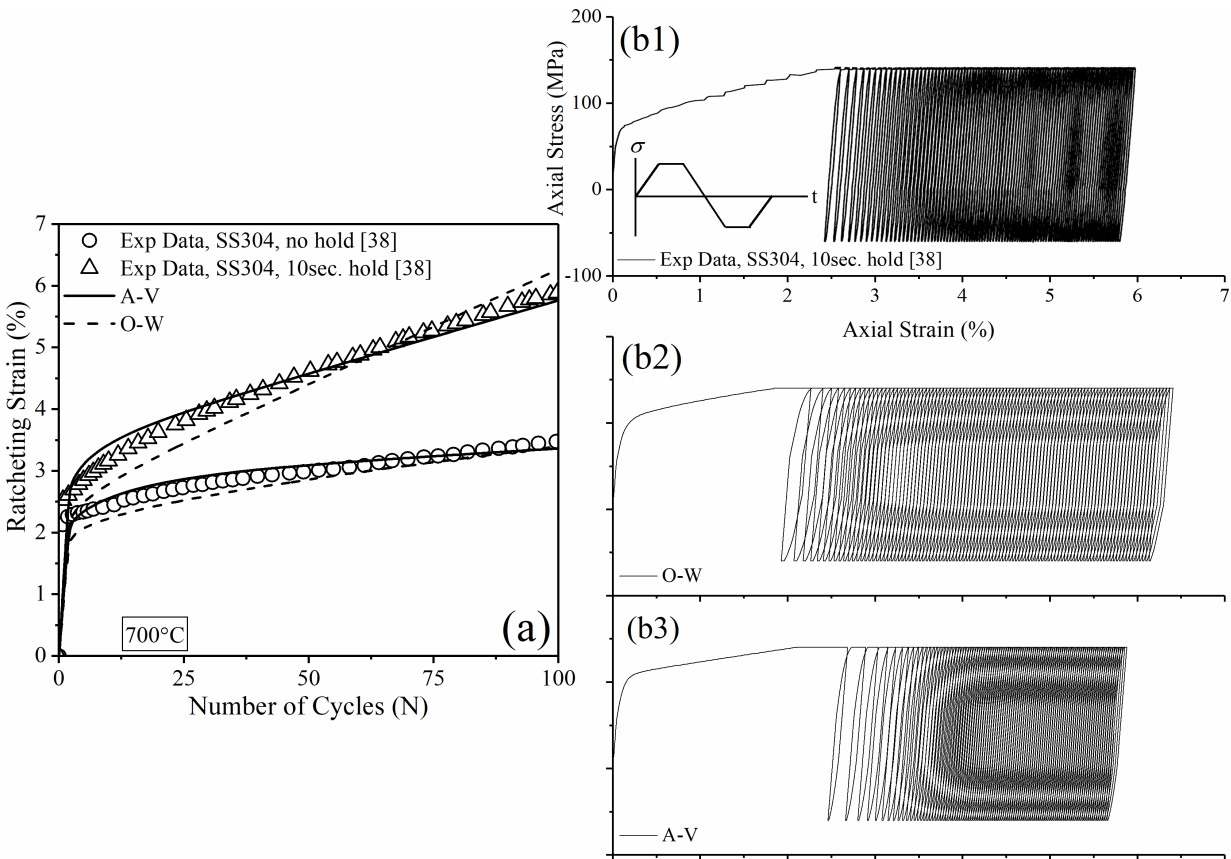


**Figure 4.23.** (a) experimental ratcheting data without and with holding time and (b) measured hysteresis loops with holding time is plotted versus those predicted by means of O-W and A-V frameworks for sample H1 tested at  $40 \pm 100$  MPa

The imposition of static loading caused the occurrence of creep, while the presence of cyclic loading led to the accumulation of ratcheting strain. The simultaneous application of these two phenomena, cyclic loading with holding time at peak/valley, resulted in a phenomenon known as creep-ratcheting. The escalation of ratcheting strain magnitude as a result of this phenomenon is attributed to the static recovery effect. The general format of kinematic hardening rules failed to address this surge in ratcheting value and resulted in underprediction with considerable margin. To address this issue, Ding et al. [60] introduced an exponential function,  $\chi(a)^{e-1} \mathbf{a}$ , into the

dynamic recovery terms of kinematic hardening rules to further enhance the magnitude of predicted ratcheting. Figure 4.24 and Figure 4.25 present the predicted ratcheting curves through the use of the O-W and A-V model for operating temperatures of ambient and 700°C. The inclusion of this function into the dynamic recovery parts has resulted in closer ratcheting prediction values than those predicted without the static recovery function.

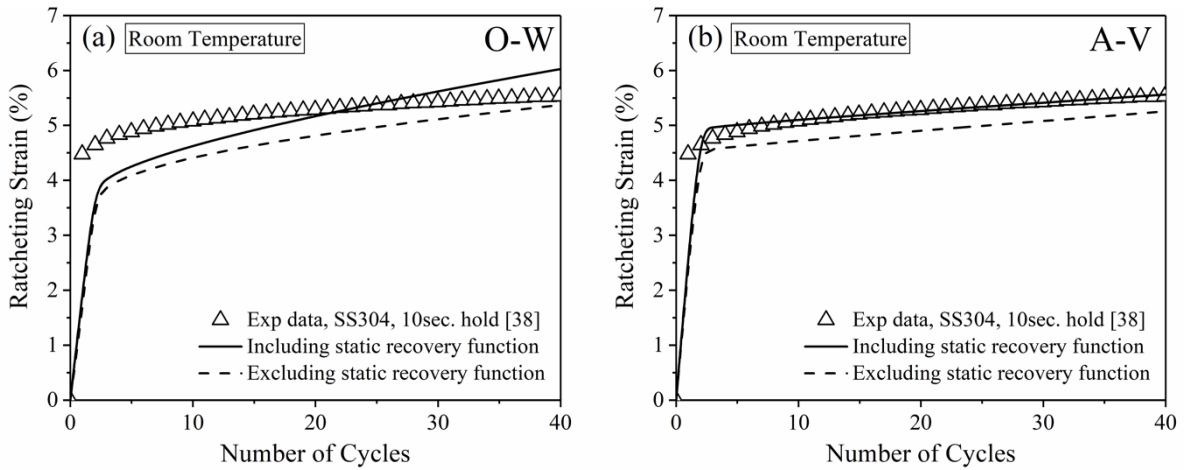


**Figure 4.24.** Predicted ratcheting curves in the presence and absence of static recovery function for sample H1 tested at room temperature by means of the (a) O-W and (b) A-V model

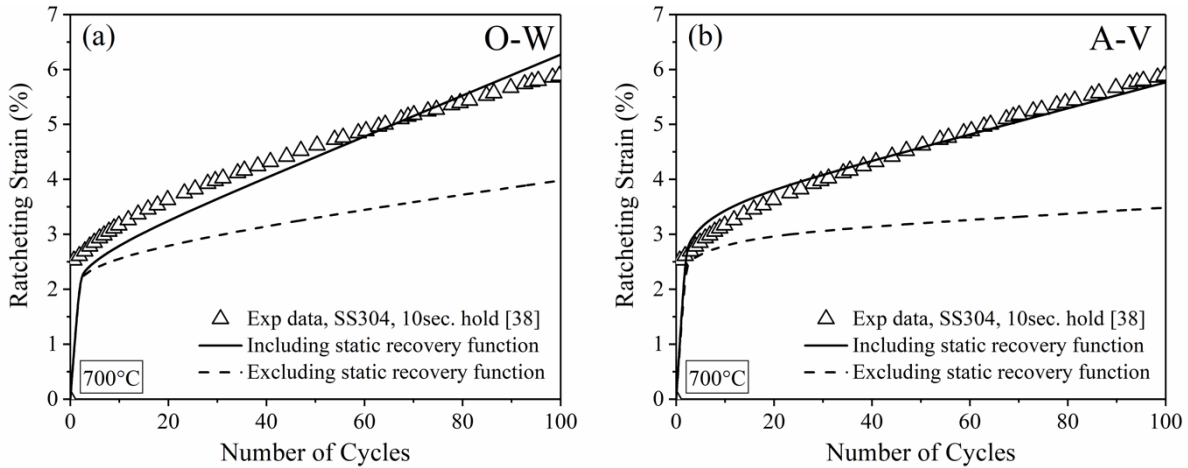


**Figure 4.25.** Predicted ratcheting results in the presence and absence of static recovery function for sample H2 tested at 700°C temperature by means of the (a) O-W and (b) A-V model

#### 4.4. Summary

Through the use of the O-W and A-V models and in the absence and presence of isotropic descriptions, the ratcheting responses of stainless steel samples were evaluated. The O-W and A-V kinematic hardening rules respectively over- and under-predicted ratcheting curves as their frameworks were constructed through the use of initial and saturated yield surfaces. Once adhered to isotropic hardening, both models resulted in comparable evolution of yield surfaces and predicted ratcheting curves. The dominance of the isotropic model in assessing ratcheting over the first 100-150 cycles in 304 steel samples was discussed and hysteresis loops within this range of cycles were generated. The inclusion of isotropic models promoted change in the width of hysteresis loops and moved the loops forward, resulting in higher strain values. The predicted results through the use of both frameworks revealed that the adherence of the Iso-C model resulted in a closer agreement with experimental data.

The impacts of stress level, rate, step, operating temperature and holding time on the ratcheting responses of visco-plastic materials were studied. Frameworks were further developed through the inclusion of the visco-plasticity constitutive equation to assess the effect of stress level and rate on the ratcheting of Z2CND18.12N austenitic and 304 stainless steel at ambient temperature. The influence of stress level, rate and step-loading condition on ratcheting rate and magnitude was discussed through these frameworks. Predicted ratcheting curves by means of the framework of the A-V model were found in more agreement to address stress level- and rate-dependency in samples of Z2CND18.12N austenitic and 304 stainless steel tested under the single-step loading condition. The capabilities of the A-V and O-W frameworks were then evaluated for samples of SS304, SS316L, U71MN under the multi-step loading condition. Predicted curves and hysteresis loops by means of the A-V model were found in closer agreement with the increase in ratcheting strains over the sequences of Low-High and the drop over the High-Low steps of loading. However, the O-W framework was yet to generate ratcheting results and hysteresis loops in size and shape comparable to measured values beyond the second step of loading.

The visco-plastic ratcheting responses of the SS304 samples tested at various step-loading conditions, stress levels, and rates at room and high temperatures were also investigated through O-W and A-V models. This alloy demonstrates no/little time-dependency at operating

temperatures between 350°C and 650°C, undergoing the dynamic strain aging phenomenon leading to a sudden escalation of ratcheting strain once mean stress increased over Low-High loading sequence in the beginning of each loading step. The dynamic strain ageing was accounted for SS304 samples at 400°C and 600°C in this study through the inclusion of an exponential function  $\psi$  into the dynamic recovery terms of the models. Time-dependency at room temperature and at 700°C was resumed where function  $\psi$  had no contribution to the ratcheting response of 304 steel samples. Over High-Low sequential loading, the ratcheting strain slightly dropped as the mean stress reduced in the transition from steps II to III. Experimental ratcheting data agreed with those predicted by means of the O-W and AV models over the first loading step. Deviations in the predicted ratcheting curves were more evident over steps II and III through use of the O-W model. The predicted ratcheting curves by the A-V model consistently followed the trend of measured values over consecutive loading steps. Time-dependent ratcheting responses of 304 steel samples was studied at an ambient temperature and an elevated temperature of 700°C while peak/valley holding times were applied. The inclusion of holding time effect resulted in creep-ratcheting and an elevation in ratcheting strain values. This escalation was accounted for through adhering an exponential function into the dynamic recovery terms of the O-W and A-V frameworks.

# CHAPTER FIVE

## CONCLUSIONS AND RECOMMENDATIONS

### 5.1. Conclusions

Ratcheting response of several steel alloys was evaluated through isotropic-kinematic hardening frameworks under various stress levels, stress rates, stress steps and sequences, operating temperatures and holding-times. Inclusion of isotropic hardening rules enabled the frameworks to follow the expansion of yield surface over asymmetric stress cycles. This adherence provided a more realistic prediction of ratcheting especially under multi-step stress loading conditions to address hardening/softening upon changes in stress levels. A unified visco-plastic flow rule was further incorporated into the framework to induce rate-dependency impact over ratcheting assessment of steel samples. Unlike elastic-plastic materials response, the visco-plastic flow rule calculated strain magnitudes at instants of applied stresses enabling hardening rules to account for rates at which stresses were applied. The use of visco-plastic flow rule was necessitated as stainless steel samples underwent the time-dependent deformation even at room temperature. The kinematic hardening rules were further developed to account for the effects of dynamic strain aging and static recovery. The former phenomenon occurred at elevated temperature resulting in rate-independency and the latter is the result of peak/valley holding times escalating magnitudes of ratcheting over stress cycles. The capability of the developed visco-plastic frameworks was compared to those of measured ratcheting values under various step-loading conditions.

The capabilities of the O-W and A-V frameworks to predict ratcheting strains and hysteresis loops in the absence and presence of isotropic descriptions were discussed through formulation and terms/coefficients. The frameworks of O-W and A-V models were constructed through use of initial and saturated yield surfaces. Once adhered to isotropic hardening, both

models resulted in comparable evolution of yield surfaces and predicted ratcheting curves. The dominance of isotropic model in assessing ratcheting over first ratcheting stage in 304 steel samples was discussed and their progressive stress-strain hysteresis loops within this stage were evaluated. Inclusion of isotropic models promoted change in the width of hysteresis loops and the loops resulting in higher strain values were moved forward. The predicted ratcheting results revealed that the adherence of the Iso-C model resulted in a closer agreement with experimental data over stage I of ratcheting. The predicted ratcheting strains and hysteresis loops based on the A–V framework were found in closer agreement with the experimental data as compared with those predicted through the O–W model.

Ratcheting response of austenitic stainless steel, 316L stainless, and U71Mn rail steels was evaluated by means of the A-V and O-W frameworks at various applied stress rates, stress levels, steps and sequences. Ratcheting progress of materials consistently increased in magnitude and rate over Low-High loading steps. However, ratcheting slightly dropped in magnitude as plastic strains were accumulated over High-Low loading steps. Ratcheting response was under-predicted through the O-W framework and the generated hysteresis loops possessed lower axial strain values as compared with experimental loops. The A-V model managed to predict ratcheting curves in closer agreements with measured values over loading steps. Hysteresis loops predicted by the A-V model agreed with size and width of measured hysteresis loops. Visco-plastic ratcheting response of SS304 samples tested at various step-loading conditions and rates demonstrated no/little time-dependency at operating temperatures between 350°C and 650°C. The minimized rate-dependency at this range of temperature was addressed through dynamic strain aging phenomenon leading to a sudden escalation of ratcheting strain once mean stress increased over Low-High loading sequence in the beginning of each loading step. The dynamic strain ageing was accounted for SS304 samples through inclusion of an exponential function  $\psi$  into the dynamic recovery term of the models. Time-dependency at room temperature and at 700°C was resumed where function  $\psi$  had no contribution in ratcheting response of 304 steel samples. Over High-Low sequential loading, ratcheting strain slightly dropped as mean stress reduced in steps II/III transition. This minor drop in ratcheting strain was associated to accumulative ratcheting strains over previous steps I and II. Experimental ratcheting data agreed with those of predicted by means of the O-W and A-V models over the first loading step. Deviations of the predicted ratcheting curves were

more evident over steps II and III through the use of the O-W model. The predicted ratcheting curves by the A-V model consistently followed trend of measured values over consecutive loading steps. In the presence of holding time at peak/valley of stress cycles, higher values of ratcheting strain were obtained. This increase was attributed to the static recovery effect caused through holding time at maximum and minimum stresses of each cycle. Inclusion of an exponential function into the dynamic recovery terms of the O-W and A-V models addressed the impact of static recovery effect and excess of predicted ratcheting strain values. The ratcheting curve predicted by the means of the A-V model at room temperature was more accurate as compared to the O-W model but both models developed curves in close agreement with obtained values at 700°C.

The predicted ratcheting curves for 304 steel samples tested at various operating temperatures were highly dependent upon the choice of kinematic hardening rules and their complexity in terms of coefficients determinations and algorithm. The A-V model is a less complex framework as compared to the O-W model since the former possesses merely three coefficients while the latter includes several coefficients to determine. Due to higher number of terms/coefficients in the O-W model, the CPU time required for ratcheting program was found to be longer than that of the A-V model.

## **5.2. Recommendations for future research**

Ratcheting phenomenon is substantially important for a reliable design of structural components undergoing asymmetric loading condition. The interaction of ratcheting and fatigue always results in severe damage and inexorable failure of load-bearing components. It is therefore essential for researchers to prioritize studies in the field of cyclic loading, particularly by concentrating on mechanistic parameters such as stress level and rate, mechanical properties, cyclic softening/hardening of materials, thermal stresses, non-proportionality under multiaxial loading conditions, microstructural characterization, and corrosive environment.

The present thesis was concentrated on developing a framework of a hardening rule to account for factors such as cyclic softening/hardening of materials, rate-dependency, operating

temperature and holding-time. More research work is recommended in the field of cyclic plasticity to attain reliable ratcheting assessment of materials at the presence of various affecting parameters. The following outlines some recommended research aspects which are lacking in literature:

- Further development of a dynamic recovery term is necessary to address dislocation interactions over the course of plastic strain accumulation. This involves microstructural features, dislocations pileups and interactions over loading and unloading paths as ratcheting is promoted over asymmetric stress cycles.
- Further investigation is required to fully address the creep-ratcheting phenomenon caused by the infusion of holding time at peak/valley of stress cycles.
- More investigations are necessary to address different types of loadings including thermal cycles and their influences on yield surface evolution. Yield surface distortion needs to be addressed as backstress increments are calculated in deviatoric stress space.
- Development of an FE code based on the Ahmadzadeh-Varvani (A-V) model in ANSYS software is required to enable researchers to employ the developed algorithm more readily.
- Literature lacks a comprehensive experimental data bank for ratcheting strain of materials under identical stress level and various stress rates, operating temperatures, and holding-times. To better understand the effect of dynamic strain aging more ratcheting experiments and examination of dislocation interaction over the loading process by the means of scanning electron microscopy (SEM) are required.

## APPENDIX A

Appendix A presents MATLAB programming code developed to assess ratcheting response of time-dependent materials under various stress levels, rates, steps and sequences, at room and elevated temperature, with an without peak/valley holding time. This program consists of the kinematic hardening rules of O-W and A-V adhered to the isotropic hardening rule of Chaboche on the basis of visco-plastic flow rule is incorporated. Table A.1 tabulates the symbols and terms utilized in the MATLAB programming codes.

**Table A.1.** Symbols and terms employed in the MATLAB programming

Symbol	Description
E	Young's modulus
$\nu$	Poisson's ratio
$n$	Unit normal tensor to stress surface
$D\sigma$	Stress tensor increment
$\epsilon$	Total strain
$D\epsilon$	Total strain increment
$D\epsilon_e$	Elastic strain increment
$D\epsilon_p$	Plastic strain increment
$Ddev\_Sig$	Deviatoric stress increment
H	Plastic modulus
a	Backstress
Da	Backstress increment
Db	Second internal variable increment
Cb2	Constant g2
Cb1	Constant g1
Ab	Constant C
a <sub>exx</sub>	Axial ratcheting strain
D	Drag stress
Nn	Viscous Exponent
Sit	Dynamic strain aging function
La, Bi	Coefficients of static recovery function
Qq, Q0, Qm, mm, Bb, NU	Isotropic hardening coefficients

## Main program

```
clc
clear all
% -----
fh = figure('Name','Stress courses generation',...
    'Position',[0,40,990,650],...
    'Resize','off',...
    'Toolbar','none',...
    'Menubar','none','Color',[0.941176 0.941176 0.941176]);
panel3 = uipanel('Parent',fh,'Title','Hystersis loops',...
    'Position',[.62 .52 .37 .48]);
axeshLoop = axes('Parent',panel3,'units','normalized',...
    'Box','on',...
    'FontSize',8,...
    'Position',[0.15 0.15 0.81 0.82]);
hLoop=plot(0,0,'-k',0,0,'-r',0,0,'ok',0,0,'or');
xlabel('\epsilon(%), -')
ylabel('\sigma(t), \tau(t), MPa')
% -----
[t, Sig, Tau, mate] = test;
% -----
panel4 = uipanel('Parent',fh,'Title','Yield surfaces',...
    'Position',[.62 .01 .37 .51]);
axeshSurf = axes('Parent',panel4,'units','normalized',...
    'Box','on',...
    'FontSize',8,...
    'Position',[0.13 0.14 0.83 0.83],...
    'XLim',[-1000 1000],...
    'YLim',[-1000 1000]);
set(get(axeshSurf,'xlabel'),'string','\surd 3 \tau(t), MPa','fontsize',8)
set(get(axeshSurf,'ylabel'),'string','\sigma(t), MPa','fontsize',8)
grid on
fi=0:pi/80:2*pi;
x=mate.R*cos(fi);
y=mate.R*sin(fi);
hp=patch(x,y,4); hold on,
h=plot(0,0,'ok','markerfacecolor','r','markersize',8);
hz=plot(0,0,'--b');
axis equal
axis manual
% -----
i=0;
a=zeros(1,9);
b=a;
DEps_p=zeros(1,9);
aa=zeros(length(t), 9);
am(1:length(mate.R),9)=0;
ar=a;
Eps=zeros(length(t),9);
Eps_p=zeros(length(t),9);
Debuging=zeros(length(t), 29);
DP=0;
```

```

Pp=0;
for j=1:length(t)-1,
Sig_start=[Sig(j) 0 0 Tau(j) 0 0 Tau(j) 0 0];
Dsig=[Sig(j+1)-Sig(j) 0 0 Tau(j+1)-Tau(j) 0 0 Tau(j+1)-Tau(j) 0 0];
[Debuging,DEps, i, a, ar, DEps_p, b,DP, Pp]=calculation(Sig_start, Dsig, i,
a, mate,j,Debuging, ar, DEps_p,b, DP, Pp);
Eps(j+1,:)=Eps(j,:)+DEps;
Eps_p(j+1,:)=Eps_p(j,:)+DEps_p;
aa(j+1,:)=a;
% -----
set(hLoop(1),'xdata',Eps(1:j+1,1)*100,'ydata',Sig(1:j+1))
set(hLoop(2),'xdata',Eps(1:j+1,4)*100,'ydata',Tau(1:j+1))
set(hLoop(3),'xdata',Eps(j+1,1)*100,'ydata',Sig(j+1))
set(hLoop(4),'xdata',Eps(j+1,4)*100,'ydata',Tau(j+1))
drawnow expose
% -----
ay=1.5*aa(j+1,1);
ax=sqrt(3)*aa(j+1,4);
set(hp,'xdata',x+ax,'ydata',y+ay)
set(h,'ydata',Sig(j+1),'xdata',sqrt(3)*Tau(j+1))
j=round(j/50)
end
k=1;
z=1;
% -----Ratcheting Calculation-----
for j=1:length(t)
if rem(t(j),.05)==0
Mexx(z,1)=max(Eps(k:j,1));
Nexx(z,1)=min(Eps(k:j,1));
aexx(z,1)=(Mexx(z,1)+Nexx(z,1))*100/2;
Mexy(z,1)=max(Eps(k:j,4));
Nexy(z,1)=min(Eps(k:j,4));
aexy(z,1)=(Mexy(z,1)+Nexy(z,1))*100/2;
k=j+1;
z=z+1;
end
end
end

```

## Calculation Subroutine

```

function [Debuging,DEps, i, a, ar, DEps_p, b,DP, Pp]=calculation(Sig_start,
Dsig, i, a, mate,j,Debuging, ar, DEps_p,b, DP, Pp);

%----- material data-----%
    Bi=?;
    La=?;
    Qq=?;
    Bb=?;
    NU=?;
    Qm=?;
    Qo=?;
    mm=?;
    A=?;
    Rr=?;
    T=?;
    SIt=?;
    BB=?;
    E=mate.E;
    ni=mate.ni;
    G=E/(2*(1+ni));
    R=mate.R+Qq.*(1-exp(-Bb.*Pp));
    SI=SIt+(1-SIt)*exp(-BB*Pp);
% -----%
Ab=?;
Cb1=?;
Cb2=?;
m=?
Delta=(Ab/Cb1);
ri_gama=?
Mi=?
D=?;
Nn=?;
%-----%
    Ddev_Sig=dev(Dsig);
    dev_Sig_start=dev(Sig_start);
%-----%
    n=nn(dev_Sig_start, a, i);
%-----%
    A_dew=dev_Sig_start;
    C_dew=A_dew+Ddev_Sig;
%-----%
    [n ,i, ar]=PlasticityCond(i, A_dew, n, a, ar, R);
%-----%
    DEps_p=zeros(1,9);
    Ff=sqrt(F(A_dew,a))-R;
%-----%
    if Ff>0
        if i==0
            A_dew=verify_A(A_dew, a, R);
            [B_dew]=intersection(A_dew, C_dew, a, R);
            A_dew=B_dew;
            AC_dew=C_dew-A_dew;

```

```

        i=i+1;
        n=nn(A_dew, a, i);
        [D_strain_p]=Delta_Strain_p(Ff, i, n, D, Nn);
        [Da,b,Db, a]=shiftsurface(Ab,Cb1,Cb2, D_strain_p, a, b, Delta,
La, Bi, m);
        a=a+Da;
        DEps_p=D_strain_p;
    else
        n=nn(dev_Sig_start, a, i);
        [D_strain_p]=Delta_Strain_p(Ff, i, n, D, Nn);
        [Da,b,Db, a]=shiftsurface(Ab,Cb1,Cb2, D_strain_p, a, b, Delta,
La, Bi, m);
        a=a+Da;
        DEps_p=D_strain_p;
    end
end
end
%-----%
DEps_e=hooklaw(Dsig, 'stress_strain', E, ni);
DEps=DEps_e+DEps_p;
end
%-----%
function n=nn(A_dew, a, i)
if i>0
    n=(A_dew-a(1,:))/norm(A_dew-a(1,:));    %eq. (20)
else
    n=[];
end
end
%-----%
function [n ,i, ar]=PlasticityCond(i, C_dew, n, a, ar, R)
if i>0
    if sqrt(F(C_dew,a))-R<0
        i=0;
        n=[];
        ar=a;
    end
else
    n=n;
    i=i;
    ar=ar;
end
end
end
%----- Yield function: Von Mises -----%
function y=F(s, aa)
y=(3/2)*(s-aa)*(s-aa)';
end
%-----Visco-Plastic strain increments (flow rule)-----%
function [D_strain_p]=Delta_Strain_p(Ff, i, n, D, Nn)
H=(Ff/D)^Nn;
D_strain_p=sqrt(3/2)*H*n;
end
%----- A-V Hardening Rule -----%

```

```

function [Da,b,Db,a]=shiftsurface(Ab,Cb1,Cb2, D_strain_p, a, b, Delta, La,
Bi)
    Db=Cb2*(a-1*b)*sqrt(((2/3)*(D_strain_p*D_strain_p')));
    b=b+Db;
    Da=(1/1)*Ab*D_strain_p-
    ((Cb1*sqrt(((2/3)*(D_strain_p*D_strain_p'))))+La*((sqrt(((3/2)*(a*a'))))^ (Bi-
1))) * (a-(sqrt(a)/Delta)^m)*b);
End
%----- O-W Hardening Rule -----%
function [Da,ai]=shiftsurface(D_strain_p, a,ai,Dai_t,Hi_t,ri_gama,M,mi, La,
Bi)
for z=1:M
    if ai(z,')==0
        dp_OW_i=0;
    else
        dp_OW_i=D_strain_p*(ai(z,+)/sqrt((ai(z,)*ai(z,)'')));
    end
    if dp_OW_i<0
        dp_OW_i=0;
    end

    Dai=ri_gama(z,2)*[(2/3)*ri_gama(z,1)*D_strain_p((sqrt((ai(z,)*ai(z,)'
)))/ri_gama(z,1))^mi*ai(z,)*dp_OW_i]-
    (La*((sqrt(((3/2)*(ai(z,)*ai(z,)''))))^ (Bi-1))) * ai(z,);
    Dai_t(z,)=Dai;
    ai(z,)=ai(z,)+Dai;
end
Da=sum(Dai_t);
end
%-----Shape memory function: Based on Chaboche 1979-----%
function [qq,dq,si,dsi]=shape(Eps_p, si, qq, n, D_strain_p, j, NN, NU)
    SS=(2/3)*((Eps_p(j,)-si(j,))*(Eps_p(j,)-si(j,)''));
    if SS-(qq^2)>=0
        N=(Eps_p(j,)-si(j,))/norm(Eps_p(j,)-si(j,));
        if n*N'>=0
            dq=NU*(n*N')*sqrt(((2/3)*(D_strain_p*D_strain_p')));
            dsi=sqrt(3/2)*(1-
NU)*(n*N')*N*sqrt(((2/3)*(D_strain_p*D_strain_p')));
        else
            dsi=zeros(1,9);
            dq=0;
        end
    else
        dsi=zeros(1,9);
        dq=0;
    end
    qq=dq+qq;
    si(j+1,)=si(j,)+dsi;
end
%-----%
function [B_dew, k0]=intersection(DewLower, DewHigher, aa, RR)
w(1)=(DewHigher-DewLower)*(DewHigher-DewLower)'; w(2)=2*(DewLower-
aa)*(DewHigher-DewLower)'; w(3)=(DewLower-aa)*(DewLower-aa)'-(2/3)*RR^2;
k0=roots(w); k0=max(k0); k0=k0(1);

```

```
B_dew=DewLower+k0*(DewHigher-DewLower);
end
%-----%
function A_dew=verify_A(A_dew, aa, RR)
delta=(1e-012)*(A_dew-aa);
if F(A_dew, aa)-RR^2>=0,
    [A_dew]=intersection(aa, A_dew, aa, RR);
    A_dew=A_dew-delta;
else
end
end
end
```

## Material properties subroutine

```
function mate = matproperty

fh = figure('Name','Material properties,...
    'Position',[100,150,640,500],...
    'Resize','off',...
    'ToolBar','none',...
    'Menubar','none','Color',[0.941176 0.941176 0.941176]);
panell = uipanel('Parent',fh,'Title','Coefficients',...
    'Position',[.01 .66 .98 .32]);
Dtextedit=0.18;
y1=0.55; %first row
y2=0.08; %second row
%--Young modulus-----%
edithE = uicontrol(panell,'Style','edit',...
    'Units','normalized',...
    'String','210000',...
    'BackgroundColor','white',...
    'FontSize',9,...
    'Position',[0.02 y1 0.2 Dtextedit]);
textxE = uicontrol(panell,'Style','text',...
    'Units','normalized',...
    'String','Young modulus, MPa',...
    'Position',[0.02 0.76 0.2 0.14]);
%--Poisson ratio-----%
edithni = uicontrol(panell,'Style','edit',...
    'Units','normalized',...
    'String','0.3',...
    'BackgroundColor','white',...
    'FontSize',9,...
    'Position',[0.02 y2 0.2 Dtextedit]);
textxni = uicontrol(panell,'Style','text',...
    'Units','normalized',...
    'String','Poisson ratio, -',...
    'Position',[0.02 0.27 0.2 0.14]);
%--Coefficient of cyclic hardening, K'-----%
edithK = uicontrol(panell,'Style','edit',...
    'Units','normalized',...
    'String','1485',...
    'BackgroundColor','white',...
    'FontSize',9,...
    'Position',[0.27 y1 0.2 Dtextedit]);
textxK = uicontrol(panell,'Style','text',...
    'Units','normalized',...
    'String','Coefficient of cyclic hardening, K'', MPa',...
    'Position',[0.27 0.76 0.2 0.23]);
%--Yield stress-----%
edithSigy = uicontrol(panell,'Style','edit',...
    'Units','normalized',...
    'String','449',...
    'BackgroundColor','white',...
    'FontSize',9,...
```

```

    'Position',[0.27 y2 0.2 Dtextedit]);
texthSigy = uicontrol(panell1,'Style','text',...
    'Units','normalized',...
    'String','Yield stress, MPa',...
    'Position',[0.27 0.27 0.2 0.14]);
%--Exponent of cyclic hardening, n'-----%
edithn = uicontrol(panell1,'Style','edit',...
    'Units','normalized',...
    'String','0.17',...
    'BackgroundColor','white',...
    'FontSize',9,...
    'Position',[0.52 y1 0.2 Dtextedit]);
texthn = uicontrol(panell1,'Style','text',...
    'Units','normalized',...
    'String','Exponent of cyclic hardening, n'', -',...
    'Position',[0.52 0.76 0.2 0.23]);
%--Radius increment of yield surfaces-----%
edithDSig = uicontrol(panell1,'Style','edit',...
    'Units','normalized',...
    'String','50',...
    'BackgroundColor','white',...
    'FontSize',9,...
    'Position',[0.52 y2 0.2 Dtextedit]);
texthDSig = uicontrol(panell1,'Style','text',...
    'Units','normalized',...
    'String','Radius increment of yield surfaces, MPa',...
    'Position',[0.52 0.27 0.2 0.23]);
%--Maximum stress, MPa-----%
edithSigmax = uicontrol(panell1,'Style','edit',...
    'Units','normalized',...
    'String','900',...
    'BackgroundColor','white',...
    'TooltipString','Maximum stress must be higher than Yield stress !',...
    'FontSize',9,...
    'Position',[0.77 y1 0.2 Dtextedit]);
texthSigmax = uicontrol(panell1,'Style','text',...
    'Units','normalized',...
    'String','Maximum stress, MPa',...
    'TooltipString','Maximum stress must be higher than Yield stress !',...
    'Position',[0.77 0.76 0.2 0.23]);
axesh = axes('Parent',fh,'units','normalized',...
    'Box','on',...
    'FontSize',8,...
    'Position',[0.1 0.11 0.86 0.51]);
set(get(axesh,'xlabel'),'string','\epsilon_a', -,'fontsize',8)
set(get(axesh,'ylabel'),'string','\sigma_a, MPa','fontsize',8)
%---buttons-----%
bhApply = uicontrol(fh,'Units','normalized',...
    'Position',[0.81 0.23 0.13 0.08],...
    'String','Apply',...
    'Callback',@buttonApply);
bhOk = uicontrol(fh,'Units','normalized',...
    'Position',[0.81 0.13 0.13 0.08],...
    'String','OK',...

```

```

        'Callback',@buttonOK);
uiwait(fh);
%-----%
function buttonApply(hObject,eventdata)
    mate.E=str2double(get(edithE,'String'));
    mate.K=str2double(get(edithK,'String'));
    mate.n=str2double(get(edithn,'String'));
    mate.ni=str2double(get(edithni,'String'));
    mate.Sig_y=str2double(get(edithSigy,'String'));
    mate.DSig=str2double(get(edithDSig,'String'));
    mate.Sigmax=str2double(get(edithSigmax,'String'));
    if mate.Sigmax<mate.Sig_y,
        f = warndlg('Maximum stress must be higher than the yield
stress.', 'Warning');
        mate.Sigmax=mate.Sig_y+mate.DSig;
        set(edithSigmax,'string',num2str(mate.Sigmax))
        uiwait(f)
    end
    Sig_ai=[0:5:mate.Sigmax];
    Eps_ai=Sig_ai/mate.E+(Sig_ai/mate.K).^(1/mate.n);
    Sig_a=[0 mate.Sig_y:mate.DSig:mate.Sigmax];
    Eps_a=Sig_a/mate.E+(Sig_a/mate.K).^(1/mate.n);
    %axes(axesh)
    plot(Eps_ai,Sig_ai,'-k',Eps_a,Sig_a,'+-b')
    xlabel('\epsilon_a, -')
    ylabel('\sigma_a, MPa')
    H=zeros(length(Sig_a)-2,1);
    for i=2:length(Sig_a)-1,
        H(i-1,1)=((3/2)*((Eps_a(i+1)-Eps_a(i))/(Sig_a(i+1)-Sig_a(i)))-
1/mate.E)^-1;
    end
    R=Sig_a(2:end)';
    mate.R=mate.Sig_y;
    mate.H=H;
end
%-----%
function buttonOK(hObject,eventdata)
    close(fh)
end
end

```

## Stress generation subroutine

```
function [t, Sig, Tau, mate] = test
global smax
fh = figure('Name','Stress courses generation',...
    'Position',[300,200,1000,618],...
    'Resize','on',...
    'Toolbar','none',...
    'Menubar','none','Color',[.8 .91 1]);
panell1 = uipanel('Parent',fh,'Title','Sinusoidal stress signals',...
    'Position',[.01 .79 .45 .20],'backgroundColor',[.8 .86 1],'FontWeight',
'bold');
panel2 = uipanel('Parent',fh,'Title','Time signal',...
    'Position',[.01 .58 .16 .20],'backgroundColor',[.8 .86 1],'FontWeight',
'bold');
panel3 = uipanel('Parent',fh,'Title','Slow start',...
    'Position',[.19 .58 .14 .20],'backgroundColor',[.8 .86 1],'FontWeight',
'bold');
panel4=uipanel('parent', fh, 'Title', 'Material Properies',...
    'Position',[.01 .05 .45 .35],'backgroundColor',[.8 .86 1],'FontWeight',
'bold');
%--Equations-----%
axeshSiga = axes('Parent',panell1,'units','pixels',...
    'Position',[7 53 136 26]);
image(imread('stresseq1.jpg','jpg'));
set(gca,'visible','off')
axeshTaua = axes('Parent',panell1,'units','pixels',...
    'Position',[9 12 136 26]);
image(imread('stresseq2.jpg','jpg'));
set(gca,'visible','off')
%--Sig_a and Tau_a-----%
texthSiga = uicontrol(panell1,'Style','text',...
    'Units','pixels',...
    'String','Stress levels (MPa)',...
    'Position',[145 85 70 27],...
    'backgroundColor',[.8 .86 1]);
edithSiga = uicontrol(panell1,'Style','edit',...
    'Units','pixels',...
    'String','400',...
    'BackgroundColor','white',...
    'FontSize',9,...
    'Position',[155 52 52 27]);
edithTaua = uicontrol(panell1,'Style','edit',...
    'Units','pixels',...
    'String','0',...
    'BackgroundColor','white',...
    'FontSize',9,...
    'Position',[155 11 52 27]);
%--Mean Stresses-----%
texthSigm = uicontrol(panell1,'Style','text',...
    'Units','pixels',...
    'String','Mean Stresses (MPa)',...
    'Position',[220 85 90 27],...
    'backgroundColor',[.8 .86 1]);
```

```

edithSigm = uicontrol(panell1,'Style','edit',...
    'Units','pixels',...
    'String','100',...
    'BackgroundColor','white',...
    'FontSize',9,...
    'Position',[237 52 52 27]);
edithTaum = uicontrol(panell1,'Style','edit',...
    'Units','pixels',...
    'String','0',...
    'BackgroundColor','white',...
    'FontSize',9,...
    'Position',[237 12 52 27]);
%--Frequencies-----%
texthfsig = uicontrol(panell1,'Style','text',...
    'Units','pixels',...
    'String','Frequencies (Hz)',...
    'Position',[310 85 66 27],...
    'backgroundColor',[.8 .86 1]);
edithfsig = uicontrol(panell1,'Style','edit',...
    'Units','pixels',...
    'String','20',...
    'BackgroundColor','white',...
    'FontSize',9,...
    'Position',[315.5 52 52 27]);
edithftau = uicontrol(panell1,'Style','edit',...
    'Units','pixels',...
    'String','20',...
    'BackgroundColor','white',...
    'FontSize',9,...
    'Position',[315.5 12 52 27]);
%--Phase shift, rad-----%
texthd = uicontrol(panell1,'Style','text',...
    'Units','pixels',...
    'String','Phase shift (rad)',...
    'Position',[380 42 60 27],...
    'backgroundColor',[.8 .86 1]);
edithd = uicontrol(panell1,'Style','edit',...
    'Units','pixels',...
    'String','0',...
    'BackgroundColor','white',...
    'FontSize',9,...
    'Position',[383 12 52 27]);
%--Time signal-----%
edithS = uicontrol(panel2,'Style','edit',...
    'Units','pixels',...
    'String','1000',...
    'BackgroundColor','white',...
    'FontSize',9,...
    'Position',[50 55 52 27]);
texthS = uicontrol(panel2,'Style','text',...
    'Units','pixels',...
    'String','Frequency sampling (Hz)',...
    'Position',[10 85 140 16],...
    'backgroundColor',[.8 .86 1]);

```

```

edithL = uicontrol(panel2,'Style','edit',...
    'Units','pixels',...
    'String','.5',...
    'BackgroundColor','white',...
    'FontSize',9,...
    'Position',[50 5 52 27]);
textL = uicontrol(panel2,'Style','text',...
    'Units','pixels',...
    'String','Length (s)',...
    'Position',[45 35 60 16],...
    'backgroundColor',[.8 .86 1]);
%--Main axes-----%
axesh = axes('Parent',fh,'units','normalized',...
    'Box','on',...
    'FontSize',8,...
    'Position',[0.525 0.525 0.45 0.45]);
set(get(axesh,'xlabel'),'string','Time, s','fontSize',8)
set(get(axesh,'ylabel'),'string','\sigma(t), \tau(t), MPa','fontSize',8)
%--Young modulus-----%
textxE = uicontrol(panel4,'Style','text',...
    'Units','pixels',...
    'String','Young modulus (MPa)',...
    'Position',[10 165 80 27],...
    'backgroundColor',[.8 .86 1]);
% SS304: 190GPa, , 42CrMo:190.5GPa, SS316L:190GPa, Copper:129
edithE = uicontrol(panel4,'Style','edit',...
    'Units','pixels',...
    'String','190000',...
    'BackgroundColor','white',...
    'FontSize',9,...
    'Position',[20 133 62 27]);
%--Poisson ratio-----%
textxni = uicontrol(panel4,'Style','text',...
    'Units','pixels',...
    'String','Poisson ratio',...
    'Position',[95 165 80 27],...
    'backgroundColor',[.8 .86 1]);
edithni = uicontrol(panel4,'Style','edit',...
    'Units','pixels',...
    'String','0.3',...
    'BackgroundColor','white',...
    'FontSize',9,...
    'Position',[105 133 62 27]);
%--Coefficient of cyclic hardening, K'-----%
textxK = uicontrol(panel4,'Style','text',...
    'Units','pixels',...
    'String','Coefficient of cyclic hardening, K'' (MPa)',...
    'Position',[180 165 100 27],...
    'backgroundColor',[.8 .86 1]);
% SS304: 1628 MPa, 42CrMo:637, SS316L:2755GPa, Copper:?
edithK = uicontrol(panel4,'Style','edit',...
    'Units','pixels',...
    'String','1628',...
    'BackgroundColor','white',...

```

```

        'FontSize',9,...
        'Position',[198 133 62 27]);
%--Exponent of cyclic hardening, n'-----%
texthn = uicontrol(panel4,'Style','text',...
    'Units','pixels',...
    'String','Exponent of cyclic hardening, n'',...
    'Position',[280 165 100 27],...
    'backgroundColor',[.8 .86 1]);
% SS304: 0.291, 42CrMo:0.097, SS316L:0.388, Copper:?
edithn = uicontrol(panel4,'Style','edit',...
    'Units','pixels',...
    'String','0.291',...
    'BackgroundColor','white',...
    'FontSize',9,...
    'Position',[298 133 62 27]);
%--Yield stress-----%
texthSigy = uicontrol(panel4,'Style','text',...
    'Units','pixels',...
    'String','Yield stress (MPa)',...
    'Position',[10 75 80 27],...
    'backgroundColor',[.8 .86 1]);
% SS304: 209 MPa, 42CrMo:310MPa, SS316L:285MPa, Copper:60
edithSigy = uicontrol(panel4,'Style','edit',...
    'Units','pixels',...
    'String','290',...
    'BackgroundColor','white',...
    'FontSize',9,...
    'Position',[20 43 62 27]);
%--Maximum stress, MPa-----%
texthSigmax = uicontrol(panel4,'Style','text',...
    'Units','pixels',...
    'String','Maximum stress (MPa)',...
    'TooltipString','Maximum stress must be higher than Yield stress !',...
    'Position',[95 75 80 27],...
    'backgroundColor',[.8 .86 1]);
edithSigmax = uicontrol(panel4,'Style','edit',...
    'Units','pixels',...
    'String','900',...
    'BackgroundColor','white',...
    'TooltipString','Maximum stress must be higher than Yield stress !',...
    'FontSize',9,...
    'Position',[104 43 62 27]);
%--Module of Plasticity , MPa-----%
texthmplastic = uicontrol(panel4,'Style','text',...
    'Units','pixels',...
    'String','Plastic Modulus (MPa)',...
    'TooltipString','Maximum stress must be higher than Yield stress !',...
    'Position',[295 75 100 27],...
    'backgroundColor',[.8 .86 1]);
edithmplastic = uicontrol(panel4,'Style','edit',...
    'Units','pixels',...
    'String','to be calculated',...
    'BackgroundColor','white',...
    'FontSize',9,...

```

```

    'Position',[294 43 100 27]);
%--Main axes-----%
axesh2 = axes('Parent',fh,'units','normalized',...
    'Box','on',...
    'FontSize',8,...
    'Position',[0.525 0.06 0.45 0.40]);
set(get(axesh2,'xlabel'),'string','\epsilon_a',-,'fontsize',8)
set(get(axesh2,'ylabel'),'string','\sigma_a, MPa','fontsize',8)
%---buttons-----%
bhSlow = uicontrol(panel3,'Units','normalized',...
    'Position',[0.22 0.64 0.54 0.32],...
    'String','Slow start',...
    'Enable','off',...
    'Callback',@buttonSlow);
texthSlow = uicontrol(panel3,'Style','text',...
    'Units','normalized',...
    'String','During time (s)',...
    'Position',[0.2 0.4 0.6 0.14],...
    'backgroundColor',[.8 .86 1]);
edithSlow = uicontrol(panel3,'Style','edit',...
    'Units','normalized',...
    'String','0.010',...
    'BackgroundColor','white',...
    'FontSize',9,...
    'Position',[0.28 0.1 0.4 .24]);
bhApply = uicontrol(fh,'Units','normalized',...
    'Position',[.35 .66 0.05 0.05],...
    'String','Apply',...
    'Callback',@buttonApply);
bhOk = uicontrol(fh,'Units','normalized',...
    'Position',[0.92 0.07 0.05 0.05],...
    'String','OK',...
    'Callback',@buttonOK);
%---buttons-----%
hh= uicontrol(panel4,'Units','pixel',...
    'Position',[380 10 55 30],...
    'String','Apply',...
    'Callback',@buttonApply2);
uiwait(fh);
%-----%
function buttonApply(hObject,eventdata)

    Sig_a=str2double(get(edithSiga,'String'));
    Tau_a=str2double(get(edithTaua,'String'));
    fsig=str2double(get(edithfsig,'String'));
    ftau=str2double(get(edithftau,'String'));
    delta=eval(get(edithd,'String'));
    fs=str2double(get(edithS,'String'));
    T=str2double(get(edithL,'String'));
    Sig_mean=str2double(get(edithSigm,'String'));
    Tau_mean=str2double(get(edithTaum,'String'));
    t=0:1/fs:T;
    Tau=Tau_a*sin(2*pi*ftau*(t+0)-delta)+ Tau_mean;
%-----without holding time-----%

```

```

for i=1:length(t),
    if t(i)<= (1/fsig)

        if t(i)<= (1/(4*fsig))
            Sig(i)= ((Sig_a)/(1/(4*fsig)))*t(i)+Sig_mean;
        elseif t(i)<= (3/(4*fsig))
            Sig(i)=
                (- (Sig_a)/(1/(4*fsig)))*(t(i)-
(1/(4*fsig)))+Sig_a+Sig_mean;%- ((2*Sig_a)/(1/(4*fsig)))*(t(i)-
(1/(4*fsig)))+Sig_a+Sig_mean;
        else
            Sig(i)=
                ((Sig_a)/(1/(4*fsig)))*(t(i)-(3/(4*fsig)))-
Sig_a+Sig_mean;% -((2*Sig_a)/(1/(4*fsig)))*(t(i)-(3/(4*fsig)))+Sig_a+Sig_mean;

        end

    else
        equ_i=t(i)-floor(t(i)./(1/(fsig)))*(1/(fsig));

        if equ_i<= (1/(4*fsig))
            Sig(i)= ((Sig_a)/(1/(4*fsig)))*equ_i+Sig_mean;
        elseif equ_i<= (3/(4*fsig))
            Sig(i)=
                (- (Sig_a)/(1/(4*fsig)))*(equ_i-
(1/(4*fsig)))+Sig_a+Sig_mean;
        else
            Sig(i)=
                ((Sig_a)/(1/(4*fsig)))*(equ_i-(3/(4*fsig)))-
Sig_a+Sig_mean;%
                -((2*Sig_a)/(1/(4*fsig)))*(equ_i-
(3/(4*fsig)))+Sig_a+Sig_mean;

        end

    end

end

%-----with holding time-----%
for i=1:length(t),
    if t(i)<= (1/fsig)

        if t(i)<= (10/(60*fsig))
            Sig(i)= ((Sig_a)/(10/(60*fsig)))*t(i)+Sig_mean;
        elseif t(i)<= (20/(60*fsig))
            Sig(i)= Sig_a+Sig_mean;
        elseif t(i)<= (40/(60*fsig))
            Sig(i)= (- (Sig_a)/(10/(60*fsig)))*(t(i)-
(20/(60*fsig)))+Sig_a+Sig_mean;%- ((2*Sig_a)/(1/(4*fsig)))*(t(i)-
(1/(4*fsig)))+Sig_a+Sig_mean;
        elseif t(i)<= (50/(60*fsig))
            Sig(i)= -Sig_a+Sig_mean;
        else
            Sig(i)= ((Sig_a)/(10/(60*fsig)))*(t(i)-(50/(60*fsig)))-
Sig_a+Sig_mean;% -((2*Sig_a)/(1/(4*fsig)))*(t(i)-
(3/(4*fsig)))+Sig_a+Sig_mean;

        end

    end

```

```

else
    equ_i=t(i)-floor(t(i)./(1/(fsig)))*(1/(fsig));

    if equ_i<= (10/(60*fsig))
        Sig(i)= ((Sig_a)/(10/(60*fsig)))*equ_i+Sig_mean;
    elseif equ_i<= (20/(60*fsig))
        Sig(i)= Sig_a+Sig_mean;
    elseif equ_i<= (40/(60*fsig))
        Sig(i)= -(Sig_a)/(10/(60*fsig))*(equ_i-
(20/(60*fsig)))+Sig_a+Sig_mean;
    elseif equ_i<= (50/(60*fsig))
        Sig(i)= -Sig_a+Sig_mean;
    else
        Sig(i)= ((Sig_a)/(10/(60*fsig)))*(equ_i-(50/(60*fsig)))-
Sig_a+Sig_mean; % -((2*Sig_a)/(1/(4*fsig)))*(equ_i-
(3/(4*fsig)))+Sig_a+Sig_mean;

    end

end

end
end
%-----%
axes(axesh)
plot(t,Sig,'.-k',t,Tau,'.-r')
xlabel('Time, s')
ylabel('\sigma(t), \tau(t), MPa')
legend('\sigma(t)', '\tau(t)')
axis tight
set(bhSlow,'Enable','on')
smax= max(abs(Sig));

end
%-----%
function buttonSlow(hObject,eventdata)
T=str2double(get(edithL,'String'));
T0=str2double(get(edithSlow,'String'));
fs=str2double(get(edithS,'String'));

if T0>T,
    f = warndlg('Time of slow start cannot be longer than time of
stress signals.', 'Warning');
    T0 = T;
    set(edithSlow,'string',num2str(T0))
    uiwait(f)
end
nr=T0*fs;
X=[Sig' Tau'];
w=sin([0:pi/2/nr:pi/2]');
w=w*ones(1,size(X,2));
X(1:size(w,1),:)=w.*X(1:size(w,1),:);
Sig=X(:,1)';
Tau=X(:,2)';
plot(t,Sig,'.-k',t,Tau,'.-r')
xlabel('Time, s')
ylabel('\sigma(t), \tau(t), MPa')

```

```

        legend('\sigma(t)', '\tau(t)')
        axis tight
    end
%-----%
    function buttonOK(hObject,eventdata)
        close(fh)
    end
%-----%
    function buttonApply2(hObject2,eventdata2)
        mate.E=str2double(get(edithE,'String'));
        mate.K=str2double(get(edithK,'String'));
        mate.n=str2double(get(edithn,'String'));
        mate.ni=str2double(get(edithni,'String'));
        mate.Sig_y=str2double(get(edithSigy,'String'));
%       mate.DSig=str2double(get(edithDSig,'String'));
        mate.Sigmax=str2double(get(edithSigmax,'String'));
        mate.R=mate.Sig_y;
        if mate.Sigmax<mate.Sig_y,
            f = warndlg('Maximum stress must be higher than the yield
stress.', 'Warning');
            mate.Sigmax=mate.Sig_y+mate.DSig;
            set(edithSigmax,'string',num2str(mate.Sigmax))
            uiwait(f)
        end
        Sig_ai=[0:5:mate.Sigmax];
        Eps_ai=Sig_ai/mate.E+(Sig_ai/mate.K).^(1/mate.n);
        Eps_a=mate.Sig_y/mate.E+(mate.Sig_y/mate.K).^(1/mate.n);
        Eps_b=smax/mate.E+(smax/mate.K).^(1/mate.n);
        mate.C=((3/2)*(((Eps_b-Eps_a)/(smax-mate.Sig_y))-1/mate.E))^-1
        axes(axesh2)
        plot(Eps_ai,Sig_ai,'-k',[Eps_a,Eps_b],[mate.Sig_y,smax],'+-b')
        xlabel('\epsilon_a, -')
        ylabel('\sigma_a, MPa')
        set(edithmplastic,'string',num2str(mate.C))
    end
end
end

```

## Deviatoric stress subroutine

```
%----- Deviatoric stress calculation, Equation (3.6) -----%
function s=dev(t);
error(nargchk(1,1,nargin))
[m n]=size(t);
if n==3
    I=[1 1 1];
elseif n==6
    I=[1 1 1 0 0 0];
elseif n==9
    I=[1 1 1 0 0 0 0 0 0];
else
    error('Improper matrix dimension')
end
s=t-((1/3)*(t*I'))*I;
```

## Hook's law subroutine

```
%----- Elastic strain calculation, Equation (3.4) -----%
function Y=hooklaw(X, td, E, ni);
error(nargchk(4,4,nargin))
[m n]=size(X);
if n==3
    I=[1 1 1];
elseif n==6
    I=[1 1 1 0 0 0];
elseif n==9
    I=[1 1 1 0 0 0 0 0 0];
else
    error('Improper matrix dimension')
end
if lower(td)=='stress_strain'
    Y=((1+ni)/E)*(X-(ni/(1+ni))*(X*I')*I);
elseif lower(td)=='strain_stress'
    Y=(E/(1+ni))*(X+(ni/(1-2*ni))*(X*I')*I);
else
    error('Improper name of transform direction')
end
```

## APPENDIX B

Experimental data employed in chapter four to evaluate ratcheting response of various steel samples are listed in Appendix B. Table B.1 presents mechanical properties of 304, austenitic Z2CND18.12N, U71Mn, and 316L steels examined in this thesis. Experimental ratcheting data in Table B.2 and Table B.3 were used to determine the influence of coupling isotropic and kinematic hardening rules. Table B.4 and Table B.5 tabulates ratcheting strain data for samples for austenitic steel Z2CND18.12N samples with respectively constant stress amplitude and mean stress. Experimental ratcheting strain data presented in Table B.6 and Table B.7 were utilized to evaluate capability of the visco-plastic framework of O-W and A-V in ratcheting response of steel samples with constant stress level and various stress rates. Table B.8 through Table B.13 lists experimentally obtained ratcheting strains of samples of SS304, SS316L and U71Mn samples subjected to various step loading spectra at room temperature, while Table B.15 through Table B.18 presents experimental ratcheting data for SS304 samples under multi-step loading condition at various elevated temperatures.

**Table B.1** Mechanical properties of studied materials

Material	$\sigma_y$ (MPa)	$E$ (GPa)	$K'$ (MPa)	$n'$
SS304 [69,70]	270	209	560	0.12
Z2CND18.12N [36]	265	165	590	0.11
U71Mn [73,74]	500	204	1854	0.28
SS316L [57,67]	200	176	430	0.13
SS304 [38,71,72]	290	211	570	0.12

**Table B.2** Experimental ratcheting strain of SS304 in Figure 4.2

150±200 MPa	
Cycles (N)	$\varepsilon_r$ (%)
0	0
1	0.4
2	0.52
3	0.6
4	0.67
5	0.72
6	0.77
7	0.81
8	0.84
9	0.87
16	1.02
32	1.24
64	1.45
127	1.66

**Table B.3** Experimental ratcheting strain of SS304 in Figure 4.7(a-c)

10±260 MPa	
Cycles (N)	$\varepsilon_r$ (%)
0	0
1	0.204
2	0.244
7	0.261
14	0.286
23	0.302
34	0.32
44	0.333
53	0.337
65	0.342
77	0.347
87	0.352
99	0.358

65±260 MPa	
Cycles (N)	$\varepsilon_r$ (%)
0	0
1	0.523
2	0.611
4	0.65
6	0.702
9	0.75
12	0.804
17	0.849
22	0.883
28	0.917
35	0.945
42	0.974
51	1.005
60	1.031
72	1.057
82	1.076
93	1.099
99	1.118

65±325 MPa	
Cycles (N)	$\varepsilon_r$ (%)
0	0
1	1.353
2	1.932
3	2.371
5	2.697
6	2.832
9	2.996
11	3.186
14	3.299
17	3.411
21	3.502
26	3.58
32	3.676
37	3.766
43	3.839
49	3.918
56	3.991
64	4.07
72	4.137
80	4.216
89	4.277
95	4.304
99	4.349

**Table B.4** Experimental ratcheting strain of Z2CND18.12 N steel with constant stress amplitude and various mean stresses in Figure 4.9a

100±200 MPa	
Cycles (N)	$\varepsilon_r$ (%)
0	0
1	0.245
16	0.491
31	0.563
46	0.608
61	0.647
76	0.68
91	0.699

125±200 MPa	
Cycles (N)	$\varepsilon_r$ (%)
0	0
1	0.537
16	1.072
31	1.199
46	1.285
61	1.35
76	1.402
91	1.446

150±200 MPa	
Cycles (N)	$\varepsilon_r$ (%)
0	0
1	1.171
16	2.117
33	2.312
50	2.448
65	2.525
84	2.591

**Table B.5** Experimental ratcheting strain of Z2CND18.12 N steel with constant mean stress and various stresses amplitude in Figure 4.9b

125±150 MPa	
Cycles (N)	$\varepsilon_r$ (%)
0	0
1	0.176
16	0.271
31	0.29
46	0.297
61	0.314
76	0.314
91	0.322

125±175 MPa	
Cycles (N)	$\varepsilon_r$ (%)
0	0
1	0.297
16	0.446
31	0.481
46	0.501
61	0.52
76	0.528
91	0.54

125±200 MPa	
Cycles (N)	$\varepsilon_r$ (%)
0	0
1	0.537
16	1.072
31	1.199
46	1.285
61	1.35
76	1.402
91	1.446

**Table B.6** Experimental ratcheting strain of Z2CND18.12 N steel with constant stress level of  $150 \pm 150$  MPa and various stress rates Figure 4.10a

$\dot{\sigma} = 1000 \text{ MPa/sec.}$	
Cycles (N)	$\varepsilon_r$ (%)
0	0
1	0.238
16	0.388
31	0.435
46	0.459
61	0.475
76	0.49
91	0.506

$\dot{\sigma} = 100 \text{ MPa/sec.}$	
Cycles (N)	$\varepsilon_r$ (%)
0	0
1	0.345
16	0.569
31	0.617
46	0.644
61	0.668
76	0.679
91	0.699

$\dot{\sigma} = 10 \text{ MPa/sec.}$	
Cycles (N)	$\varepsilon_r$ (%)
0	0
1	0.51
16	0.877
31	0.979
46	1.038
61	1.085
76	1.125
91	1.156

**Table B.7** Experimental ratcheting strain of SS304 with constant stress level of  $78 \pm 234$  MPa and various stress rates Figure 4.10b and Figure 4.10c

$\dot{\sigma} = 65 \text{ MPa/sec.}$		$\dot{\sigma} = 13 \text{ MPa/sec.}$		$\dot{\sigma} = 2.6 \text{ MPa/sec.}$	
Cycles (N)	$\varepsilon_r$ (%)	Cycles (N)	$\varepsilon_r$ (%)	Cycles (N)	$\varepsilon_r$ (%)
0	0	0	0	0	0
1	2.325	1	3.313	1	4.003
2	2.735	2	3.666	2	4.339
3	2.948	3	3.795	3	4.457
4	3.128	4	3.89	4	4.541
5	3.279	5	3.958	5	4.597
6	3.403	6	4.02	6	4.636
7	3.504	7	4.059	7	4.681
8	3.57	8	4.104	8	4.721
9	3.638	9	4.132	9	4.749
10	3.7	10	4.166	10	4.771
11	3.745	11	4.193	11	4.794
12	3.784	12	4.215	12	4.816
13	3.824	13	4.244	13	4.839
14	3.856	14	4.266	14	4.856
15	3.884	15	4.289	15	4.873
16	3.913	16	4.311	16	4.889
17	3.941	17	4.328	17	4.911
19	3.986	19	4.362	19	4.939
21	4.025	21	4.395	21	4.967
23	4.065	23	4.418	23	4.995
25	4.093	25	4.452	25	5.018
27	4.126	27	4.474	27	5.04
29	4.155	29	4.497	29	5.063
31	4.183	31	4.518	31	5.086
33	4.21	33	4.541	33	5.102
35	4.227	35	4.558	35	5.119
37	4.255	37	4.575	37	5.136
39	4.272	39	4.591	39	5.153

**TableB.8** Experimental ratcheting strain of SS304 over three steps of loading in Figure 4.11

Step I (78±248 MPa)		Step II (117±248 MPa)		Step III (78±248 MPa)	
Cycles (N)	$\varepsilon_r$ (%)	Cycles (N)	$\varepsilon_r$ (%)	Cycles (N)	$\varepsilon_r$ (%)
0	0	51	2.313	101	3.733
1	0.87	52	2.553	102	3.722
2	1.03	53	2.69	103	3.733
3	1.113	54	2.806	104	3.733
4	1.175	55	2.892	105	3.733
5	1.198	56	2.963	106	3.742
6	1.238	57	3.037	107	3.733
7	1.261	58	3.08	109	3.733
8	1.281	59	3.123	111	3.733
9	1.301	60	3.185	113	3.722
10	1.335	61	3.217	115	3.733
11	1.355	62	3.268	117	3.742
13	1.386	64	3.322	---	---
15	1.407	66	3.374	---	---
17	1.438	68	3.416	---	---
19	1.46	70	3.448	---	---
21	1.492	72	3.479	---	---
23	1.512	74	3.522	---	---
25	1.534	76	3.553	---	---
27	1.534	78	3.585	---	---
29	1.555	80	3.605	---	---
31	1.586	82	3.627	---	---
33	1.597	84	3.648	---	---
35	1.606	86	3.659	---	---
37	1.629	88	3.679	---	---
39	1.649	90	3.701	---	---
41	1.66	92	3.722	---	---
43	1.671	94	3.722	---	---
45	1.703	96	3.753	---	---
47	1.703	98	3.773	---	---
49	1.712	100	3.796	---	---
50	1.723	---	---	---	---

**Table B.9** Experimental ratcheting strain of SS316L over four steps of loading in Figure 4.12

Step I (0±195 MPa)		Step II (39.7±195 MPa)		Step III (66.2±195 MPa)		Step IV (105.8±195 MPa)	
Cycles (N)	$\varepsilon_r$ (%)	Cycles (N)	$\varepsilon_r$ (%)	Cycles (N)	$\varepsilon_r$ (%)	Cycles (N)	$\varepsilon_r$ (%)
0	0	31	0.212	41	0.694	51	2.408
1	0.004	32	0.241	42	0.783	52	2.624
2	0.004	33	0.256	43	0.835	53	2.727
5	0.004	34	0.264	44	0.873	54	2.795
7	0.012	35	0.271	45	0.894	55	2.846
10	0.012	36	0.271	46	0.917	56	2.898
12	0.004	37	0.279	47	0.932	57	2.921
15	0.004	38	0.279	48	0.947	58	2.942
17	0.012	39	0.286	49	0.961	59	2.972
20	0.012	40	0.286	50	0.961	60	2.987
22	0.012	---	---	---	---	---	---
27	0.004	---	---	---	---	---	---
30	0.004	---	---	---	---	---	---

**Table B.10** Experimental ratcheting strain of U71Mn over seven steps of loading in Figure 4.13

Cycles (N)	$\epsilon_r$ (%)	Cycles (N)	$\epsilon_r$ (%)	Cycles (N)	$\epsilon_r$ (%)	Cycles (N)	$\epsilon_r$ (%)
Step I (0±449 MPa)		Step III (359±449 MPa)		Step V (308±449 MPa)		Step VII (411±449 MPa)	
0	0	41	3.444	80	6.797	121	7.684
2	0	43	3.613	81	6.675	123	8.036
5	0	44	3.765	84	6.644	125	8.252
8	0	46	3.901	86	6.644	127	8.435
10	0	49	4.026	87	6.644	129	8.573
12	0	51	4.131	90	6.658	131	8.739
14	0	53	4.225	93	6.644	134	8.895
16	0	55	4.331	95	6.675	136	9.094
18	0	57	4.422	97	6.658	139	9.291
20	0	60	4.513	100	6.658	---	---
Step II (308±449 MPa)		Step IV (411±449 MPa)		Step VI (359±449 MPa)		---	---
21	2.033	61	5.082	101	6.797	---	---
24	2.31	63	5.45	104	6.888	---	---
27	2.51	66	5.708	106	6.966	---	---
31	2.662	68	5.893	108	7.027	---	---
34	2.801	70	6.093	111	7.088	---	---
37	2.906	73	6.259	113	7.118	---	---
40	3.014	75	6.414	115	7.193	---	---
---	---	77	6.55	117	7.257	---	---
---	---	---	---	120	7.301	---	---

**Table B.11** Experimental ratcheting strain of U71Mn over four steps of loading in Figure 4.14a

Step I (205±411 MPa)		Step II (256±411 MPa)		Step III (308±411 MPa)		Step IV (256±411 MPa)	
Cycles (N)	$\varepsilon_r$ (%)	Cycles (N)	$\varepsilon_r$ (%)	Cycles (N)	$\varepsilon_r$ (%)	Cycles (N)	$\varepsilon_r$ (%)
0	0	21	1.616	41	2.287	61	2.702
1	0.957	23	1.711	43	2.409	65	2.706
3	1.083	25	1.772	45	2.473	68	2.713
5	1.151	27	1.814	47	2.531	72	2.709
7	1.197	29	1.86	49	2.58	74	2.713
10	1.239	32	1.902	51	2.626	77	2.713
13	1.277	34	1.932	54	2.664	79	2.713
16	1.33	37	1.962	58	2.729	---	---
20	1.368	40	2.005	60	2.763	---	---

**Table B.12** Experimental ratcheting strain of U71Mn over six steps of loading in Figure 4.14b

Cycles (N)	$\varepsilon_r$ (%)	Cycles (N)	$\varepsilon_r$ (%)	Cycles (N)	$\varepsilon_r$ (%)
Step I (359±321 MPa)		Step III (359±449 MPa)		Step V (359±385 MPa)	
0	0	41	2.941	83	8.275
1	0.775	44	3.264	87	8.289
2	1.515	47	3.464	89	8.259
5	1.59	50	3.62	91	8.275
8	1.621	53	3.787	94	8.289
11	1.637	56	3.943	96	8.289
14	1.651	60	4.126	Step VI (359±321 MPa)	
16	1.651	Step IV (359±513 MPa)		101	8.306
20	1.668	61	4.832	102	8.32
Step II (359±385 MPa)		63	5.308	104	8.289
21	2.004	66	5.878	106	8.289
24	2.191	69	6.445	110	8.306
27	2.282	72	6.968	112	8.306
30	2.357	75	7.46	116	8.306
33	2.421	78	7.967	119	8.289
36	2.435	80	8.306	---	---
40	2.513	---	---	---	---

**Table B.13** Experimental ratcheting strain of SS316L over four steps of loading in Figure 4.14c

Step I (52±195 MPa)		Step I (52±221 MPa)		Step I (52±247 MPa)		Step I (52±195 MPa)	
Cycles (N)	$\epsilon_r$ (%)						
0	0	21	1.295	41	2.742	62	3.457
1	0.544	22	1.513	42	2.951	63	3.457
1	0.623	23	1.573	43	3.056	64	3.475
2	0.657	24	1.617	44	3.108	65	3.465
3	0.684	25	1.652	45	3.168	66	3.475
5	0.692	25	1.686	46	3.213	67	3.457
5	0.702	27	1.696	47	3.257	69	3.465
6	0.719	28	1.731	48	3.292	70	3.475
7	0.719	29	1.756	50	3.317	71	3.457
8	0.727	30	1.765	51	3.344	72	3.465
9	0.744	32	1.783	52	3.37	74	3.465
10	0.744	33	1.808	53	3.396	75	3.457
11	0.754	35	1.817	55	3.413	77	3.475
12	0.762	36	1.827	56	3.44	78	3.465
13	0.762	37	1.835	58	3.465	80	3.465
15	0.771	38	1.844	59	3.483	---	---
16	0.771	40	1.862	60	3.457	---	---
17	0.781	---	---	---	---	---	---
18	0.781	---	---	---	---	---	---
20	0.781	---	---	---	---	---	---

**Table B.14** Experimental ratcheting strain of SS304 at 700°C in Figure 4.17

40±100 MPa			
Cycles (N)	$\varepsilon_r$ (%)	Cycles (N)	$\varepsilon_r$ (%)
0	0	37	2.876
1	2.128	40	2.914
2	2.257	43	2.934
3	2.296	46	2.966
4	2.321	49	2.985
5	2.334	52	3.011
6	2.353	55	3.031
7	2.38	58	3.057
9	2.411	61	3.088
11	2.45	64	3.134
13	2.528	67	3.166
15	2.559	70	3.198
17	2.598	73	3.224
19	2.624	76	3.243
21	2.669	79	3.269
23	2.695	82	3.308
25	2.728	85	3.34
27	2.766	88	3.366
29	2.779	91	3.392
31	2.812	93	3.412
33	2.837	96	3.45
35	2.856	100	3.476

**Table B.15** Experimental ratcheting strain of SS304 over three steps of loading at 200°C in

Figure 4.18

Step I (39±248 MPa)		Step II (78±248 MPa)		Step III (39±248 MPa)	
Cycles (N)	$\varepsilon_r$ (%)	Cycles (N)	$\varepsilon_r$ (%)	Cycles (N)	$\varepsilon_r$ (%)
0	0	31	5.971	81	7.192
1	3.322	32	6.14	82	7.192
2	3.437	33	6.214	82	7.192
3	3.522	34	6.351	83	7.183
4	3.616	35	6.445	86	7.183
5	3.679	36	6.573	87	7.192
6	3.753	37	6.635	88	7.183
7	3.805	38	6.71	89	7.183
8	3.858	39	6.781	90	7.192
9	3.932	41	6.824	91	7.192
10	3.984	42	6.887	92	7.183
12	4.027	44	6.929	93	7.192
13	4.069	45	6.972	95	7.183
14	4.101	46	7.003	96	7.172
15	4.132	48	7.024	98	7.172
16	4.163	49	7.046	---	---
17	4.195	51	7.055	---	---
18	4.215	52	7.086	---	---
19	4.237	53	7.098	---	---
20	4.258	55	7.109	---	---
21	4.278	57	7.12	---	---
22	4.3	58	7.129	---	---
23	4.312	60	7.14	---	---
25	4.32	61	7.16	---	---
26	4.332	63	7.172	---	---
27	4.343	64	7.183	---	---
28	4.352	66	7.203	---	---
29	5.595	68	7.203	---	---
30	5.868	70	7.223	---	---
---	---	71	7.223	---	---
---	---	73	7.257	---	---
---	---	75	7.246	---	---
---	---	76	7.277	---	---
---	---	78	7.277	---	---
---	---	79	7.203	---	---

**Table B.16** Experimental ratcheting strain of SS304 over three steps of loading at 400°C in

Figure 4.19

Step I (39±248 MPa)		Step II (78±248 MPa)		Step III (39±248 MPa)	
Cycles (N)	$\varepsilon_r$ (%)	Cycles (N)	$\varepsilon_r$ (%)	Cycles (N)	$\varepsilon_r$ (%)
0	0	51	4.786	101	4.887
1	2.599	52	4.849	102	4.86
2	2.763	54	4.887	104	4.887
3	2.801	56	4.912	105	4.873
4	2.839	58	4.923	107	4.86
5	2.851	59	4.936	108	4.86
6	2.875	61	4.923	111	4.849
7	2.902	63	4.923	112	4.86
8	2.941	65	4.923	114	4.835
10	2.941	67	4.936	116	4.86
12	2.977	69	4.936	119	4.86
14	2.977	70	4.923	---	---
16	3.004	72	4.923	---	---
17	3.004	73	4.923	---	---
19	3.028	75	4.936	---	---
21	3.042	76	4.936	---	---
22	3.042	78	4.95	---	---
24	3.042	80	4.95	---	---
26	3.042	81	4.936	---	---
27	3.053	82	4.936	---	---
29	3.042	84	4.95	---	---
31	3.053	86	4.936	---	---
32	3.053	88	4.936	---	---
34	3.053	90	4.936	---	---
36	3.053	91	4.936	---	---
38	3.053	93	4.95	---	---
40	3.066	94	4.95	---	---
41	3.053	96	4.95	---	---
43	3.066	98	4.936	---	---
45	3.053	100	4.95	---	---
47	3.053	---	---	---	---
49	3.053	---	---	---	---
50	3.053	---	---	---	---

**Table B.17** Experimental ratcheting strain of SS304 over three steps of loading at 600°C in

Figure 4.21

Step I (26±195 MPa)		Step II (39±195 MPa)		Step III (26±195 MPa)	
Cycles (N)	$\varepsilon_r$ (%)	Cycles (N)	$\varepsilon_r$ (%)	Cycles (N)	$\varepsilon_r$ (%)
0	0	51	3.318	102	3.37
1	3.244	52	3.37	103	3.37
2	3.28	53	3.381	105	3.356
4	3.332	55	3.381	107	3.37
5	3.343	58	3.395	109	3.356
6	3.356	60	3.395	111	3.356
7	3.356	62	3.395	113	3.356
9	3.356	64	3.395	114	3.37
10	3.356	66	3.395	116	3.343
11	3.356	68	3.395	117	3.356
13	3.343	70	3.395	119	3.356
14	3.356	73	3.395	---	---
16	3.356	75	3.395	---	---
18	3.356	76	3.395	---	---
19	3.343	79	3.408	---	---
21	3.356	80	3.408	---	---
24	3.356	82	3.408	---	---
26	3.356	84	3.395	---	---
28	3.356	86	3.408	---	---
29	3.356	87	3.408	---	---
31	3.356	89	3.408	---	---
33	3.356	91	3.408	---	---
35	3.356	92	3.408	---	---
37	3.343	95	3.408	---	---
39	3.343	97	3.395	---	---
40	3.343	98	3.408	---	---
42	3.343	100	3.408	---	---
43	3.343	---	---	---	---
45	3.343	---	---	---	---
47	3.343	---	---	---	---
49	3.332	---	---	---	---

**Table B.18** Experimental ratcheting strain of SS304 over three steps of loading at 700°C in

Figure 4.22

Step I (0±102 MPa)		Step II (26±102 MPa)		Step III (50±102 MPa)	
Cycles (N)	$\varepsilon_r$ (%)	Cycles (N)	$\varepsilon_r$ (%)	Cycles (N)	$\varepsilon_r$ (%)
0	0	21	0.241	41	1.698
1	0	22	0.328	42	2.003
2	0	23	0.392	43	2.219
4	0	25	0.431	44	2.382
5	0	26	0.482	45	2.522
6	0	27	0.518	47	2.623
7	0	29	0.569	48	2.738
9	0	30	0.594	50	2.839
10	0	32	0.645	51	2.953
11	0	33	0.684	52	3.018
12	0	34	0.734	53	3.105
14	0	36	0.773	55	3.194
15	0	38	0.798	56	3.284
16	0	40	0.86	57	3.359
18	0	---	---	58	3.46
19	0	---	---	59	3.55
20	0	---	---	60	3.662

## REFERENCES

- [1] Das D, Chakraborti PC. Effect of stress parameters on ratcheting deformation stages of polycrystalline OFHC copper. *Fatigue Fract Eng Mater Struct* 2011;34:734–42.
- [2] Lim C-B, Kim KS, Seong JB. Ratcheting and fatigue behavior of a copper alloy under uniaxial cyclic loading with mean stress. *Int J Fatigue* 2009;31:501–7.
- [3] Paul SK, Sivaprasad S, Dhar S, Tarafder S. Ratcheting and low cycle fatigue behavior of SA333 steel and their life prediction. *J Nucl Mater* 2010;401:17–24.
- [4] Gaudin C, Feaugas X. Cyclic creep process in AISI 316L stainless steel in terms of dislocation patterns and internal stresses. *Acta Mater* 2004;52:3097–110.
- [5] Rodriguez P. Serrated plastic flow. *Bull Mater Sci* 1984;6:653–63.
- [6] Ananthakrishna G. Current theoretical approaches to collective behavior of dislocations. *Phys Rep* 2007;440:113–259.
- [7] Ludwik P. *Elemente der technologischen Mechanik*. Springer-Verlag; 2013.
- [8] Bairstow L. The elastic limits of iron and steel under cyclical variations of stress. *Phil Trans R Soc Lond A* 1911;210:35–55.
- [9] Coffin LF. The deformation and fracture of a ductile metal under superimposed cyclic and monotonic strain. *Achiev. High Fatigue Resist. Met. Alloy.*, ASTM International; 1970:53-76.
- [10] Chaboche JL. A review of some plasticity and viscoplasticity constitutive theories. *Int J Plast* 2008;24:1642–93.
- [11] Khan AS, Huang S. *Continuum theory of plasticity*. John Wiley & Sons; 1995.
- [12] Lee D, Zaverl F. A generalized strain rate dependent constitutive equation for anisotropic metals. *Acta Metall* 1978;26:1771–80.
- [13] Chaboche JL, Van KD, Cordier G. Modelization of the strain memory effect on the cyclic hardening of 316 stainless steel. *SMiRT'5, Div." L, Berlin, LI 1.3*; 1979.
- [14] Ohno N. A constitutive model of cyclic plasticity with a nonhardening strain region. *J Appl Mech* 1982;49:721–7.
- [15] Nouailhas D, Cailletaud G, Policella H, Marquis D, Dufailly J, Lieurade HP, et al. On the description of cyclic hardening and initial cold working. *Eng Fract Mech* 1985;21:887–95.

- [16] Kang G, Gao Q, Yang X. A visco-plastic constitutive model incorporated with cyclic hardening for uniaxial/multiaxial ratcheting of SS304 stainless steel at room temperature. *Mech Mater* 2002;34:521–31.
- [17] Prager W, Mathematics BUD of A, Research USO of N, Ships USNDB of. A New Method of Analyzing Stresses and Strains in Work-hardening Plastic Solids. Division of Applied Mathematics, Brown University; 1955.
- [18] Armstrong PJ. A mathematical representation of the multiaxial Bauschinger effect. CEBG Rep RD/B/N, 731 1966.
- [19] Bower AF, Johnson KL. The influence of strain hardening on cumulative plastic deformation in rolling and sliding line contact. *J Mech Phys Solids* 1989;37:471–93.
- [20] Chaboche JL. Viscoplastic constitutive equations for the description of cyclic and anisotropic behaviour of metals. *Bull Acad Pol Sci, Ser Sci Tech* 1977;25:33–42.
- [21] Ohno N, Wang J-D. Kinematic hardening rules with critical state of dynamic recovery, part I: formulation and basic features for ratcheting behavior. *Int J Plast* 1993;9:375–90.
- [22] Ohno N, Wang J-D. Kinematic hardening rules with critical state of dynamic recovery, Part II: application to experiments of ratcheting behavior. *Int J Plast* 1993;9:391–403.
- [23] Jiang Y, Sehitoglu H. Modeling of cyclic ratcheting plasticity, part I: development of constitutive relations. *J Appl Mech* 1996;63:720–5.
- [24] McDowell DL. Stress state dependence of cyclic ratcheting behavior of two rail steels. *Int J Plast* 1995;11:397–421.
- [25] Chen X, Jiao R, Kim KS. On the Ohno–Wang kinematic hardening rules for multiaxial ratcheting modeling of medium carbon steel. *Int J Plast* 2005;21:161–84.
- [26] Ahmadzadeh GR, Varvani-Farahani A. Ratcheting assessment of steel alloys under uniaxial loading: a parametric model versus hardening rule of Bower. *Fatigue Fract Eng Mater Struct* 2013;36:281–92.
- [27] Hamidinejad SM, Varvani-Farahani A. Ratcheting assessment of steel samples under various non-proportional loading paths by means of kinematic hardening rules. *Mater Des* 2015;85:367–76.
- [28] Karvan P, Varvani-Farahani A. Ratcheting assessment of 304 steel samples by means of two kinematic hardening rules coupled with isotropic hardening descriptions. *Int J Mech*

- Sci 2018;149:190–200.
- [29] Karvan P, Varvani-Farahani A. Isotropic-kinematic hardening framework to assess ratcheting response of steel samples undergoing asymmetric loading cycles. *Fatigue Fract Eng Mater Struct* 2019;42:295–306.
- [30] Ahmadzadeh GR, Varvani-Farahani A. Ratcheting assessment of materials based on the modified Armstrong–Frederick hardening rule at various uniaxial stress levels. *Fatigue Fract Eng Mater Struct* 2013;36:1232–45.
- [31] Loffing-Cueni D, Flores SY, Sauter D, Daidié D, Siegrist N, Meneton P, et al. Dietary Sodium Intake Regulates the Ubiquitin-Protein Ligase Nedd4-2 in the Renal Collecting System. *J Am Soc Nephrol* 2006;17:1264–74.
- [32] Chaboche JL, Nouailhas D. A unified constitutive model for cyclic viscoplasticity and its applications to various stainless steels. *J Eng Mater Technol* 1989;111:424–30.
- [33] Perzyna P. The constitutive equation for work-hardening and rate sensitive plastic materials. *Proc. Vib. Probl.* 1963;4:281–90.
- [34] Chaboche J-L. Constitutive equations for cyclic plasticity and cyclic viscoplasticity. *Int J Plast* 1989;5:247–302.
- [35] Kang G, Gao Q. Uniaxial and non-proportionally multiaxial ratcheting of U71Mn rail steel: experiments and simulations. *Mech Mater* 2002;34:809–20.
- [36] Yu D, Chen G, Yu W, Li D, Chen X. Visco-plastic constitutive modeling on Ohno–Wang kinematic hardening rule for uniaxial ratcheting behavior of Z2CND18. 12N steel. *Int J Plast* 2012;28:88–101.
- [37] Karvan P, Varvani-Farahani A. Ratcheting assessment of visco-plastic alloys at ambient temperature by means of the A-V and O-W hardening rule frameworks. *Mech Mater* 2019;130:95–104.
- [38] Kang G, Kan Q, Zhang J, Sun Y. Time-dependent ratchetting experiments of SS304 stainless steel. *Int J Plast* 2006;22:858–94.
- [39] Zhao W, Yang S, Wen G, Ren X. Fractional-order visco-plastic constitutive model for uniaxial ratcheting behaviors. *Appl Math Mech* 2019;40:49–62.
- [40] Yoshida F. Uniaxial and biaxial creep-ratcheting behavior of SUS304 stainless steel at room temperature. *Int J Press Vessel Pip* 1990;44:207–23.

- [41] Mizuno M, Mima Y, Abdel-Karim M, Ohno N. Uniaxial Ratchetting of 316FR Steel at Room Temperature— Part I: Experiments. *J Eng Mater Technol* 2000;122:29–34.
- [42] Chen G, Chen X, Niu C-D. Uniaxial ratcheting behavior of 63Sn37Pb solder with loading histories and stress rates. *Mater Sci Eng A* 2006;421:238–44.
- [43] Wen M, Li H, Yu D, Chen G, Chen X. Uniaxial ratcheting behavior of Zircaloy-4 tubes at room temperature. *Mater Des* 2013;46:426–34.
- [44] Hong S. The tensile and low-cycle fatigue behavior of cold worked 316L stainless steel: influence of dynamic strain aging. *Int J Fatigue* 2004;26:899–910.
- [45] Sarkar A, Nagesha A, Sandhya R, Mathew MD. Effect of mean stress and stress amplitude on the ratcheting behaviour of 316LN stainless steel under dynamic strain aging regime. *Mater High Temp* 2012;29(4):351-358.
- [46] Yu D, Chen X, Yu W, Chen G. Thermo-viscoplastic modeling incorporating dynamic strain aging effect on the uniaxial behavior of Z2CND18. 12N stainless steel. *Int J Plast* 2012;37:119–39.
- [47] de Almeida LH, Le May I, Emygdio PRO. Mechanistic Modeling of Dynamic Strain Aging in Austenitic Stainless Steels. *Mater Charact* 1998;41:137–50.
- [48] Haupt A, Munz D, Scheibe W, Schinke B, Schmitt R, Sklenicka V. High temperature creep and cyclic deformation behaviour of AISI 316 L(N) austenitic steel and its modelling with unified constitutive equations. *Nucl Eng Des* 1996;162:13–20.
- [49] Kang G, Liu Y, Ding J, Gao Q. Uniaxial ratcheting and fatigue failure of tempered 42CrMo steel: damage evolution and damage-coupled visco-plastic constitutive model. *Int J Plast* 2009;25:838–60.
- [50] Taleb L, Cailletaud G. An updated version of the multimechanism model for cyclic plasticity. *Int J Plast* 2010;26:859–74.
- [51] Larsson R, Nilsson L. On the modelling of strain ageing in a metastable austenitic stainless steel. *J Mater Process Technol* 2012;212:46–58.
- [52] Ho K. Extension of the viscoplasticity theory based on overstress (VBO) to capture non-standard rate dependence in solids. *Int J Plast* 2002;18:851–72.
- [53] Miller AK, Sherby OD. A simplified phenomenological model for non-elastic deformation: Predictions of pure aluminum behavior and incorporation of solute strengthening effects.

- Acta Metall 1978;26:289–304.
- [54] Wang W, Zheng X, Yu J, Lin W, Wang C, Xu J. Time-dependent ratcheting of 35CrMo structural steel at elevated temperature considering stress rates. *Mater High Temp* 2017;34:172–8.
- [55] Zheng X, Wang J, Gao J, Ma L, Yu J, Xu J. Rate-dependent low cycle fatigue and ratcheting of 25Cr2MoVA steel under cyclic pulsating tension. *Mater High Temp* 2018;35:482–9.
- [56] Zheng X, Wang W, Guo S, Xuan F. Viscoplastic constitutive modelling of the ratchetting behavior of 35CrMo steel under cyclic uniaxial tensile loading with a wide range of stress amplitude. *Eur J Mech A/Solids* 2019;76:312–20.
- [57] Kang G, Gao Q. Uniaxial Ratcheting of Ss316L Stainless Steel At High Temperature : Experiments and Simulations. SMiRT18-F01-5; 2005.
- [58] Abdel-Karim M, Ohno N. Kinematic hardening model suitable for ratchetting with steady-state. *Int J Plast* 2000;16:225–40.
- [59] Krempl E, McMahon JJ, Yao D. Viscoplasticity based on overstress with a differential growth law for the equilibrium stress. *Mech Mater* 1986;5:35–48.
- [60] Ding J, Kang G, Kan Q, Liu Y. Constitutive model for uniaxial time-dependent ratcheting of 6061-T6 aluminum alloy. *Comput Mater Sci* 2012;57:67–72.
- [61] Goodall IW, Hales R, Walters DJ. On constitutive relations and failure criteria of an austenitic steel under cyclic loading at elevated temperature. *Creep Struct.*, Springer; 1981, p. 103–27.
- [62] Ohno N, Kachi Y. A constitutive model of cyclic plasticity for nonlinear hardening materials. *J Appl Mech* 1986;53:395–403.
- [63] Kang GZ, Gao Q. Temperature-dependent cyclic deformation of SS304 stainless steel under non-proportionally multiaxial load and its constitutive modeling. *Key Eng. Mater.*, vol. 274, Trans Tech Publ; n.d., p. 247–52.
- [64] Varvani-Farahani A. A comparative study in descriptions of coupled kinematic hardening rules and ratcheting assessment over asymmetric stress cycles. *Fatigue Fract Eng Mater Struct* 2017;40:882–93.
- [65] Gao Q, Kang GZ, Yang XJ. Uniaxial ratcheting of SS304 stainless steel at high temperatures: visco-plastic constitutive model. *Theor Appl Fract Mech* 2003;40:105–11.

- [66] The MathWorks Inc. MATLAB Version R2015b. Massachusetts, USA 2015.
- [67] Kang GZ, Li Y, Gao Q, Kan QH, Zhang J. Uniaxial ratchetting in steels with different cyclic softening/hardening behaviours. *Fatigue Fract Eng Mater Struct* 2006;29:93–103.
- [68] Jiang Y, Kurath P. An investigation of cyclic transient behavior and implications on fatigue life estimates. *J Eng Mater Technol* 1997;119:161–70.
- [69] Kang G, Liu Y, Li Z. Experimental study on ratchetting-fatigue interaction of SS304 stainless steel in uniaxial cyclic stressing. *Mater Sci Eng A* 2006;435:396–404.
- [70] Kang GZ, Li YG, Zhang J, Sun YF, Gao Q. Uniaxial ratcheting and failure behaviors of two steels. *Theor Appl Fract Mech* 2005;43:199–209.
- [71] Kang G, Gao Q, Cai L, Sun Y. Experimental study on uniaxial and nonproportionally multiaxial ratcheting of SS304 stainless steel at room and high temperatures. *Nucl Eng Des* 2002;216:13–26.
- [72] Kang G, Li Y, Gao Q. Non-proportionally multiaxial ratcheting of cyclic hardening materials at elevated temperatures: Experiments and simulations. *Mech Mater* 2005;37:1101–18.
- [73] Kang G, Gao Q, Yang X. Experimental study on the cyclic deformation and plastic flow of U71Mn rail steel. *Int J Mech Sci* 2002;44:1647–63.
- [74] Kang G. A visco-plastic constitutive model for ratcheting of cyclically stable materials and its finite element implementation. *Mech Mater* 2004;36:299–312.
- [75] Abdel-Karim M. An extension for the Ohno–Wang kinematic hardening rules to incorporate isotropic hardening. *Int J Press Vessel Pip* 2010;87:170–6.
- [76] Chen X, Chen X, Yu W, Li D. Ratcheting behavior of pressurized 90 elbow piping subjected to reversed in-plane bending with a combined hardening model. *Int J Press Vessel Pip* 2016;137:28–37.